<u>İSTANBUL TECHNICAL UNIVERSITY ★ INSTITUTE OF SCIENCE AND TECHNOLOGY</u>

EVALUATION OF STRESS INTENSITY FACTORS OF PATCHED CRACKS BY FINITE ELEMENT ANALYSIS

M.S. Thesis by
Emre CİVAN

Department : **Aeronautics and Astronautics Engineering**

Programme: **Aeronautics and Astronautics Engineering**

JUNE 2008

İSTANBUL TECHNICAL UNIVERSITY ★ INSTITUTE OF SCIENCE AND TECHNOLOGY

EVALUATION OF STRESS INTENSITY FACTORS OF PATCHED CRACKS BY FINITE ELEMENT ANALYSIS

M.S. Thesis by
Emre CİVAN
511041036

Date of submission : 5 Mayıs 2008
Date of defence examination: 9 Haziran 2008

Supervisor (Chairman): Assist. Prof. Dr. H. İbrahim KESER
Members of the Examining Committee: Prof.Dr. Zahit MECİTOĞLU
Assoc. Prof.Dr. Erol UZAL

JUNE 2008

İSTANBUL TEKNİK ÜNİVERSİTESİ ★ FEN BİLİMLERİ ENSTİTÜSÜ

YAMA TAMİRLİ ÇATLAKLARIN GERİLME ŞİDDET FAKTÖRLERİNİN SONLU ELEMANLAR METODUYLA HESAPLANMASI

YÜKSEK LİSANS TEZİ
Emre CİVAN
511041036

Tezin Enstitüye Verildiği Tarih : 5 Mayıs 2008
Tezin Savunulduğu Tarih : 9 Haziran 2008

Tez Danışmanı : **Yard. Doç.Dr. H. İbrahim KESER**
Diğer Jüri Üyeleri: **Prof.Dr. Zahit MECİTOĞLU**

Doç. Dr. Erol UZAL

HAZİRAN 2008

PREFACE

I express my sincere gratitude to my supervisor, Assist. Prof Dr. H. İbrahim Keser, for his valuable advises and continual support through the project.

Special thanks to Prof. Dr. İbrahim Özkol and Assoc. Prof. Dr. İrfan Kaymaz from Ataturk University for his efforts in helping and supporting me with his great knowledge and experience.

Finally, I would like to express my thanks to my beloved family and my fiancee for supporting me in all parts of my life.

İstanbul 2008 Emre Civan

TABLE OF CONTENTS

LIST OF TABLES

Page Number

LIST OF FIGURES

Page Number

LIST OF SYMBOLS

a : Half crack length
β : Coefficient, β = 1 for plane stress and $\beta = 1 - \nu^2$ for plane strain
E : Modulus of Elasticity
E' : coefficient, E' = E for plane stress and $E' = E/(1-\nu^2)$ for plane strain
f(θ) : Correction factor that depends on specimen and crack geometry
g(θ) : Geometric correction factor for displacement equation
G : Strain energy release rate
G_c : Critical work required to create a new unit crack area.
Φ : Complex stress function
γ : Surface energy connected with traction-free crack surfaces
H : Half height of the plate
κ : Coefficient, $\kappa = 3-4\nu$ for plane strain and $\kappa = 3-\nu/1+\nu$ for plane stress
K : Stress intensity factor
K_I : Stress intensity factor for opening mode (Mode I)
K_{II} : Stress intensity factor sliding mode (Mode II)
K_{III} : Stress intensity factor tearing mode (Mode III)
K_{IC} : Plane strain fracture toughness
K_c : Fracture toughness
L : Half length of the plate
μ : Shear modulus
ν : Poisson ratio
θ : Cylindrical coordinate of a point with respect to the crack tip
r : Cylindrical coordinate of a point with respect to the crack tip
R : Resistance to fracture
σ_0 : Uniaxial tensile stress
σ : Uniformly distributed axial tension applied to the ends of the plate
t : Thickness of the plate
t' : Thickness of the patch
u : Displacement in local x axis
v : Displacement in local y axis
w : Displacement in local z axis
w : Half width of the patch
Y : Dimensionless geometry correction factor or stress intensity factor
Z : Analytical function of the complex variable z = x + iy

YAMA TAMİRLİ ÇATLAKLARIN GERİLME ŞİDDET FAKTÖRLERİNİN SONLU ELEMANLAR METODUYLA HESAPLANMASI

ÖZET

Çatlak bulunduran yapısal elemanlar üzerlerine yapıştırılan yamalar sayesinde, Gerilme Şiddet Faktörlerini (GŞF, SIF: Stress Intensity Factor) azaltarak, mekanik dayanımını yükseltmek ve yorulma ömrünü uzatmak suretiyle tamir etmek mümkündür. Dahası, bu tip tamirler çok kolaylıkla uygulanabilirler. Yapıştırmalı yamalı tamirler hizmet şartları altında uzun süre dayanımlarını muhafaza edebilirler. Önemle belirtilmelidir ki, kötü tamir edilmiş bir yapı, hiç tamir edilmemiş bir yapıya nazaran daha tehlikelidir. Bu yüzden, verimli yama tamirlerinin dizayn edilmesi önem arzetmektedir.

Eğer çatlak bulunan Mode I (Şekil 2.2) yükleme altındaki bir yapısal parça yama uygulanmak suretiyle tamir edilirse çatlak ucundaki gerilme şiddet faktör değerleri düştüğü için yapının mekanik özellikleri iyileşecektir. Gerilme şiddet faktörleri yamanın mekanik, geometrik ve yapıştırma özelliklerine bağlı olarak değişir. Yama uygulanmış çatlakların, gerilme şiddet faktör değerlerinin kapalı çözümleri sadece bazı özel durumlarda mevcuttur.

Bu çalışmada, öncelikle simetrik sonlu dikdörtgen 2H uzunluğunda, 2L genişliğinde, t kalınlığında, ortasında 2a boyunda çatlak içeren bir plağın gerilme şiddet faktörleri hesaplanmıştır. σ_0 değerinde yayılı eksenel çekme kuvveti plağın ucuna uygulanmıştır. Kullanılan malzeme lineer elastik ve izotropik kabul edilmektedir. Plağın yan kenarlarında gerilme yoktur.

Çalışmanın ikinci safhasında ise, üzerine w genişliğinde kare bir yama yapıştırılan kare bir plağın kırılma mekanik özellikleri incelenmiştir. Çatlak bölgesi $t^{'} = t$ kalınlığında olan bir yama ile tamir edilmiştir.

Geliştirilen çatlak modeli aynı zamanda plak üzerindeki elastik gerilme alanını tanımlayabilecek üç ayrı yoğunluktaki ağ konfigurasyonları ile çözdürülmüştür. Ağ yoğunluğu kaba, orta ve iyi olmak üzere basamaklar halinde artırılarak edinilmiş çözümün yakınsaması incelenmiştir.

Çatlak bulunan plaktaki gerilme alanını tanımlayabilmek için ticari bir yazılım olan ANSYS programı kullanılmak suretiyle sonlu elemanlar çözümleri elde edilmiştir. Gerilme şiddet faktörleri değerleri lineer elastik sahada çözülmüş ve sonuçları analitik hesaplamalarla kıyaslanmıştır. Simeriden dolayı plağın sadece çeyreği göz önüne alınmıştır.

ANSYS yazılımıyla hesaplanan sonuçları tablolaştırma ve toplu işlem yapmak için MATLAB kullanılmıştır. NASGRO yazılımı, gerilme şiddet faktörü çözüm tabloları ve daha önceki çalışmalar elde edilen sonuçların doğruluğunu sağlamak amaçlı olarak kullanılmıştır.

Diğer incelenen konularsa, çatlak ucu eleman uzunluğunun çatlak uzunluğuna oranının etkisi, Elastisite modülünün etkisi, Poisson oranı etkisi, yama kalınlığının GŞF üzerindeki etkisi, gerilme ve GŞF değerlerinin çatlak uzunluğuna ve yama boyutlarına olan bağlılığıdır. Gerilme şiddet faktörü değerlerinin makul bir hassasiyet içinde bulunabilmesi için, üç farklı ağ yoğunluğu kullanılmıştır. Ayrıca sonsuz plak şartları incelenmiş ve çıkan sonuçların literatürdeki sonuçlar ile kıyaslaması ve sağlaması yapılmıştır.

Sonuçlar grafik ve tablolar vasıtasıyla sunulmuştur. Çıkan sonuçların daha önceki çalışmalarla ve analitik çözümlerle mükemmel uyum sağladığı görülmüştür.

Bu tezin esas katkısı, farklı plak konfigurasyonları ve yama şekilleri için yama tamirli veya tamirsiz Gerilim Şiddet Faktörlerini hesaplayabilecek güvenilir bir sonlu elemanlar modeli oluşturmaktır.

EVALUATION OF STRESS INTENSITY FACTORS OF PATCHED CRACKS BY FINITE ELEMENT ANALYSIS

SUMMARY

Many cracked structural components can be repaired by using bonded overlay patches which, mainly by reducing the stress-intensity factor (SIF), improve the mechanical resistance and increase fatigue life. Furthermore, such repairs can easily be applied. Bonded repairs have been shown to provide high level of bond durability under service conditions. It should be pointed out that a badly repaired structure can be more dangerous than the corresponding unrepaired structure. For such a reason, the design of efficient patch repairs is a crucial task.

If a cracked structural component under Mode I (Opening Mode) loading (Figure 2.2) is repaired by employing a patch, the mechanical behaviour improves since the stresses near the crack tip (and consequently the Stress Intensity Factor) decrease due to their deviation from the cracked plate to the patch. The stress intensity factors are reduced depending on the mechanical, geometrical and bond properties of the patch adopted. Closed form solutions of the stress intensity factors related to patched cracks exist only for particular cases.

In this study, first of all a symmetrical finite rectangular plate with a height of 2H, width of 2L, thickness equal to t contains a transverse symmetrical crack of width 2a is examined to evaluate Stress Intensity Factor. Uniformly distibuted axial tension of intensity σ_0 is applied to the ends of the plate. The material of the plate is assumed to be linearly elastic and isotropic. Both edges of the strip are free of stresses.

At the second stage of the problem, the fracture behaviour of a square cracked plate with a square patch with a width of w bonded on the plate surface is analysed. The cracked zone is assumed to be patched with a plate having thickness $t' = t$.

These crack models have also been investigated by taking meshing configuration into account to obtain excellent predictions of the elastic stress field in the plate. Mesh density refinement will be increased incrementally in order to verify that the required accuracy has been attained.

Solution for these problems are obtained by means of finite element method to determine the stress field in the cracked plate by using commercial software ANSYS. Stress distributions and stress intensity factors (SIF) are computed in linear elastic field and compared with analytical calculations. Because of the symmetry only quarter of the whole model is being examined for both models.

MATLAB code is written in order to achieve the tabulation of the results obtained by ANSYS. NASGRO software [44], and stress intensity solutions tabulated handbooks and previous studies in the literature are used for the verification of the results.

Other topics handled are the effect of ratio of crack tip element length to crack length (2a), Young's Modulus (E), Poisson's ratio (ν) and thickness of bonded patch on the calculation of SIF, stress and SIF dependancy of the model to crack length and patch dimensions. In order to analyze the stress intensity factor with a reasonable accuracy and to examine the mesh dependency of the results, three different mesh densities used. Also infinite plate conditions are examined and and the results obtained are verified.

Results are presented in graphical and tabular forms. Tabulated results are in perfect agreement with previous studies and analytical solutions.

The main contribution of this thesis is the development of a reliable finite element model for the evaluation of Stress Intensity Factors on various configuration and shape of patch repaired and unrepaired plates.

1. INTRODUCTION

1.1. Introduction to Fracture Mechanics and Patch Repairs

The presence of cracks increases the time and effort spent on maintenance and repair; they may ultimately lead to component fracture and subsequent structural failure, which in extreme cases can endanger human life. When failure of a structure occurs, it is mostly unexpected, sudden, and unfortunate, and it is natural for us to focus attention on minimizing the undesired consequences when designing and analyzing modern-day structures. The study of crack behavior, prevention and analysis of fracture of materials is known as fracture mechanics.

Since cracks cannot be eliminated, procedures must be devised to quantify and predict the behaviour of cracked structures under service conditions. The cracks may be present as small flaws in the material manufacturing stage, they may arise during fabrication or they may be the result of damage (fatigue, impact corrosion etc.) to the completed structure [1].

Systematic scientific rules must be devised to characterise cracks and their effects and to predict if and when they may become unsafe during the structures operational service life. The prime characterization and prediction parameter of fracture mechanics is Stress Intensity Factor.

Linear elastic fracture mechanics principles are used to relate the stress magnitude and distribution near the crack tip to the remote stresses applied to the cracked component, the crack size and shape and the material properties of the cracked component [1].

Damage of structural components is quite common in many engineering fields (mechanical, aerospace, automotive, marine, nuclear, civil, etc.). Whenever the required safety level of a damaged structure is not attained, temporary repair, permanent repair or replacement are three possible actions to be performed. Repairs in components with out-of-tolerance defects represent the easiest way to achieve the requested safety level in a short time and at low costs [13].

Many cracked structural components can be repaired by using bonded overlay patches which, mainly by reducing the Stress Intensity Factor (SIF), improve the mechanical resistance and increase fatigue life. Furthermore, such repairs can easily be applied. Bonded repairs have been shown to provide high level of bond durability under service conditions. It should be pointed out that a badly repaired structure can be more dangerous than the corresponding unrepaired structure. For such a reason, the design of efficient patch repairs is a crucial task [13].

1.2. Literature Review

It is not possible to describe whole contributions to the analytical, numerical and experimental methods of linear elastic fracture mechanics in this limited space. However, it is important to outline the milestones to cover the development of Linear Elastic Fracture Mechanics until now.

By the end of the 19th century, the effect of crack on the structural strength was widely known, but its nature and influence was still unknown. In 1913, Inglis published the first significant work in the development of fracture mechanics. The work was an analytical formulation of stresses in a plate in the vicinity of a two-dimensional elliptical hole. The plate was pulled at both ends perpendicular to the ellipse as shown in Figure 1.1. Inglis observed that the corner of the ellipse (point A) was feeling the most pressure and as the ellipse gets longer and thinner the stresses at *A* become larger [2]. He examined local stresses at the tip of the ellipse and estimated that the stress concentration was approximately

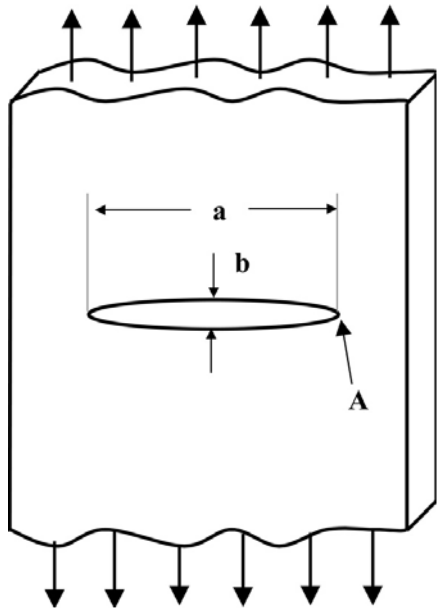

Figure 1.1: Stresses in a plate in the vicinity of a two-dimensional elliptical hole

$$2\left(\frac{a}{b}\right) \quad \text{or} \quad 2\sqrt{\frac{a}{\rho}} \tag{1.1}$$

where ρ is the root radius at the tip of the ellipse. Inglis evaluated various hole geometries and realized that it is not really the shape of the hole that matters but the length of hole perpendicular to the load and the curvature at the end of the hole that matters in cracking. He also noticed that pulling in a direction parallel to the hole does not produce a great effect.

The basic ideas leading to the start of modern fracture mechanics can be attributed to a theory of fracture strength of glass, which was published by A.A. Griffith in 1920 [2]. Using Inglis' work as a foundation, Griffith proposed an energy balance approach to study the fracture phenomenon in cracked bodies. A great contribution to the ideas about breaking strength of materials emerged when Griffith suggested that the weakening of material by a crack could be treated as an equilibrium problem. He proposed that the reduction in strain energy of a body when the crack propagates could be equated to the increase in surface energy due to the increase in the surface area. He developed a relationship between crack length (a), surface energy connected with traction-free crack surfaces (2γ), and applied stress, which is given by

$$\sigma^2 = \frac{2\gamma E}{\pi a} \tag{1.2}$$

The establishment of fracture mechanics is closely related to some well known disasters during the World War II. It is an interesting fact that the scientific curiosity towards fracture mechanics became a significantly important engineering discipline after the unfortunate failures of Liberty ships [3].

Griffith's work was ignored for over twenty years until several hundred liberty ships fractured extensively during World War II. The failures occurred primarily because of the change from riveted to welded construction and the major factor was the combination of poor weld properties with stress concentrations, and poor choice of brittle materials in the construction.

Research into this problem was led by George Rankine Irwin at the Naval Research Laboratory in Washington, DC. It was the research during this period that resulted in the development and definition of what we now refer to as linear-elastic fracture mechanics (LEFM). A major breakthrough occurred in the early 1950s when Irwin and Kies and Irwin provided the extension of Griffith theory for an arbitrary crack and proposed the criteria for the growth of this crack [3]. The criterion was that the strain energy release rate (G) must be larger than the critical work (G_c), which is required to create a new unit crack area.

Irwin also related strain energy release rate to the stress field at the crack tip using Westergaard's work [46]. Westergaard had developed a semi-inverse technique for analyzing stresses and displacements ahead of a crack tip. Using Westergaards' method, Irwin [45] showed that the stress field in the area of the crack tip is completely determined by a quantity K called the stress intensity factor [1]. Using the method of virtual work, Irwin presented a relationship between the energy release rate and the stress intensity factor as

$$\sigma_{ij} = \left[\frac{K}{\sqrt{2\pi r}}\right] f_{ij}(\theta) + ... \tag{1.3}$$

$$K^2 = EG \tag{1.4}$$

where r and θ are cylindrical coordinates of a point with respect to the crack tip shown in Figure 1.2. f_{ij} is defined as the geometric correction factor and will be explained in detail in later chapters. E is Young's modulus, and K is the stress intensity factor (SIF).

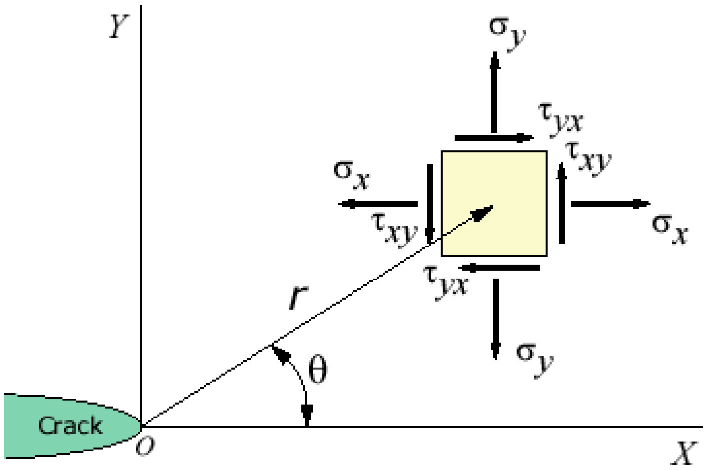

Figure 1.2: Definition of the coordinate axis ahead of a crack tip. The z direction is normal to the page.

Their research also resulted in a new materials property, fracture toughness, which is denoted by K_{Ic}, and is now universally accepted as the defining property of fracture mechanics.

The vast increase in the use of high strength metals and the reduction in design safety factors motivated a large number of researchers after World War II, to investigate this phenomena. Other serious failures that were experienced during that period were those of the de Havilland "Comet" commercial aircraft [4]. After about a year in service, three aircraft failed, resulting in the tragic loss of several lives. In 1955, Wells [2] used fracture mechanics to show that the fuselage failures in several Comet jet aircraft resulted from fatigue cracks reaching a critical size. These cracks were initiated at windows and were caused by insufficient local reinforcement in combination with square corners, which produced higher stress concentrations. After investigations, all of these failures seemed understandable in terms of the new fracture strength points of view. The evaluation method was straightforward, a value of G_c was established from laboratory tests on precracked specimens and the value of the driving force G that tended to extend the starting crack was computed using appropriate stress analysis methods. The comparison showed that the fracture toughness had not been large enough to prevent crack propagation in these failure cases.

In 1957, Williams [2] developed an infinite series that defined stress around a crack for any geometry. The use of the optical method “photoelasticity” to examine the stress fields around the tip of a running crack was published by Wells and Post in 1958.

In 1960, a significant contribution to the development of LEFM was put forth when Paris [3] advanced an idea to apply fracture mechanics principles to fatigue crack growth. The work was a landmark in the fatigue aspects of fracture mechanics, and yielded the equation Linear elastic fracture mechanics is not valid when significant plastic deformation precedes failure.

After the fundamentals of fracture mechanics were established, scientists began to concentrate on the plasticity of the crack tips. Although earlier theoretical developments were aimed at understanding brittle crack behavior, it became apparent from experiments that except for a few, most materials are ductile and therefore linear elastic analysis should be modified accordingly [3].

In 1968, Rice [47] modeled the plastic deformation as nonlinear elastic behavior and extended the method of energy release rate to nonlinear materials. He showed that the energy release rate can be expressed as a path-independent line integral, called the J integral. The plastic zone size and the crack opening displacement were found to correlate with the elastic stress intensity factor criterion [2]. The elastic-plastic failure parameter is designated J_{Ic} and is conventionally converted to K_{Ic} as given by

$$K_{Ic} = \sqrt{\frac{EJ_{Ic}}{1-\upsilon^2}} \tag{1.5}$$

Rice's theory has since dominated the development of fracture mechanics in United States. Meanwhile, Wells [1] proposed a parameter called crack tip opening displacement (CTOD), which led the fracture mechanics research in Europe.

The successful experiments in 1971 by Begley [4], led to the publication of a standard procedure for J testing of metals in 1981. In 1976, Sih [2] introduced the strain–energy density concept, which was a departure from classical fracture mechanics. He was able to characterize mixed-mode extension problems with this method, which also provided the direction of the crack propagation in addition to the amplitude of the stress field.

Contemporary research and development in fracture mechanics focuses on several interesting areas, such as dynamic fracture mechanics, interface fracture mechanics, shear ruptures in earthquakes, stress corrosion cracking, environmental effects on fatigue crack propagation, fracture of novel materials such as nanocomposites and graded materials. Experimental techniques have progressed enough to investigate fracture in materials at nanometer length scales and nanosecond time resolution. However, experimental techniques that could provide spatial and temporal resolution simultaneously at the nanolevel are still not available.

From this point on, some contemporary representative examples of previous stress intensity factor evaluation studies of cracks mainly by finite element method will be presented.

The performance of several superconvergent techniques to extract stress intensity factors from numerical solutions computed with the generalized finite element method is investigated by Pereira and Duarte [5]. Several numerical examples demonstrating the convergence of the computed SIF and the flexibility of the proposed implementation are also presented. The path independence of the extraction methods is investigated in their work.

Lin and Smith [6] worked on the evaluation of stress intensity factors for two symmetric quarter-elliptical corner cracks subjected to remote tension by using both the quarter-point displacement and J-integral methods based on three-dimensional finite element analyses.

Some examples of linear elastic and elastic-plastic problems to evaluate fracture parameters is solved by Araujo and Bittencourt [7] by using Displacement Correlation Technique (DCT), Modified Crack Closure Method and J-integral evaluation methods accomplished by means of Equivalent Domain Integrals.

Guinea and Planas [8] analyzed the influence of element size, element shape, and mesh arrangement on numerical values of K_I obtained by the displacement method, and gave some guidelines to obtain K_I values within a few percent difference of the exact value. Three different displacement-based extrapolation techniques were also analyzed in their studies.

Utomo [9] evaluated two methods of stress intensity factor calculation, Quarter Point Displacement Technique (QPDT) and Displacement Correlation Technique

(DCT). Their work focuses on the comparison of results found by their experiments and the finite element analysis by both QPDT and DCT methods if they are in good agreement. They used compact tension specimen and cracked beam in order to evaluate abovementioned methods.

Lim and Johnston [10] investigated on the performances of Quarter Point Displacement Technique (QPDT) and Displacement Correlation Technique (DCT) to resolve the common problem that, which of these methods provide more accurate results that is in better agreement with the analytical solutions.

Tsamasphyros and Vrettos [11] developed codes for the solution of composite patch repaired crack problems by implementing a mesh generator routine for the creation of the geometry and a finite element routine for the calculation of Stress Intensity Factors.

Aour and Rahmani [12] developed a special super-element using boundary elements based on the usual finite element technique of total potential energy minimization in order to develop a combined finite element/boundary element method approach. The application of the quarterpoint elements in finite element method and J-integrals techniques were examined using the proposed coupling FEM–BEM. The accuracy and efficiency of the proposed approach have been assessed for the evaluation of stress intensity factors.

Brighenti and Carpinteri [13] worked on the problem of the optimal shape of patch repairs for cracked plates by applying a genetic algorithm. The optimum design procedure consists in evaluating the patch topology which minimises the stress-intensity factor function of the repaired plate under Mode I loading while keeping constant the total patched area by implementing a finite element code embedded in a genetic algorithm.

1.3. Statement of the Problem and Methods of Solution

Damage of structural components is quite common in many engineering fields (mechanical, aerospace, automotive, marine, nuclear, civil, etc.) [13]. Whenever the required safety level of a damaged structure is not attained, temporary repair, permanent repair or replacement are three possible actions to be performed. Repairs in components with out-of-tolerance defects represent the easiest way to achieve the requested safety level in a short time and at low costs.

Many cracked structural components can be repaired by using bonded overlay patches which, mainly by reducing the stress-intensity factor (SIF), improve the mechanical resistance and increase fatigue life [14]. Furthermore, such repairs can easily be applied. Bonded repairs have been shown to provide high level of bond durability under service conditions. It should be pointed out that a badly repaired structure can be more dangerous than the corresponding unrepaired structure. For such a reason, the design of efficient patch repairs is a crucial task.

If a cracked structural component under Mode I loading is repaired by employing a patch, the mechanical behaviour improves since the stresses near the crack tip (and consequently the stress intensity factor) decrease due to their deviation from the cracked plate to the patch. Note that the stress intensity factors are reduced depending on the mechanical, geometrical and bond properties of the patch adopted. Closed form solutions of the stress intensity factors related to patched cracks exist only for particular cases.

In this thesis, a symmetrical finite rectangular plate with a height of 2H, width of 2L, thickness equal to t contains a transverse symmetrical crack of width 2a as shown in Figure 1.3. is examined to evaluate stress intensity factor. Uniformly distributed axial tension of intensity σ is applied to the ends of the plate. The material of the plate is assumed to be linearly elastic and isotropic. Both edges of the strip are free of stresses.

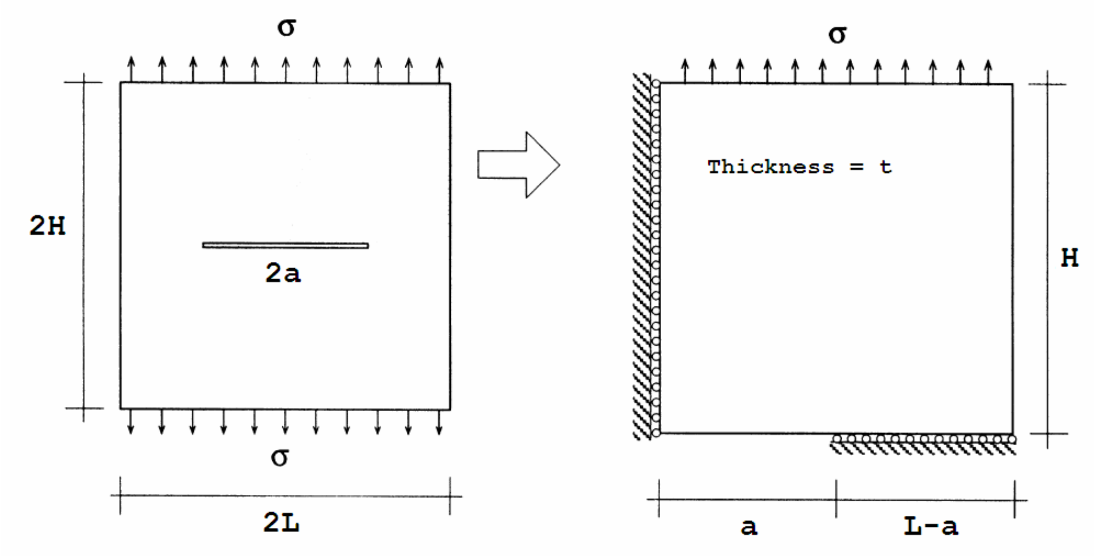

Figure 1.3: Center cracked plate geometry

After the patchless model described above is examined, the fracture behaviour of a square cracked plate with a square patch with a width of 2w bonded on the plate surface as shown in Figure 1.4 is analysed. The cracked zone is assumed to be patched with a plate having thickness $t' = t$.

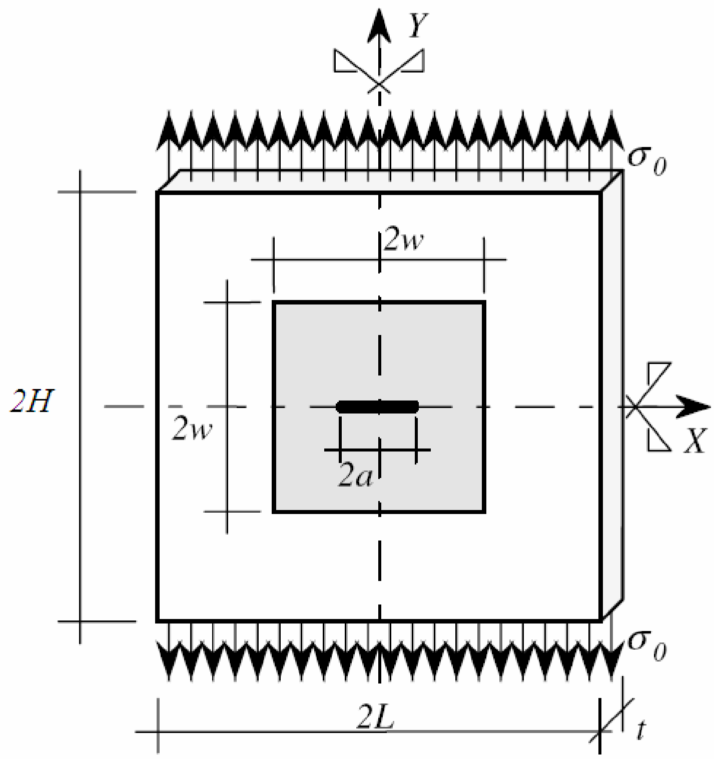

Figure 1.4: A square cracked plate with a square patch bonded on the plate surface

These crack models have also been investigated by taking meshing configuration into account to obtain predictions of the elastic stress field in the plate. Mesh density refinement will be increased incrementally in order to verify that the adequate accuracy has been attained. To achieve that, coarse, medium and fine mesh densities will be applied to each model.

Solution for these problems are obtained by means of finite element method to determine the stress field in the cracked plate by using commercial software ANSYS. Stress distributions and stress intensity factors (SIF) are computed in linear elastic field and compared with previous works [16, 38, 39]. Because of the symmetry only quarter of the whole model is being examined for both models. The bond between the cracked plate and the patch is assumed to be complete, i.e. without any interface between the two structural components.

MATLAB code is written in order to achieve the tabulation of the results obtained by ANSYS. NASGRO, and stress intensity solutions tabulated handbooks [15, 21, 37] and previous studies in the literature [8, 16] are used for the verification of the results.

For calculations, 3-D solid models were created by extruding 8-noded plane (PLANE82) elements given in Appendix B into 20-noded volumetric brick elements (SOLID95) presented in Appendix C.

Other topics handled are the effect of ratio of crack tip element length to crack length, Young's Modulus, Poisson’s ratio and thickness of bonded patch on the calculation of SIF, stress and SIF dependancy of the model to crack length and patch dimensions. In order to analyze the stress intensity factor with a reasonable accuracy and to examine the mesh dependency of the results, three different mesh densities (coarse, medium, fine) used. Also infinite plate conditions are examined and the results obtained are verified [8, 13, 16, 38, 39, 40].

2. STRESS INTENSITY FACTORS

2.1. Introduction

The stress intensity factor is a fundamental quantity that governs the stress field near the crack tip and it can be used to predict the failure of a cracked plate. The stress intensity factor depends on both the geometrical configuration and the loading conditions of the body.

By means of various techniques, the stress, strain, and displacement fields associated with a crack embedded in an elastic solid can be solved analytically [3]. One of such method is due to Westergaard, who introduced the following complex stress function,

$$\Phi = \mathrm{Re}\,\overline{\overline{Z}} + y\,\mathrm{Im}\,\overline{Z} \tag{2.1}$$

where Z = Z(z) is an analytical function of the complex variable z = x + iy. Here

$$\overline{Z} = \int Z(z)dz \tag{2.2.a}$$

$$\overline{\overline{Z}} = \int\int Z(z)dzdz \tag{2.2.b}$$

For a two dimensional continuous elastic medium, Airy stress function is described as

$$\sigma_{xx} = \frac{\partial^2\Phi}{\partial y^2} \tag{2.3.a}$$

$$\sigma_{yy} = \frac{\partial^2\Phi}{\partial x^2} \tag{2.3.b}$$

$$\tau_{xy} = -\frac{\partial^2\Phi}{\partial x\partial y} \tag{2.3.c}$$

Applying Equation (2.1) gives

$$\sigma_{xx} = \operatorname{Re} Z - y \operatorname{Im} Z' \tag{2.4.a}$$

$$\sigma_{yy} = \operatorname{Re} Z + y \operatorname{Im} Z' \tag{2.4.b}$$

$$\tau_{xy} = -y \operatorname{Re} Z' \tag{2.4.c}$$

Note that the imaginary part of the stresses vanishes when y = 0. In addition, the shear stress vanishes when y = 0, implying that the crack plane is a principal plane. Thus the stresses are symmetric about θ = 0 and Equation (2.4) implies Mode I (Figure 2.2) loading.

The Westergaard stress function (Equation 2.1), in its original form, is suitable for solving a limited range of crack problems. Consider a through crack in an infinite plate subject to biaxial remote tension (Figure 2.1). If the origin is defined at the center of the crack, the Westergaard stress function (Equation 2.1) is given by

$$Z(z) = \frac{\sigma}{\sqrt{1-(a/z)^2}} \tag{2.5}$$

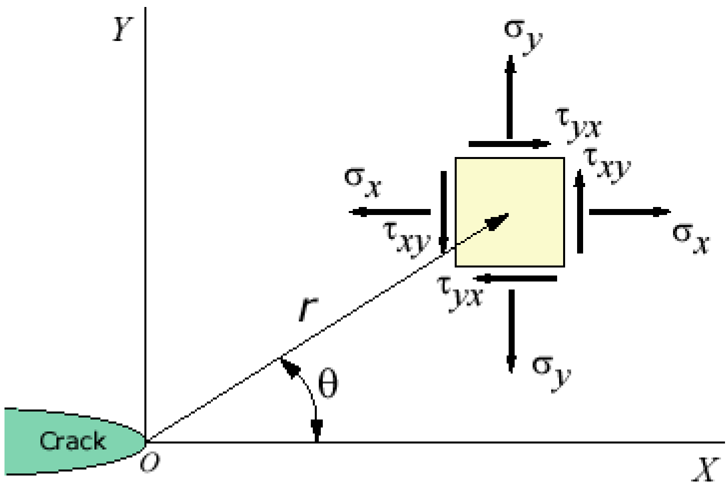

Figure 2.1: Through crack in an infinite plate subject to biaxial remote tension

Where σ is the remote stress and a is the half-crack length. For –a < x < a, Z is pure imaginary, while Z is real for |x| > |a|. The normal stresses on the crack plane are given by

$$\sigma_{xx} = \sigma_{yy} = \operatorname{Re} Z = \frac{\sigma x}{\sqrt{x^2 - a^2}} \tag{2.6}$$

Now consider the horizontal distance from each crack tip, $x^* = x - a$, Equation (2.6) becomes

$$\sigma_{xx} = \sigma_{yy} = \frac{\sigma\sqrt{a}}{\sqrt{2x^*}} \tag{2.7}$$

for $x^* << a$. Thus the Westergaard [46] approach leads to the expected inverse square-root singularity. One advantage of this analysis relates the local stresses to the global stress and crack size.

By transforming the origin to the right-hand crack tip, i.e., $z = a + re^{-i\theta}$, all the stress components can be derived. In the limit of small enough values of r/a, Equation (2.5) can be expressed as

$$Z = \frac{\sigma\sqrt{a}}{\sqrt{2r}} e^{-i\theta/2} \tag{2.8}$$

From differentiation of Equation (2.5),

$$Z'(z) = \frac{-\sigma a^2}{\left(z^2 - a^2\right)^{3/2}} \tag{2.9}$$

Hence

$$Z' = \frac{\sigma a}{2r} e^{-3i\theta/2} \tag{2.10}$$

For the configuration shown in Figure 2.1, the stresses can be expressed in a simple form, noting equation (2.4),

$$\sigma_{ij} = \frac{K}{\sqrt{2\pi r}} f_{ij}(\theta) \tag{2.11}$$

and displacement

$$u_i = \frac{K}{2\mu}\sqrt{\frac{r}{2\pi}}g(\theta) \tag{2.12}$$

where the K terms are the stress intensity factors which embody the loading and geometry conditions.

2.2. Fracture Modes

A crack in a solid can be stressed in three different modes, as illustrated in Figure 2.2. Normal stresses give rise to the "opening mode" or Mode I loading. The displacements of the crack surfaces are perpendicular to the plane of the crack. Mode I is opening or tensile mode where the crack surfaces move directly apart. Mode II is sliding or in-plane shear mode where the crack surfaces slide over one another in a direction perpendicular to the leading edge of the crack. Mode III is tearing and antiplane shear mode where the crack surfaces move relative to one another and parallel to the leading edge of the crack [4]. The stress intensity factor is usually given a subscript to denote the mode of loading, i.e., K_I, K_{II}, K_{III}.

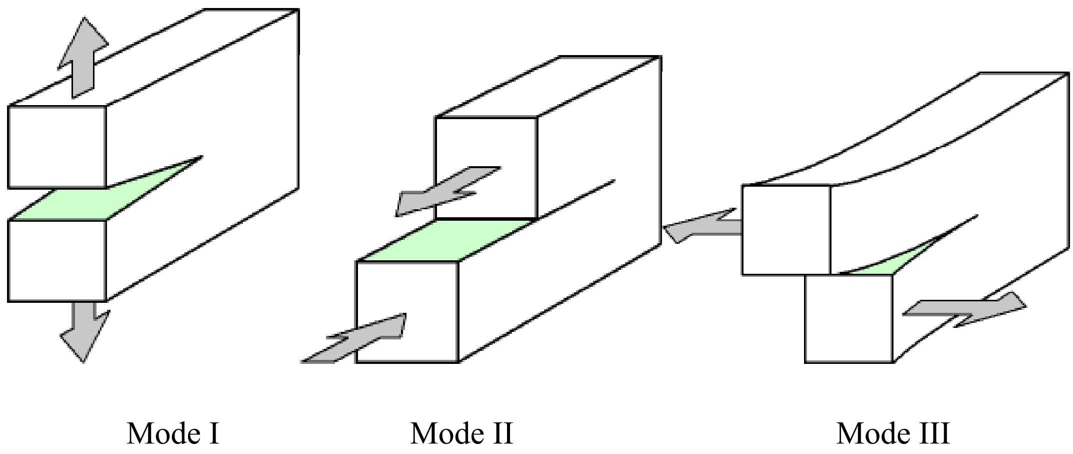

Figure 2.2: The three modes of loading that can be applied to a crack

90% of the fracture mechanics engineering problems are of the Mode I type, another 8% of the combined-mode type, which, immediately upon initiation of loading, transform into Mode I crack behavior [1]. For practical reasons, Mode I is the most important, and therefore only the K_I parameter is considered throughout the study.

For certain cracked configurations subjected to external forces, it is possible to derive closed-form expressions for the stresses in the body, assuming isotropic linear elastic material behavior. Westergaard [46], Irwin [45], Sneddon [48] and Williams [49] were among the first to publish such solutions.

Irwin [45] solved several two-dimensional crack problems in linear elasticity and showed that the stress field in the vicinity of the crack-tip was always of the same form. He showed that the stress-field component σ_{ij} at the point (r,θ) near the crack tip is given by

$$\sigma_{ij}(r,\theta) = \frac{K}{\sqrt{2\pi r}} f_{ij}(\theta) + \text{other terms}, \tag{2.13}$$

where the origin of the polar coordinates (r,θ) is at the crack tip and $f_{ij}(\theta)$ contains trigonometric functions. As the coordinate r approaches zero the leading term in Equation (2.13) dominates; the other terms are constant or tend to zero. The constant K in the first term is known as the Stress Intensity Factor. It therefore follows that the stress field in the vicinity of the crack tip is characterized by the stress intensity factor. In general K will be a function of the crack size and shape, the type of loading and the geometrical configuration of the structure. The stress intensity factor is often written in the following form.

$$K = Y\sigma\sqrt{\pi a} \tag{2.14}$$

where σ is a stress, a is a measure of the crack length and Y is a non-dimensional function of the geometry.

The symbol K (with the appropriate subscripts) is widely used in the literature dealing with a multitude of theoretical and experimental studies of fracture phenomena and materials science in general. It does refer to a specific zone near the crack tip, as shown in Figure 2.3. In this zone, the stress field is completely described by the stress intensity factor, K, and the stresses are given by the following equations:

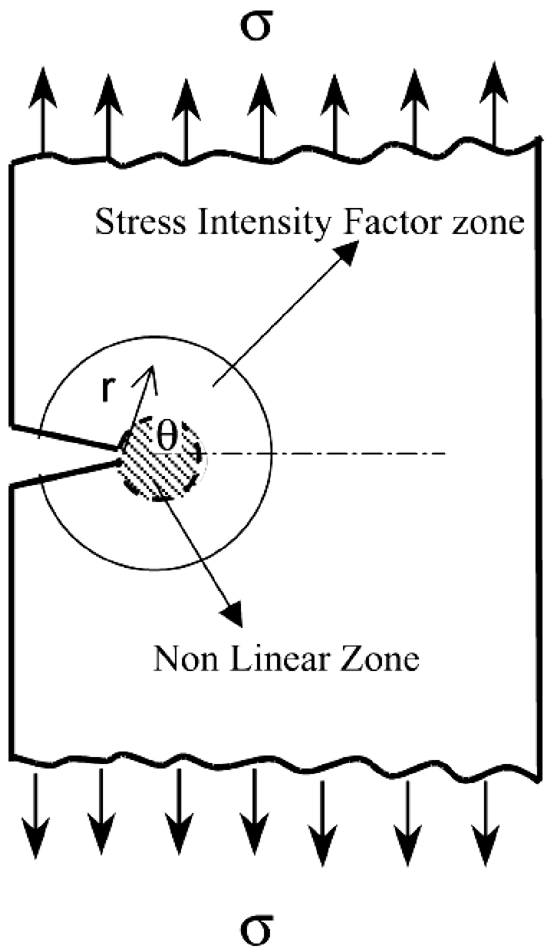

Figure 2.3: Stress intensity factor zone representation

$$\sigma_{xx} = \frac{K_I}{\sqrt{2\pi r}}\cos\left(\frac{\theta}{2}\right)\left[1-\sin\left(\frac{\theta}{2}\right)\sin\left(\frac{3\theta}{2}\right)\right] \quad + \text{other terms} \tag{2.15.a}$$

$$\sigma_{yy} = \frac{K_I}{\sqrt{2\pi r}}\cos\left(\frac{\theta}{2}\right)\left[1+\sin\left(\frac{\theta}{2}\right)\sin\left(\frac{3\theta}{2}\right)\right] \quad + \text{other terms} \tag{2.15.b}$$

$$\tau_{xy} = \frac{K_I}{\sqrt{2\pi r}}\cos\left(\frac{\theta}{2}\right)\sin\left(\frac{\theta}{2}\right)\cos\left(\frac{3\theta}{2}\right) \quad + \text{other terms} \tag{2.15.c}$$

$$\sigma_{zz} = \begin{cases} 0 & \text{Plane stress} \\ \upsilon(\sigma_{xx}+\sigma_{yy}) & \text{Plane strain} \end{cases} \tag{2.15.e}$$

$$\tau_{xz}, \tau_{yz} = 0 \tag{2.15.f}$$

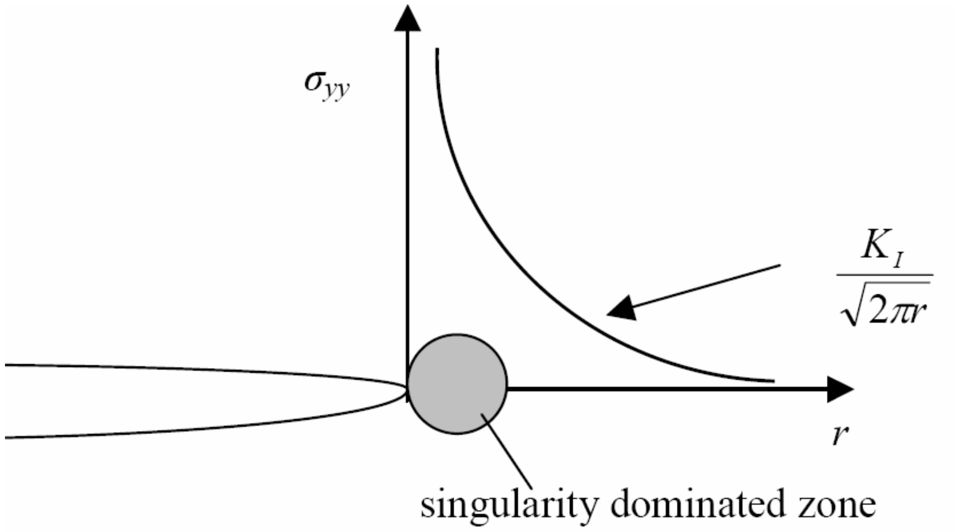

Figure 2.4 Stress normal to crack plane in Mode I loading

Figure 2.4 is a schematic plot of σ_{yy}, the stress normal to the crack plane vs. distance from the crack tip. If we consider the Mode I singular field on the crack plane, where θ = 0, Equation (2.15) becomes:

$$\sigma_{yy} = \frac{K_I}{\sqrt{2\pi r}} \tag{2.16}$$

Clearly the actual stress normal to the crack plane σ_{yy} is higher than that given by Equation (2.16). Hence this equation is valid only near the crack tip, where $1/\sqrt{r}$ singularity dominates the stress field. This is defined as the singularity dominated zone, as shown in Figure 2.4. Stresses far from the crack tip are governed by the remote boundary conditions. The stress intensity factor defines the amplitude of the crack-tip singularity. That is, stresses near the crack tip increase in proportion to K. Moreover, the stress intensity factor completely defines the crack tip conditions; if K is known, it is possible to solve for all components of stress, strain, and displacement as a function of r and θ. This single-parameter description of crack tip conditions turns out to be one of the most important concepts in fracture mechanics.

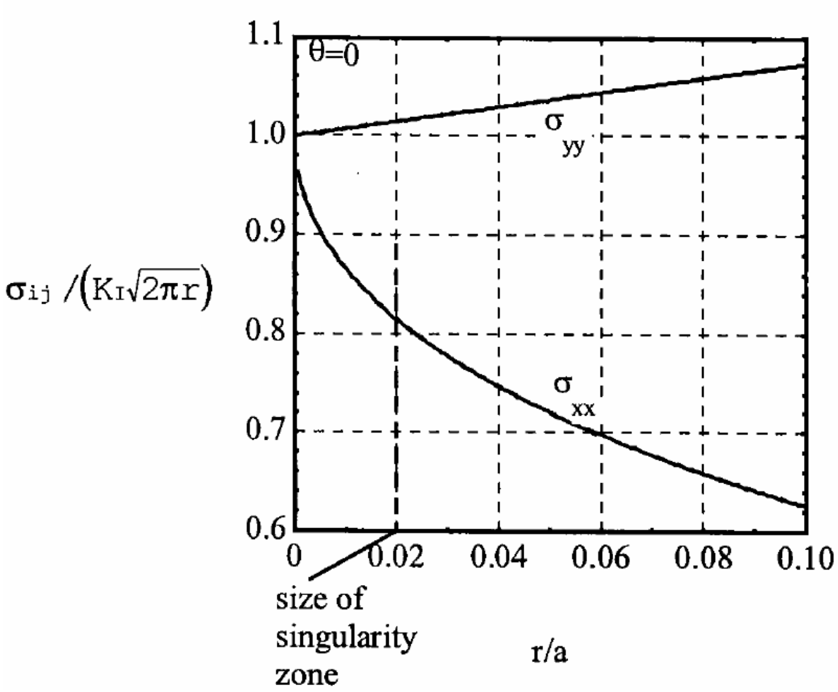

Figure 2.5: Ratio of actual stresses on the crack plane to the singularity limit

The size of this zone can be estimated by considering the ratio of the actual stress on the crack plane to the singularity limit. This is depicted in Figure 2.5. Note that the stress in the y direction is close to the singularity limit for relatively large distances from the crack tip, but the x stress diverges considerably from the near-tip limit. Let us arbitrarily define the singularity zone as the region within which the deviation is less than 20% for the x stress; this represents a value of r/a = 0.02. In other words, the term "singularity zone" is approximately one-fiftieth of the half crack size [17].

2.3. Fracture Criterion

When a solid is fractured, work is performed to create new material surfaces in a thermodynamically irreversible manner [4]. In Griffith's theory of ideally brittle materials, the work of fracture is spent in the rupture of cohesive bonds. The fracture surface energy γ, which represents the energy required to form a unit of new material surface, corresponds to a normal separation of atomic planes.

However the energy required for the rupture of atomic bonds is only a small portion of the dissipated energy in the fracture process. There are situations where the irreversible work associated with fracture is confined to a small process zone adjacent to the crack surfaces, while the remaining material is deformed elastically.

In such a case the various work terms associated with fracture may be lumped together in a macroscopic term R (resistance to fracture) which represents the work required for the creation of a unit of new material surface. R may be considered as a material parameter.

For an ideally brittle material, the energy dissipated in plastic deformation is negligible and can be omitted. The energy balance during crack growth can be written as

$$G = 2\gamma \tag{2.17}$$

where the factor 2 appearing on the right-hand side of the equation refers to the two new material surfaces formed during crack growth.

When the zones of plastic deformation around the crack tip are very small, the plastic strain energy can be omitted, and the work rate supplied to the body for crack growth is represented by Equation (2.17). In such circumstances, fracture is assumed to occur when the strain energy release rate G, which represents the energy pumped into the fracture zone from the elastic bulk of the solid, becomes equal to the energy required for the creation of a unit area of new material R. The fracture condition is

$$G_I = G_c = R \tag{2.18}$$

Equation (2.18) is usually expressed in terms of the opening-mode stress intensity factor K_I. By introducing a new material parameter K_c from the equation

$$K_c = \sqrt{\frac{ER}{\beta}} \tag{2.19}$$

where, $\beta = 1$ for plane stress and $\beta = 1-\upsilon^2$ for plane strain. The relation between strain energy release rate G and stress intensity factor is defined as,

$$G_I = \frac{K_I^2}{E} \text{ for plane stress} \tag{2.20}$$

$$G_I = \frac{\left(1-\upsilon^2\right)K_I^2}{E} \text{ for plane strain} \tag{2.21}$$

and by substituting G_I in terms of K_I from Equation (2.20) or (2.21), we can write Equation (2.19) as

$$K_I = K_c \tag{2.22}$$

Equation (2.22) expresses the critical stress intensity factor fracture criterion. The left-hand side of the equation depends on the applied load, the crack length and the geometrical configuration of the cracked plate. The right-hand side is a material parameter and can be determined experimentally. Note that Equation (2.22) was derived from the global energy balance of the continuum; it expresses the law of conservation of energy.

From a comprehensive investigation and analysis of the structural failures, following general conclusions can be drawn [4].

- Most fractures were mainly brittle in the sense that they were accompanied by very little plastic deformation, although the structures were made of materials with ductile behavior at ambient temperatures.
- Most brittle failures occurred in low temperatures.
- Usually, the nominal stress in the structure was well below the yield stress of the material at the moment of failure.
- Most failures originated from structural discontinuities including holes, notches, reentrant corners, etc.
- The origin of most failures, excluding those due to poor design, was pre-existing defects and flaws, such as cracks accidentally introduced into the structure. In many cases the flaws that triggered fracture were clearly identified.
- The structures that were susceptible to brittle fracture were mostly made of high-strength materials which have low notch or crack toughness (ability of the material to resist loads in the presence of notches or cracks).
- Fracture usually propagated at high speeds which, for steel structures, were in the order of 1000 m/s. The observed crack speeds were a fraction of the longitudinal sound waves in the medium [18].

Plane-Strain Fracture Toughness

Fracture toughness is an indication of the amount of stress required to propagate a preexisting flaw. It is a very important material property since the occurrence of flaws is not completely avoidable in the processing, fabrication, or service of a material/component. Flaws may appear as cracks, voids, metallurgical inclusions, weld defects, design discontinuities, or some combination thereof. Since engineers can never be totally sure that a material is flaw free, it is common practice to assume that a flaw of some chosen size will be present in some number of components and use the linear elastic fracture mechanics (LEFM) approach to design critical components [17]. This approach uses the flaw size and features, component geometry, loading conditions and the material property called fracture toughness to evaluate the ability of a component containing a flaw to resist fracture.

Laboratory experiments indicate that K_c varies with the thickness B of the specimen tested. The form of variation of K_c with B is shown in Figure 2.6. For increasing thickness beyond a critical minimum value, B_c, plane strain conditions dominate and the fracture toughness remains the same. The critical value of stress intensity factor in region III for plane strain conditions is denoted by K_{Ic} in Figure 2.6 and is independent of the specimen thickness [4].

K_{Ic} is one of the most important parameters in fracture mechanics called the plane-strain fracture toughness. This is the critical value of stress intensity K_I at which fracture takes place. Broek [1] provides a strong argument for using the K_{Ic} symbol, regardless of the state of stress.

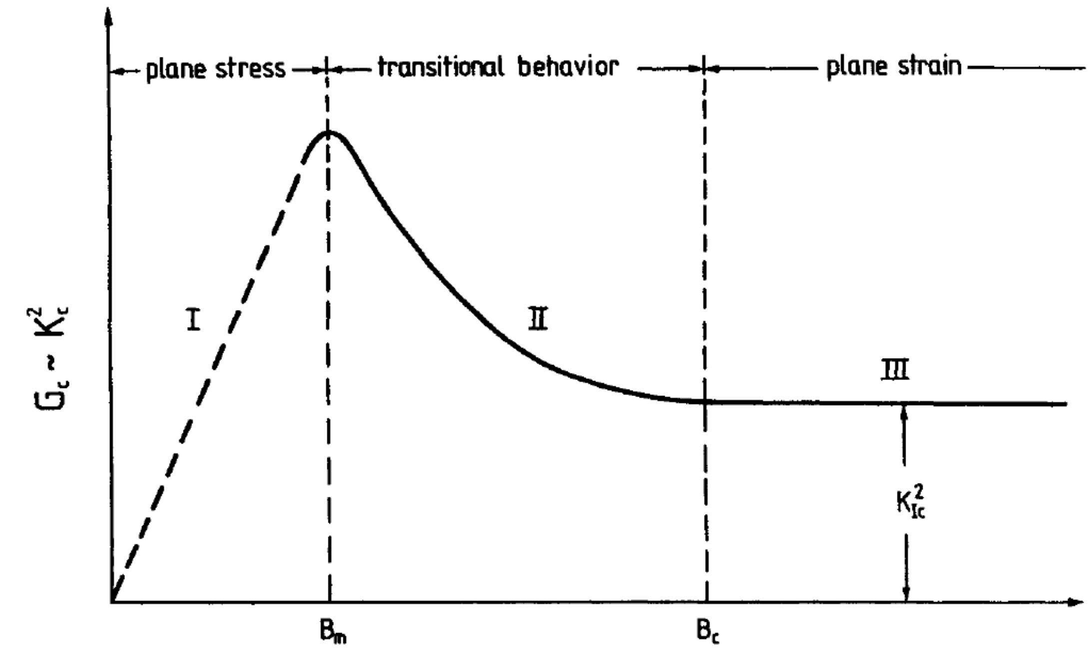

Figure 2.6: Critical fracture toughness G_c (or K^2_c) versus plate thickness B.

With the correct fracture toughness symbol in place, one of the simplest formulas of fracture mechanics can be written as

$$K_{Ic} = \sigma(\pi a)^{1/2} \tag{2.23}$$

This equation is intended for an infinite plate under uniform tensile stress where the length of a through-thickness crack is 2a, as indicated in Figure 2.7. This is essentially the Griffith crack. Although Eq. (2.23) is rather elementary and assumes no geometrical correction, it contains three important parameters reflecting the fundamental principles of a quantitative evaluation of structural integrity of mechanical and structural components in the face of a potential failure due to cracks. Here the nominal stress applied to the structural member is denoted by σ. The design parameter a is the half-length of a through-thickness crack (or a similar flaw) in a wide plate. Finally K_{Ic} represents the fracture toughness of the material for static-loading and plane-strain conditions of the maximum constraint. This is a material property that depends on ductile or brittle behavior as the case may be. It is necessary to emphasize that the K_{Ic} parameter can only be determined from tests [4]. ASTM has standardized the testing procedures and specimen geometries for measuring the plane-strain fracture toughness of metallic materials (ASTM standard E 399 [50]).

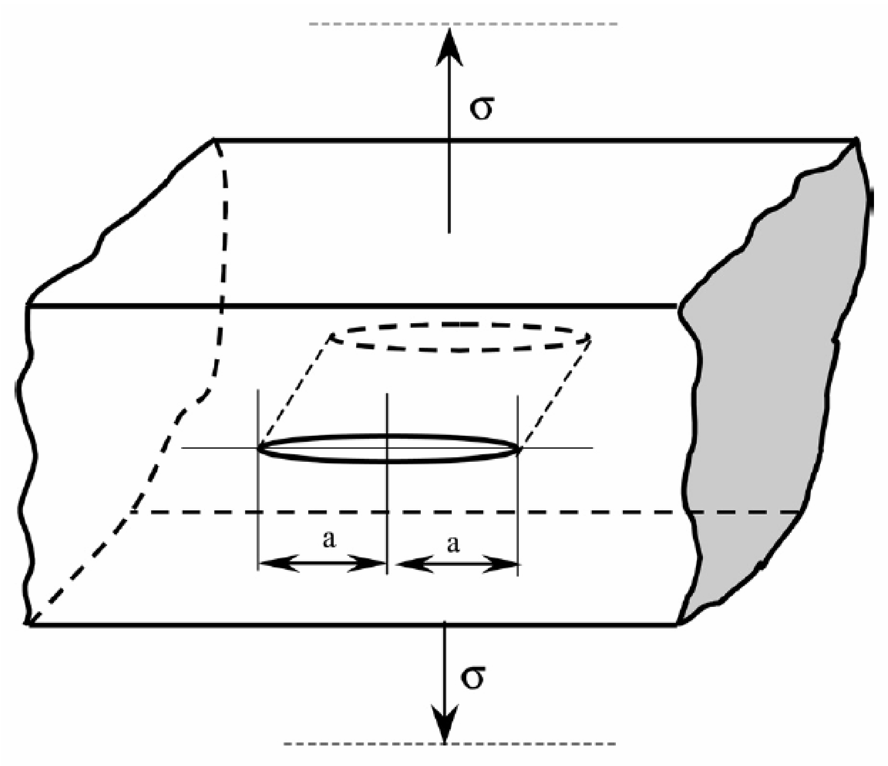

Figure 2.7: Infinitely wide plate with a typical through-thickness crack.

2.4. Methods of Solution

The development of methods, which quantify the effects of the presence of cracks on material performance, has led to the evolution of the theory of fracture mechanics. The various approaches to evaluate crack stability and its propagation path are important applications of fracture mechanics. Crack behavior analysis involves the evaluation of parameters such as the energy release rate (J) and stress intensity factors (SIFs).

In linear fracture mechanics analysis, determination of the stress intensity factor is always a major consideration and has to be evaluated. It is known that, under LEFM assumptions, the stress, strain, and displacement fields in the near crack-tip region are determined by the stress intensity factors (SIF's). The SIFs are also used in the determination of direction and velocity of crack propagation.

2.4.1. Analytical Methods

2.4.1.1. Elasticity theory

The equations of 2D elasticity can be formulated in terms of complex variable theory, thus allowing the powerful methods of analytic function theory and conformal mapping to be applied. With such methods the solutions to a great number of fracture problems have been found. Analytical solutions are useful not only to calculate stress intensity factors for physical problems that can be approximated by these idealizations, but as building blocks for more complex solutions and as examples against which to test computational methods for calculating stress intensity factors [2].

2.4.1.2 Energy and compliance methods

The energy and compliance methods are useful in the case where a test specimen or structure can be modeled using beam or plate theory. In such cases if the energy or stiffness of the structure can be determined as a function of crack length, or area, then the energy release rate and stress intensity factor can be computed.

The energy release rate (J) can be used as a crack propagation criteria, and when it exceeds a critical value the crack may propagate. Using this critical value, the fracture toughness for a crack, with any size in a given material, is determined. It is also possible to determine the maximum crack size that a material supports under a given loading state. Therefore, the critical value of the energy release rate is a measure of the material resistance to cracking.

2.4.2 Stress Intensity Handbooks and Software

Using a variety of methods, including boundary collocation, energy approaches and conformal mapping solutions for stress intensity factors for a great many practical problems have been calculated by numerous researchers over the years. In an effort spanning decades these results have been tabulated in easy to use, well organized handbooks [15]. Generally these handbooks provide equations for stress intensity factors as a function of the geometry and dimensions of the crack and of the object containing the crack. The results are given a graphs, equations and tables of coefficients. A sampling of stress intensity factor solutions for common fracture test specimens is given in Table 2.1.

Taking the use of tabulated solutions further, software packages such as NASCRAC commercial software and NASGRO commercial software integrate stress intensity factor solutions, material property databases and a graphical user interface to provide tools for the estimation of allowable loads, fatigue life and other calculations of interest in practical applications.

Table 2.1: Stress intensity solutions for several fracture test specimen geometries. E′ = E (plane stress), E′ = E/(1 − ν2) (plane strain). [15]

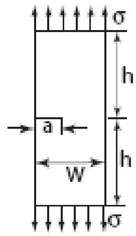	**Single Edge Notch Tension (SENT)** $h/W > 1$ $K_I = \sigma\sqrt{\pi a}F(a/W)$ $F(a/W) = 0.265(1 - a/W)^4 + \frac{.857+.265a/W}{(1-a/W)^{3/2}}$
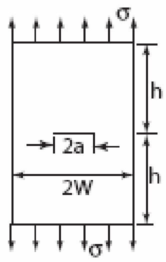	**Center Cracked Tension (CCT)** $h/W > 3$ $K_I = \sigma\sqrt{\pi a}F(a/W)$ $F(a/W) = \sqrt{\sec\frac{\pi a}{2W}}[1 - .025(a/W)^2 + .06(a/W)^4]$
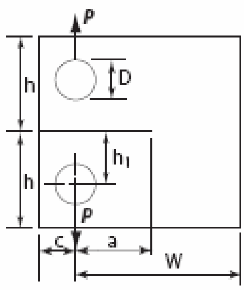	**ASTM Standard Compact Tension (CT)** $h = 0.6W$, $h_1 = 0.275W$, $D = 0.25W$, $c = 0.25W$, thickness, $B = W/2$ $K_I = \frac{P}{WB}\sqrt{a}F(a/W)$ $F(a/W) = 29.6 - 185.5(a/W) + 655.7(a/W)^2 - 1017.(a/W)^3 + 638.9(a/W)^4$
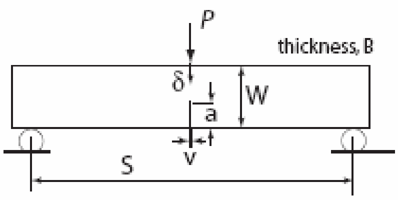	**Three Point Bend (Single Edge Notch Bend, SENB),** $S/W = 4$ $K_I = \frac{PS}{BW^{3/2}}F(a/W)$ $F(a/W) = \frac{3(a/W)^{1/2}[1.99-(a/W)(1-a/W)(2.15-3.93a/W+2.7(a/W)^2)]}{2(1+2a/W)(1-a/W)^{3/2}}$ Load-line disp, $\delta = \frac{P}{E'B}\left(\frac{S}{W-a}\right)^2[1.193 - 1.98a/W + 4.478(a/W)^2 - 4.443(a/W)^3 + 1.739(a/W)^4]$ CMOD, $v = \frac{4\sigma a}{E'}[0.76 - 2.28a/W + 3.87(a/W)^2 - 2.04(a/W)^3 + 0.66/(1-a/W)^2]$, $\sigma = \frac{6PS}{4BW^2}$

2.4.3 Boundary collocation method

Boundary collocation is a method for the computation of stress intensity factors based on the eigenfunction expansion of the crack tip stress fields. The general idea is that given traction boundary conditions for a certain problem, express the tractions at a finite number of locations, called collocation points, in terms of the eigenfunction expansion with unknown coefficients. For each collocation point you will have one equation for the unknown coefficients. As long as you use at least as many collocation points as unknowns in the expansion, you can then solve the resulting system of equations for the eigenfunction coefficients. The value of the coefficient corresponding to the $r^{-1/2}$ stress singularity is the stress intensity factor [1].

2.4.4 Experimental Methods

In some cases it may not be practical to determine stress intensity factors from analytical or computational methods. For example, perhaps the loading is not known, or is dynamic, or information about parts of the structure that would be needed for a FEM analysis are missing. In such cases one may wish to determine the stress intensity factor experimentally, based on local measurements of stress, strain and displacement.

2.4.5 Computational Methods

Despite the wide range of problems which have been solved and tabulated in the handbooks, many problems in fracture mechanics involve complex geometries that cannot be well approximated by the handbook solutions. The use of computational methods such as the finite element method, boundary element method and dislocation based methods is invaluable for studying fracture in real-world problems.

Among these computational methods, finite element method is the most popular one due to its wide ranging use in engineering design and due to its very flexible and extendable nature in order to apply to nonlinear and dynamic problems and also in practice to calculate the stress intensity factor.

In the so-called indirect method the stress intensity factor is obtained through extrapolation of curve fitting to the values of a stress or a displacement component calculated at certain interior locations. In the direct method, special crack-tip elements are used and the stress intensity factors are directly calculated. The special elements developed for this purpose seem to be quite numerous among which one may mention the circular core element, the enriched element, the singular triangle, the quarter-point element, and specialized hybrid elements [19]. In all these techniques the basic idea is to design the elements adjacent to the crack tip in such a way that the displacements are forced to vary according to the asymptotic distributions given by Equation 2.16. The properly calculated local amplitudes would then give K_1 and K_2. This method will be investigated in detail in the following chapters.

$$u \cong \frac{K_I}{8\mu}\sqrt{2r}\left[(2\kappa-1)\cos\frac{\theta}{2}-\cos\frac{3\theta}{2}\right] \quad (2.24a)$$

$$v \cong \frac{K_I}{8\mu}\sqrt{2r}\left[(2\kappa+1)\sin\frac{\theta}{2}-\sin\frac{3\theta}{2}\right] \quad (2.24b)$$

Fundamental to the use of the finite element method for LEFM is the extraction of accurate SIF's from the finite element results. A large number of different techniques for extracting SIF's have been presented in the literature [5, 6, 8].

Techniques for extracting SIF's fall into one of two categories: direct approaches, which correlate the SIF's with FEM results directly, and "energy" approaches, which first compute energy release rates [19].

2.4.5.1 Stress correlation

Stress intensity factors are defined as [23]

$$\begin{pmatrix} K_I \\ K_{II} \\ K_{III} \end{pmatrix} = \lim_{r\to 0}\sqrt{2\pi r}\begin{pmatrix} \sigma_{22}(r,0) \\ \sigma_{12}(r,0) \\ \sigma_{32}(r,0) \end{pmatrix} \quad (2.25)$$

If the stress along θ = 0 can be calculated, then the stress intensity factor can be determined by extrapolation back to r = 0 [20]. For example, in Mode-I, use the FEM method to compute the stresses at points ahead of the crack tip, then plot $K_I = \lim_{r\to 0}\sigma_{22}(r,0)\sqrt{2\pi r}$ vs. r. Extrapolate this curve back to r = 0 to determine K_I. Advantages of this method are that it is quite simple, it can be used with any finite element program, no special postprocessing is needed, only one analysis is needed, different modes of stress intensity factors are easily computed and stress intensity factors can be computed along a 3D crack front by taking stresses on lines normal to the crack front at different positions. The accuracy of the method will depend on mesh refinement and the ability of the mesh to capture the crack tip stress singularity. The method is easily generalized to use the stresses on any angle θ, which may be desirable since, depending on the mesh used, the integration points may not lie on θ = 0.

2.4.5.2 Displacement correlation technique

This technique correlates the nodal displacements from a finite element analysis, at specific locations, with the analytic solutions to obtain the stress intensity factors and will be investigated under analytical study section 3.2 in further detail due to its importance.

2.4.5.3 Global energy and compliance

For cracks that grows straight ahead,

$$J = \frac{K_I^2}{E'} + \frac{K_{II}^2}{E'} + \frac{K_{III}^2}{2\mu} \tag{2.26}$$

Thus if the problem involves only a single mode of loading, then the stress intensity factor can be extracted by finding the energy release rate.

2.4.5.4 Crack closure integrals

The crack closure integral, for 2D cracks that grow straight ahead, can be rewritten in terms of energy release rates for Mode I, related to a stress intensity factor, For the crack with length a grows to a new length a +Δa,

Crack Closure Integral: $G = \lim_{\Delta a \to 0} \frac{1}{\Delta a} \int_0^{\Delta a} \sigma_{i2}(x_1, 0) u_i (\Delta a - x_1, \pi) dx_1$ (2.27)

for Mode I: $G = G_I$

$$G_I = \frac{K_I^2}{E'}$$

$$G_I = \lim_{\Delta a \to 0} \frac{1}{\Delta a} \int_0^{\Delta a} \sigma_{22}(x_1, 0) u_2 (\Delta a - x_1, \pi) dx_1 \tag{2.28}$$

The crack closure integral can be approximated in a finite element computation and used to extract individual stress intensity factors [4].

2.4.5.5 Domain integral

Perhaps the most accurate and elegant method for computing the energy release rate is to calculate the J integral by converting the line integral into a domain integral which can easily be calculated using the known finite element shape functions.

The J integral for a 2D body is:

$$J = \int_{\Gamma} \left(U_d dx_2 - T \frac{\partial u}{\partial x_1} ds \right) = \int_{\Gamma} U_d n_1 - \sigma_{ij} \frac{\partial u_i}{\partial x_1} n_j ds \tag{2.29}$$

Consider the close path

$$\Gamma_n = \Gamma_0 + \Gamma_s^+ + \Gamma_s^- - \Gamma \tag{2.30}$$

Introduce a weight function $q(x_1,x_2)$ that is equal to unity on Γ and zero on Γ_0 and Γ_s.

The J integral along the new path is:

$$J = -\oint_{\Gamma_n} \left(U_d \delta_{1j} - \sigma_{ij} \frac{\partial u_i}{\partial x_1} \right) q n_j ds \tag{2.31}$$

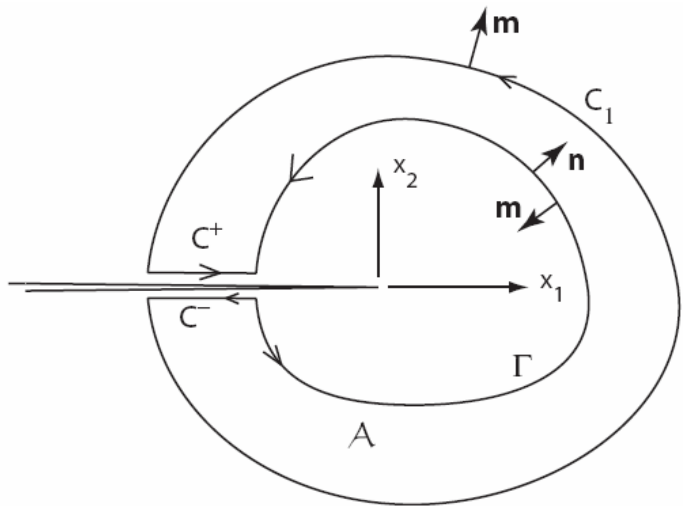

Figure 2.8: Contours for derivation of domain integral calculation of J.

Apply the divergence theorem to transform the integral along the close contour into a domain integral:

$$J = -\int_A \left(U_d \frac{\partial q}{\partial x_1} - \sigma_{ij} \frac{\partial u_i}{\partial x_1} \frac{\partial q}{\partial x_j} \right) dA - \int_A \left(\frac{\partial U_d}{\partial x_1} - \frac{\partial}{\partial x_j} \left(\sigma_{ij} \frac{\partial u_i}{\partial x_1} \right) \right) q dA \tag{2.32}$$

where the second term vanishes for elastic problems. Thus J may be calculated as an area integral over any annular region surrounding the crack tip. The domain integral approach is generally very accurate even with modest mesh refinement since it does not rely on capturing the exact crack tip singular stress field, rather on correctly computing the strain energy in the region surrounding the crack tip [2].

3. ANALYTICAL STUDY

3.1 Crack Tip Singular Elements

The finite element method has been employed extensively in fracture mechanics to model the stress singularity at the crack tip. The application of the finite element method to fracture mechanics for calculating stress intensity factors which measure the amplitude of the crack tip singularity requires special care.

All of the methods for computing stress intensity factors rely on the accurate calculation of the stress, displacement and energy fields. Since all of the methods use information from a small distance away from the crack tip they are somewhat forgiving of errors induced by not capturing the exact crack tip singular stress field. However, more accurate results could be obtained by capturing the crack tip singular stress field. Since we know that in elastic materials the crack tip stresses are singular as $1/\sqrt{r}$ this singularity can be built into the finite element calculation from the start. A number of methods to produce singular crack tip stresses have been developed, some of which require special elements and some of which can be used with standard elements. Some cause displacement incompatibility between the singular and regular elements.

The early finite element calculations for stress intensity factors, involving the use of relatively small standard elements in the vicinity of the crack tip, have been found to be unreliable and are not recommended [21]. In the past, several papers have appeared in the literature which report on the application of singular point elements to fracture mechanics. Amongst those, the quarter point element conceived by Barsoum [22] has found considerable popularity because of its simplicity and ease of implementation. Thus we will focus on quarter-point elements that can be implemented using standard elements.

In linear elastic fracture mechanics analysis, determination of the stress intensity factor at the crack tip is often a major consideration and has to be evaluated as accurately as possible. In order to insure convergence to the correct solution it is necessary that the elements which surround the crack tip are capable of representing the corresponding singularity. In the finite element method the displacement field and the coordinates are interpolated using shape functions [23]. Let x = x_1, y = x_2, u = u_1, v = u_2. Consider the 2D, 8 node isoparametric element shown in Figure 3.1. The parent element in the (ξ, η) space is mapped to an element in the physical space (x, y) using the shape functions, $N_i(\xi, \eta)$ and nodal coordinates (x_i, y_i),

$$x(\xi,\eta) = \sum_{i=1}^{8} N_i(\xi,\eta)x_i \tag{3.1a}$$

$$y(\xi,\eta) = \sum_{i=1}^{8} N_i(\xi,\eta)y_i \tag{3.1b}$$

The displacements are interpolated in the same way, i.e.

$$u(\xi,\eta) = \sum_{i=1}^{8} N_i(\xi,\eta)u_i \tag{3.2a}$$

$$v(\xi,\eta) = \sum_{i=1}^{8} N_i(\xi,\eta)v_i \tag{3.2b}$$

The shape functions have the property that N_i = 1 at node i and N_i = 0 at all other nodes. The shape functions for the 8 node element are

$$N_1 = \frac{-(\xi-1)(\eta-1)(1+\eta+\xi)}{4} \tag{3.3a}$$

$$N_2 = \frac{(\xi+1)(\eta-1)(1+\eta-\xi)}{4} \tag{3.3b}$$

$$N_3 = \frac{(\xi+1)(\eta+1)(-1+\eta+\xi)}{4} \tag{3.3c}$$

$$N_4 = \frac{-(\xi-1)(\eta+1)(-1+\eta-\xi)}{4} \tag{3.3d}$$

$$N_5 = \frac{(1-\xi^2)(1-\eta)}{2} \tag{3.3e}$$

$$N_6 = \frac{(1+\xi)(1-\eta^2)}{2} \tag{3.3f}$$

$$N_7 = \frac{(1-\xi^2)(1+\eta)}{2} \tag{3.3g}$$

$$N_8 = \frac{(1-\xi)(1-\eta^2)}{2} \tag{3.3h}$$

Let us calculate the strain along the bottom of the 8 node element, i.e. along $\eta = -1$. The relevant shape functions on $\eta = -1$ are

$$N_1 = -\frac{1}{2}\xi(1-\xi) \tag{3.4a}$$

$$N_2 = \frac{1}{2}\xi(1+\xi) \tag{3.4b}$$

$$N_5 = (1-\xi^2) \tag{3.4c}$$

These functions are plotted in Figure 3.2 [23].

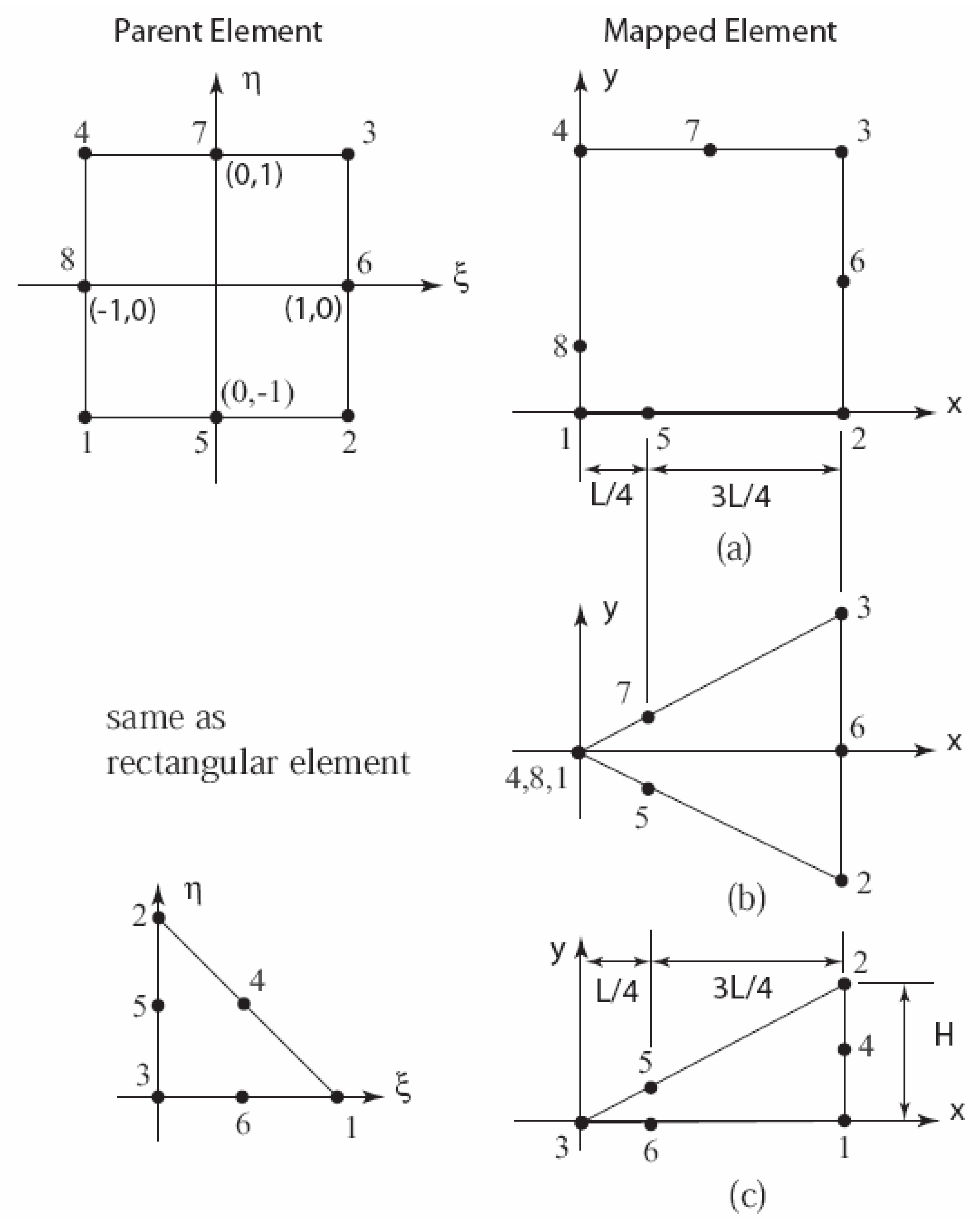

Figure 3.1: Parent elements in (ξ, η) plane and mapped quarter-point elements. (a) 8 node rectangular element, (b) Triangular element formed by collapsing nodes 4,8,1 to a single point. With the collapsed node element the element edges must be straight in order to obtain accurate solutions (c) Natural triangular element. (Recommended element for linear problems.)

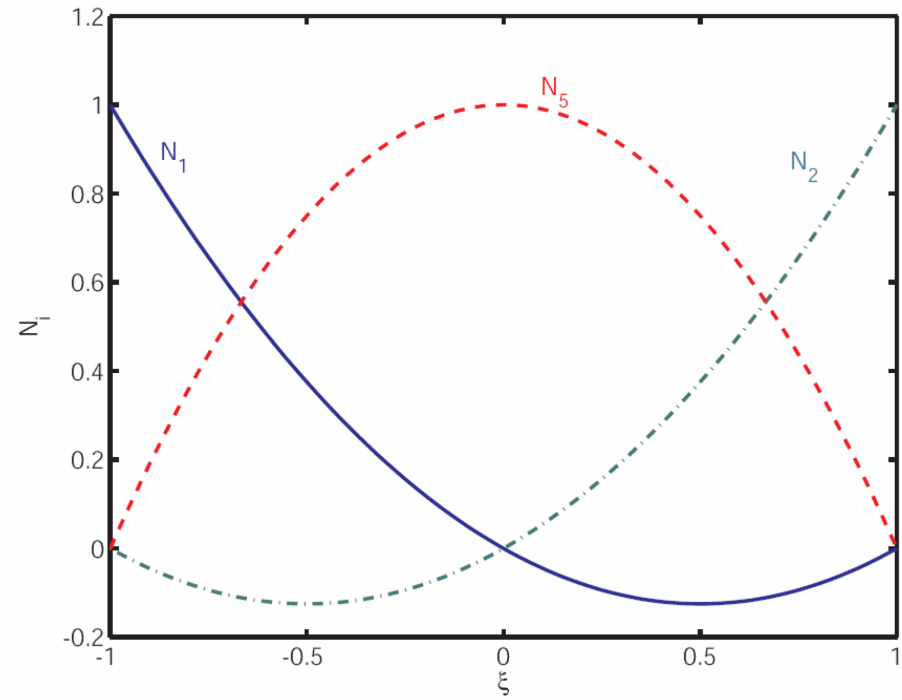

Figure 3.2: Shape functions for the 8 node element along η = −1.

The normal strain γ_{xx} is

$$\gamma_{xx} = \frac{\partial u}{\partial x} = \sum_{i=1,2,5} \frac{\partial N_i}{\partial \xi}\frac{\partial \xi}{\partial x} u_i \tag{3.5}$$

where $\partial N_1 / \partial \xi = \xi - 1/2, \partial N_2 / \partial \xi = \xi + 1/2$ and $\partial N_5 / \partial \xi = -2\xi$

Consider first the case in which the node 5 (mid-side node) is located at the center of the element, so that $x_1 = 0$, $x_2 = L$, $x_5 = L/2$. Applying equations (3.1) and (3.4),

$$x(\xi) = \frac{\xi(1+\xi)}{2}L + (1-\xi^2)\frac{L}{2}$$

$$= \frac{L}{2} + \frac{\xi L}{2}$$

Thus $\xi = (2x - L)/L$ and $\partial \xi / \partial x = 2/L$. Since none of the $\partial N_i/\partial \xi$ are singular, and since $\partial \xi/\partial x$ is non-singular, Equation (3.5) results in a non-singular strain. Now let us move the position of node 5 to the quarter-point, i.e. let $x_5 = L/4$, keeping $x_1 = 0$ and $x_2 = L$. Now

$$x(\xi) = \frac{\xi(1+\xi)}{2}L + (1-\xi^2)\frac{L}{4}$$

$$= \frac{L}{4}\left(\xi^2 + 2\xi + 1\right)$$

Solve for ξ and differentiate,

$$\xi(x) = -1 + 2\sqrt{\frac{x}{L}}$$

$$\frac{\partial \xi}{\partial x} = \frac{1}{\sqrt{xL}}$$

Let $u_1 = 0$ then from equation (3.5), γ_{xx} along $\eta = 1$ is

$$\gamma_{xx} = \frac{1}{\sqrt{xL}}\left[-2\xi u_5 + \left(\frac{1}{2} + \xi\right)u_2\right]$$

$$\gamma_{xx} = \frac{1}{\sqrt{xL}}\left[\frac{u_2}{2} + \left(u_2 - 2u_5\right)\xi\right]$$

Substituting $\xi = -1 + 2\sqrt{x/L}$ and simplifying.

$$\gamma_{xx} = \frac{4}{L}\left(\frac{u_2}{2} - u_5\right) + \frac{1}{\sqrt{xL}}\left(2u_5 - \frac{u_2}{2}\right) \tag{3.6}$$

Thus simply moving the mid-side nodes to the quarter points results in the desired $1/\sqrt{r}$ singularity. Other elements can also be used. The triangular element formed by collapsing the $\xi = -1$ side nodes to one point and moving the mid-side nodes to x = L/4 as shown in Figure 3.1(b)Figure 3.2 also has $1/\sqrt{r}$ singularity.

The rectangular element has the drawback that it does not allow the crack to be surrounded by singular elements and hence to accurately capture the θ variation of stress, which might be needed for crack direction calculations. In addition, except along the element edges, the $1/\sqrt{r}$ singularity exists only in a small region near the crack tip. The collapsed element has the drawback that the meshing will be somewhat more difficult to implement and that unless the element edges are straight, as shown in Figure 3.1(b), the $1/\sqrt{r}$ does not exist on straight lines coming from the crack tip and the accuracy in computing K will be degraded [24].

A better choice might be the natural triangle quarter point element shown in Figure 3.1(c) [24]. Not only can the crack tip be easily surrounded by elements, the meshing is simple and the element gives the $1/\sqrt{r}$ on all lines coming from the crack tip. The shape functions for the 6 node triangular element are

$$N_1 = (2\xi - 1)\xi$$

$$N_2 = (2\eta - 1)\eta$$

$$N_3 = (2(1 - \xi - \eta) - 1)(1 - \xi - \eta)$$

$$N_4 = 4\xi\eta$$

$$N_5 = 4\eta(1 - \xi - \eta)$$

$$N_6 = 4\xi(1 - \xi - \eta)$$

Consider the edge along the x axis, $\eta = 0$ in the parent element. With $x_6 = L/4$ and $x_1 = L$,

$$x = x_1 N_1 + x_6 N_6$$

$$= L(2\xi - 1)\xi + \frac{L}{4} 4\xi(1 - \xi)$$

$$= L\xi^2$$

Thus $\xi = \sqrt{\frac{x}{L}}$

The u displacement along this line is

$$u = u_1 N_1(\xi,0) + u_6 N_6(\xi,0) + u_3 N_3(\xi,0)$$

$$u = u_1(2\xi - 1)\xi + u_3(2(1 - \xi) - 1)(1 - \xi) + u_6 4\xi(1 - \xi)$$

Substituting $\xi = \sqrt{\frac{x}{L}}$ and simplifying

$$u = u_3 + \sqrt{\frac{x}{L}}\left[4u_6 - 3u_3 - u_1\right] + \frac{x}{L}\left[2u_1 + 2u_3 - 4u_6\right] \tag{3.7}$$

$$\gamma_{xx} = \frac{\partial u}{\partial x} = \frac{1}{\sqrt{xL}}\left[-\frac{u_1}{2} - \frac{3u_3}{2} + 2u_6\right] + \frac{1}{L}\left[2u_1 + 2u_3 - 4u_6\right] \tag{3.8}$$

Thus the natural triangle quarter-point element has constant and $1/\sqrt{r}$ strain terms, reproducing the first two terms of the Williams crack tip solution. Note that the full strain field can be shown to have $1/\sqrt{r}$ singularity, see [24].

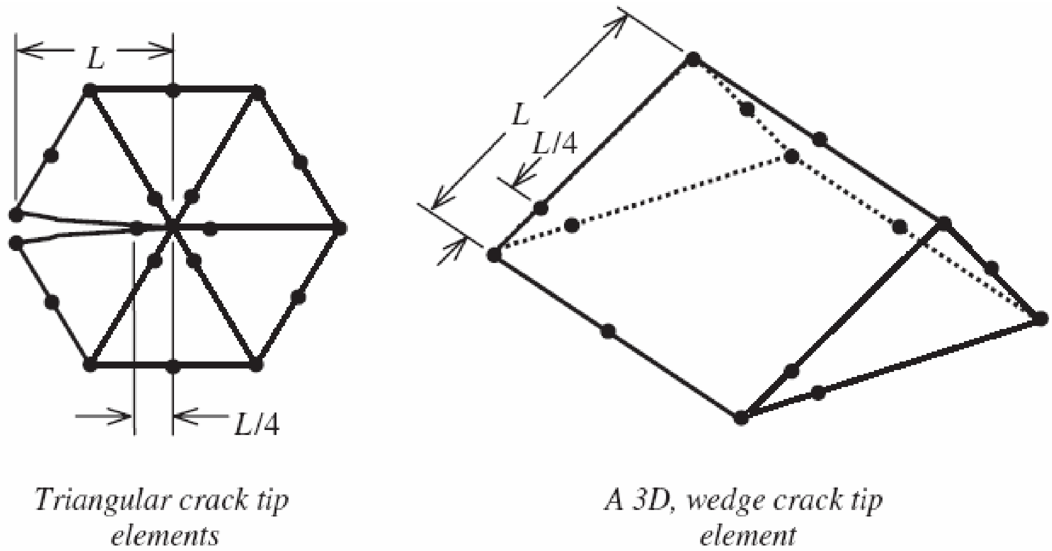

Figure 3.3: Examples of crack tip elements

With any of these elements accuracy per unit computational time should be significantly better than with the use of non singular elements [23]. For example, Banks-Sills and Sherman [25] compared displacement extrapolation, J integral and total energy approaches using singular and non-singular elements. For a central cracked plate under tension using 100 8-node elements displacement extrapolation had an error in stress intensity factor of 5.4% using regular elements and 1.8% using quarter point elements. For the same problem, using the total energy method with a mesh of 121 8-node elements the error was 2.4% using regular elements and 0.37% using quarter point elements.

3.2 Displacement Correlation Technique

This technique is one of the simplest and historically one of the first techniques used to extract SIF's from FEM results [20]. It is a direct approach. Displacement Correlation technique correlates the nodal displacements for one point in the mesh from a finite element analysis, with the analytic solutions to obtain the stress intensity factors.

For Mode I, the analytical expression for the crack opening displacement δ(r) at a distance r from the crack tip along the crack face is of the form

$$\delta(r) = K_I\left(\frac{\kappa+1}{\mu}\right)\sqrt{\frac{r}{2\pi}} \tag{3.9}$$

where μ is the shear modulus, κ = 3-4ν for plane strain and κ = 3-ν/1+ν for plane stress, and ν is the Poisson’s ratio. The crack opening can be also described by a displacement expansion where the higher order terms are neglected [19]. This expression is given by

$$\delta(r) = \left(4(u_b - u_d) - (u_c - u_e)\right)\sqrt{\frac{r}{L}} \tag{3.10}$$

where u are the relative displacements normal to crack face at nodes, and L is the element size (Figure 3.4). From equations (3.9) and (3.10)

$$K_I = \left(\frac{\mu}{\kappa+1}\right)\sqrt{\frac{2\pi}{L}}\left(4(u_b - u_d) - (u_c - u_e)\right) \tag{3.11}$$

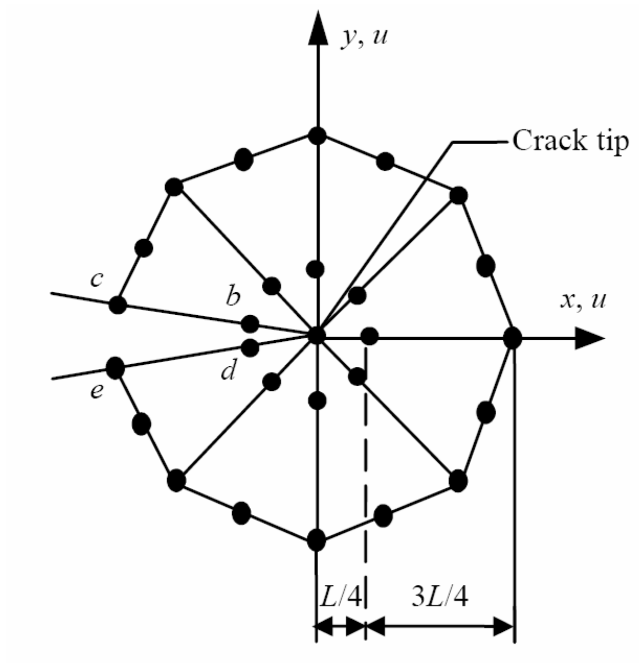

Figure 3.4: Quarter-point elements at the crack tip

3.3. Quarter-Point Displacement Technique

The quarter-point displacement method uses the out-of-plane displacement value at the quarter-point behind the crack tip, as shown in Figure 3.4, to extract the SIF through the following relationship

$$K_I = \left(\frac{2\mu}{\kappa+1}\right)\sqrt{\frac{2\pi}{L}}\left(u_b - u_d\right) \tag{3.12}$$

where μ is the shear modulus, κ = 3 -4ν for plane strain and κ = 3-ν/1+ν for plane stress, ν is the Poisson's ratio, L is the quarter-point element length along crack face, u_b, u_d is the local displacement normal to crack face as depicted in Figure 3.4. This equation can be derived from the well-known displacement solution adjacent to the crack tip for Mode I crack, i.e.

$$u_z = \frac{2(1+\upsilon)K}{E}\sqrt{\frac{r}{2\pi}}\sin\frac{\theta}{2}\left(2 - 2\upsilon - \cos^2\frac{\theta}{2}\right) \tag{3.13}$$

An important point to emphasize is that the only difference between the two techniques is that the The Quarter Point Displacement Technique (QPDT) estimates the stress intensity factor (SIF) from the displacements of one nodal pair while the

Displacement Correlation Technique (DCT) utilizes the relative displacements between two nodal pairs [19].

Modelling the singularity at the crack tip is an essential part in predicting crack propagation using fracture mechanics, but being able to model the singularity is not sufficient, since stress intensity factor is the most important parameter in fracture mechanics to check if the crack propagates, the proper method should be available for this task to be done [10].

Of these techniques, the DCT is more widely employed, although the QPDT is marginally simpler to implement. Presumably this has been motivated by Shih et al. [26], who independently suggested that the DCT is more rational in formulation than the QPDT. In addition, limited numerical analyses presented by the former appeared to favour the DCT. However recent studies by Yehia and Shephard [41] on a much wider range of problems indicated that both techniques tend to converge to the same value as the quarter-point element size is refined. Hence displacement correlation technique is employed to calculate fracture parameters throughout the study.

3.4 Calculation of Stress Intensity Factors by Finite Element Method

The analysis uses a fit of the nodal displacements in the vicinity of the crack. The actual displacements at and near a crack for linear elastic materials are [27]:

$$u = \frac{K_I}{4G}\sqrt{\frac{r}{2\pi}}\left((2\kappa-1)\cos\frac{\theta}{2}-\cos\frac{3\theta}{2}\right)-\frac{K_{II}}{4G}\sqrt{\frac{r}{2\pi}}\left((2\kappa+3)\sin\frac{\theta}{2}+\sin\frac{3\theta}{2}\right)+O(r)$$

$$v = \frac{K_I}{4G}\sqrt{\frac{r}{2\pi}}\left((2\kappa-1)\sin\frac{\theta}{2}-\sin\frac{3\theta}{2}\right)-\frac{K_{II}}{4G}\sqrt{\frac{r}{2\pi}}\left((2\kappa+3)\cos\frac{\theta}{2}+\cos\frac{3\theta}{2}\right)+O(r)$$

$$w = \frac{2K_{III}}{G}\sqrt{\frac{r}{2\pi}}\sin\frac{\theta}{2}+O(r) \qquad (3.14)$$

where

u, v, w= Displacements in a local Cartesian coordinate system as shown in Figure 3.5

r, θ = coordinates in a local cylindirical coordinate system as shown in Figure 3.5

G = Shear modulus

K_I, K_{II}, K_{III} = Stress intensity factors relating to deformation shapes shown in Figure 2.2.

$\kappa = 3 - 4\nu$ if plane strain or axisymmetric

$\kappa = \dfrac{3-\upsilon}{1+\upsilon}$ if plane stress

ν = Poisson's ratio

O(r) = Terms of order r or higher

Evaluating Equation 3.14 at $\theta = \pm\ 180.0°$ and dropping the higher order terms yields:

$$u = +\frac{K_{II}}{2G}\sqrt{\frac{r}{2\pi}}(1+\kappa) \tag{3.15a}$$

$$v = +\frac{K_{I}}{2G}\sqrt{\frac{r}{2\pi}}(1+\kappa) \tag{3.15b}$$

$$w = +\frac{2K_{III}}{G}\sqrt{\frac{r}{2\pi}} \tag{3.15c}$$

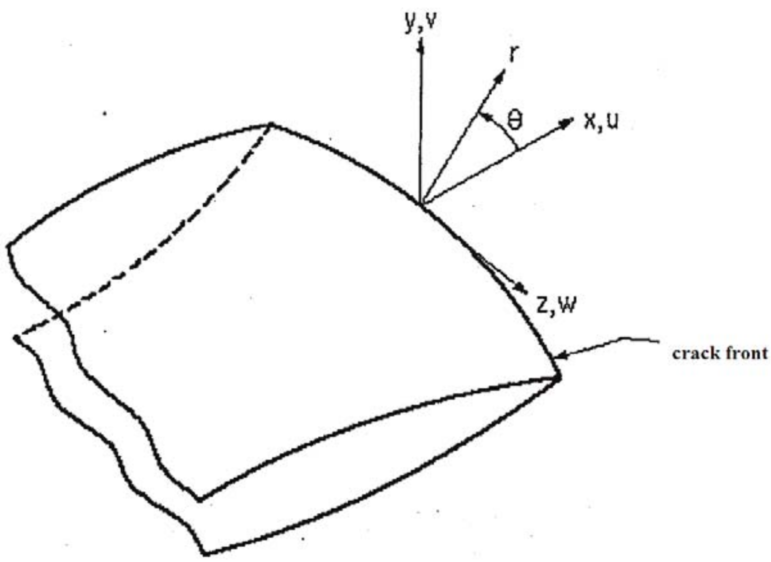

Figure 3.5: Local coordinates measured from a 3-D crack front

For models symmetric about the crack plane (half-crack model), Equation 3.15 can be reorganized to give:

$$K_I = \sqrt{2\pi}\frac{2G}{1+\kappa}\frac{|v|}{\sqrt{r}} \tag{3.16a}$$

$$K_{II} = \sqrt{2\pi}\frac{2G}{1+\kappa}\frac{|u|}{\sqrt{r}} \tag{3.16b}$$

$$K_{III} = \sqrt{2\pi}\,2G\frac{|w|}{\sqrt{r}} \tag{3.16c}$$

The final factor $\frac{|v|}{\sqrt{r}}$ needs to be evaluated based on the nodal displacements and locations. As shown in Figure 3.6, three points are available. v is normalized so that v at node I is zero. Then A and B are determined so that

$$\frac{|v|}{\sqrt{r}} = A + Br \tag{3.17}$$

at points J and K. Next, let r approach 0:

$$\lim_{r \to 0} \frac{|v|}{\sqrt{r}} = A \tag{3.18}$$

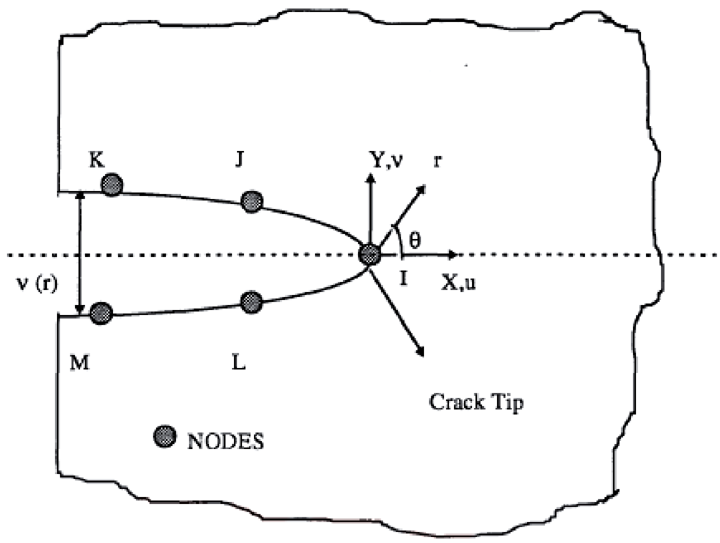

Figure 3.6: Nodes Used for the Approximate Crack-Tip Displacements

Thus Equation 3.16. becomes,

$$K_I = \sqrt{2\pi} \frac{2GA}{1+\kappa} \tag{3.19}$$

4. FINITE ELEMENT SOLUTION BY ANSYS

4.1 General Remarks about Finite Element Method

The Finite Element Method (F.E.M.) is a procedure for obtaining approximate solutions to continuum problems [28]. It involves conceptually dividing the body under consideration into elements and assuming an approximate form for the solution within each element. The Finite Element Method is a good choice for solving partial differential equations over complex domains when the domain changes, when the desired precision varies over the entire domain, or when the solution lacks smoothness.

The FEM is one of the most important developments in computational methods to occur in the 20th century. In just a few decades, the method has evolved from one with applications in structural engineering to a widely utilized and richly varied computational approach for many scientific and technological areas.

There are many practical engineering problems for which we cannot obtain exact solutions. This inability to obtain an exact solution may be attributed to either the complex nature of governing differential equations or the difficulties that arise from dealing with the boundary and initial conditions. To deal with such problems, we resort to numerical approximations. In contrast to analytical solutions, which show the exact behavior of a system at any point within the system, numerical solutions approximate exact solutions at discrete points, called nodes. The first step of any numerical procedure is discretization. This process divides the medium of interest into a number of small subregions and nodes. There are two common classes of numerical methods: (1) finite difference methods and (2) finite element methods. With finite difference methods, the differential equation is written for each node, and the derivatives are replaced by difference equations. This approach results in a set of simultaneous linear equations. Although finite difference methods are easy to understand and employ simple problems, they become difficult to apply to problems with complex geometries or complex boundary conditions. This situation is also true for problems with nonisotropic material properties.

In contrast, the finite element method uses integral formulations rather than difference equations to create a system of algebraic equations. Moreover, an approximate continuous function is assumed to represent the solution for each element. The complete solution is then generated by connecting or assembling the individual solutions, allowing for continuity at the interelemental boundaries.

Usually the problem addressed is too complicated to be solved satisfactorily by classical analytical methods. The problem may concern stress analysis, heat conduction, or any of several other areas. The finite element procedure produces many simultaneous algebraic equations, which are generated and solved on a digital computer.

Finite element calculations are performed on personal computers, mainframes, and all sizes between. Results are rarely exact. However, errors are decreased by processing more equations, and results accurate enough for engineering purposes are obtainable at reasonable cost.

The finite element method originated as a method of stress analysis. It is used to analyze both linear and nonlinear systems. Nonlinear analysis includes material yielding, creep or cracking; aeroelastic response; buckling and postbuckling response; contact and friction; etc. The finite element method is used for both static and dynamic analyses. In its most general form, the method is not restricted to structural (or mechanical) systems. Today finite elements are also used to analyze problems of heat transfer, fluid flow, lubrication, electric and magnetic fields, and many others.

In the foregoing example, and in general, the finite element method models a structure as an assemblage of small parts (elements). Each element is of simple geometry and therefore is much easier to analyze than the actual structure. In essence, a complicated solution by a model that consists of piecewise-continuous simple solutions is approximated. Elements are called "finite" to distinguish them from differential elements in calculus.

An important ingredient in a finite element analysis is the behavior of the individual elements. A few good elements may produce better results than many poorer elements.

The "finite element method" is a method of piecewise approximation in which the approximating function φ is formed by connecting simple functions, each defined over a small region (element). And a "finite element" is a region in space in which a function φ is interpolated from nodal values of φ on the boundary of the region in such a way that interelement continuity of φ tends to be maintained in the assemblage [28].

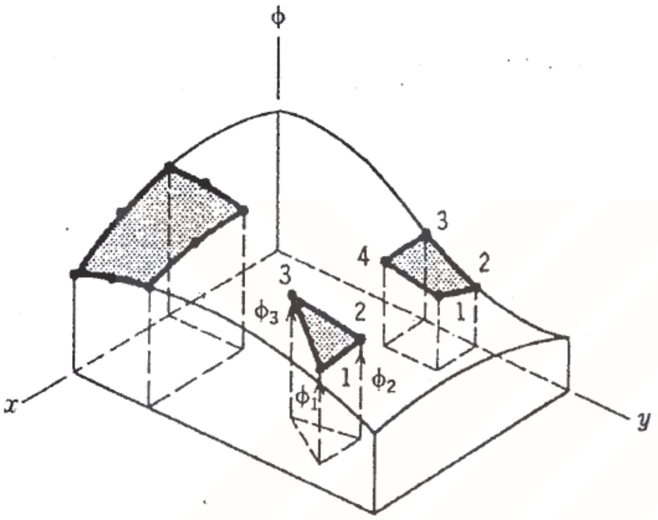

Figure 4.1: A function of φ=φ(x,y) that varies smoothly over a rectangular region in the xy plane, and typical elements that might be used to approximate it.

Let's consider function φ, which might represent any of several physical quantities, varies smoothly in the actual structure as seen in Figure 4.1. A finite element model typically yields a piecewise-smooth representation of φ . Between elements there may be jumps in the x and y derivatives of φ. Within each element φ is a smooth function that is usually represented by a simple polynomial. For the triangular element, the linear polynomial

$$\varphi = a_1 + a_2 x + a_3 y \tag{4.1}$$

is appropriate, where the a, are constants. These constants can be expressed in terms of φ_1, φ_2 and φ_3, which are the values of φ at the three nodes. Triangles model the actual φ by a surface of flat triangular facets. For the four-node quadrilateral, the "bilinear" function

$$\varphi = a_1 + a_2 x + a_3 y + a_4 xy \qquad (4.2)$$

is appropriate. The eight node quadrilateral in Figure 4.1 has eight a, in its polynomial expansion and can represent a parabolic surface.

Equations 4.1 and 4.2 are interpolations of function in terms of the position (x,y) within an element. That is, when the a, have been determined in terms of nodal values φ_i, Equations 4.1 and 4.2 define φ within an element in terms of the φi, and the coordinates. Clearly, if the mesh of elements is not too coarse and if the φ_i happened to be exact, then φ away from nodes would be a good approximation. Nodal values φ_i, are close to exact if the mesh is not too coarse and if the element properties are properly formulated.

The problem that which element type should be used is unfortunately not simple. An element that is good in one problem area may be poor in another. Even in a specific problem area an element may behave well or badly, depending on the particular geometry, loading and boundary conditions.

A finite element analysis typically involves the following steps. Steps 1, 4, and 5 require decisions by the analyst and provide input data for the computer program. Steps 2, 3, 6 and 7 are carried out automatically by the computer program.

1. Divide the structure or continuum into finite elements. Mesh generation programs, called preprocessors, help the user in doing this work.

2. Formulate the properties of each element. In stress analysis, this means determining nodal loads associated with all element deformation states that are allowed

3. Assemble elements to obtain the finite element model of the structure.

4. Apply the known loads: nodal forces and/or moments in stress analysis.

5. In stress analysis, specify how the structure is supported. This step involves setting several nodal displacements to known values (which often are zero).

6. Solve simultaneous linear algebraic equations to determine nodal degrees of freedom (nodal displacements in stress analysis).

7. In stress analysis, calculate element strains from the nodal degrees of freedom and the element displacement field interpolation, and finally calculate stresses from strains. Output interpretation programs, called postprocessors, help the user sort the output and display it in graphical form.

The power of the finite element method resides principally in its versatility. The method can be applied to various physical problems. The body analyzed can have arbitrary shape, loads, and support conditions. The mesh can mix elements of different types, shapes, and physical properties. This great versatility is contained within a single computer program. User-prepared input data controls the selection of problem type, geometry, boundary conditions, element selection, and so on.

Another attractive feature of finite elements is the close physical resemblance between the actual structure and its finite element model. The model is not simply an abstraction. This seems especially true in structural mechanics, and may account for the finite element method having its origin there. The piecewise approximation of the physical field (continuum) on finite elements provides good precision even with simple approximating functions. Simply increasing the number of elements can achieve increasing precision.

The finite element method also has disadvantages. A specific numerical result is found for a specific problem: a finite element analysis provides no closed-form solution that permits analytically study of the effects of changing various parameters. A computer, a reliable program, and intelligent use are essential. A general purpose program has extensive documentation, which cannot be ignored. Experience and good engineering judgement are needed in order to define a good model. Many input data are required and volumnious output must be sorted and understood. [29]

Basically, the procedure to be followed to obtain a model with a crack for in 3-D is as follows:

- Enter input parameters
- Define keypoints accordingly,
- Define lines by keypoints.

- Define areas by lines,
- Choose 2-D, 8-noded quadrilateral elements for area meshing, choose 3-D 20-noded quadrilateral elements for volumetric meshing,
- Apply extruding operation according to requirement to get a 3-D model,
- Position the local coordinate system on the crack tip
- Mesh the structure in such a way that crack tip is surrounded by singular elements
- Apply loading (i.e., define Degree Of Freedom, Forces, and so on)
- Solve
- Create a path along the crack face
- Obtain the nodal solutions for stress intensity factors
- A detailed expalantion of the modelling will be given in Section 4.4

4.2. Sources of Error

There are three sources of error in the finite element method: errors due to approximation of the domain (discretization error), errors due to approximation of the element behavior (formulation error), and errors due to use of finite precision arithmetic.

Discretization error is due to the approximation of the domain with a finite number of elements of fixed geometry. For instance, consider the analysis of a rectangular plate with a centrally located hole (Figure 4.2(a)). Due to symmetry, it is sufficient to model only-one quarter of the plate. If the region is subdivided into triangular elements (a triangular mesh or grid), the circular hole is approximated by a series of straight lines. If a few large triangles are used in a coarse mesh, (Figure 4.2 (b)), greater discretization error results than if a large number of small elements are used in a fine mesh, (Figure 4.2 (c)). Other geometric shapes may be chosen for the elements. For example, with quadrilateral elements that can represent curved sides, the circuler hole is more accurately approximated (Figure 4.2 (d)). Hence, discretization error may be reduced by grid refinement. The grid can be refined by using more elements of the same type but of smaller size (h-refinement) or by using elements of a different type (p-refinement).

Formulation error results from the use of finite elements that do not precisely describe the behavior of continuum. For instance, a particular element might be formulated on the assumption that displacements vary linearly over the domain. Such an element would contain no formulation error when used to model a prismatic bar under constant tensile load; in this case, the assumed displacement matches the actual displacement. If the same bar were subjected to uniformly distributed body force, then the actual displacements vary quadratically and formulation error would exist.

Formulation error can be minimized by proper selection element type and appropriate grid refinement. Numerical error is a consequence of round-off during floating-point computations and the error associated with numerical integration procedures. This source of error is.dependent on the order in which computations are performed in the program and the use of double or extended precision variables and functions. The use of bandwith minimization can help control numerical error. Generally, in a well-designed finite element program, numerical error is small relative to formulation error [30].

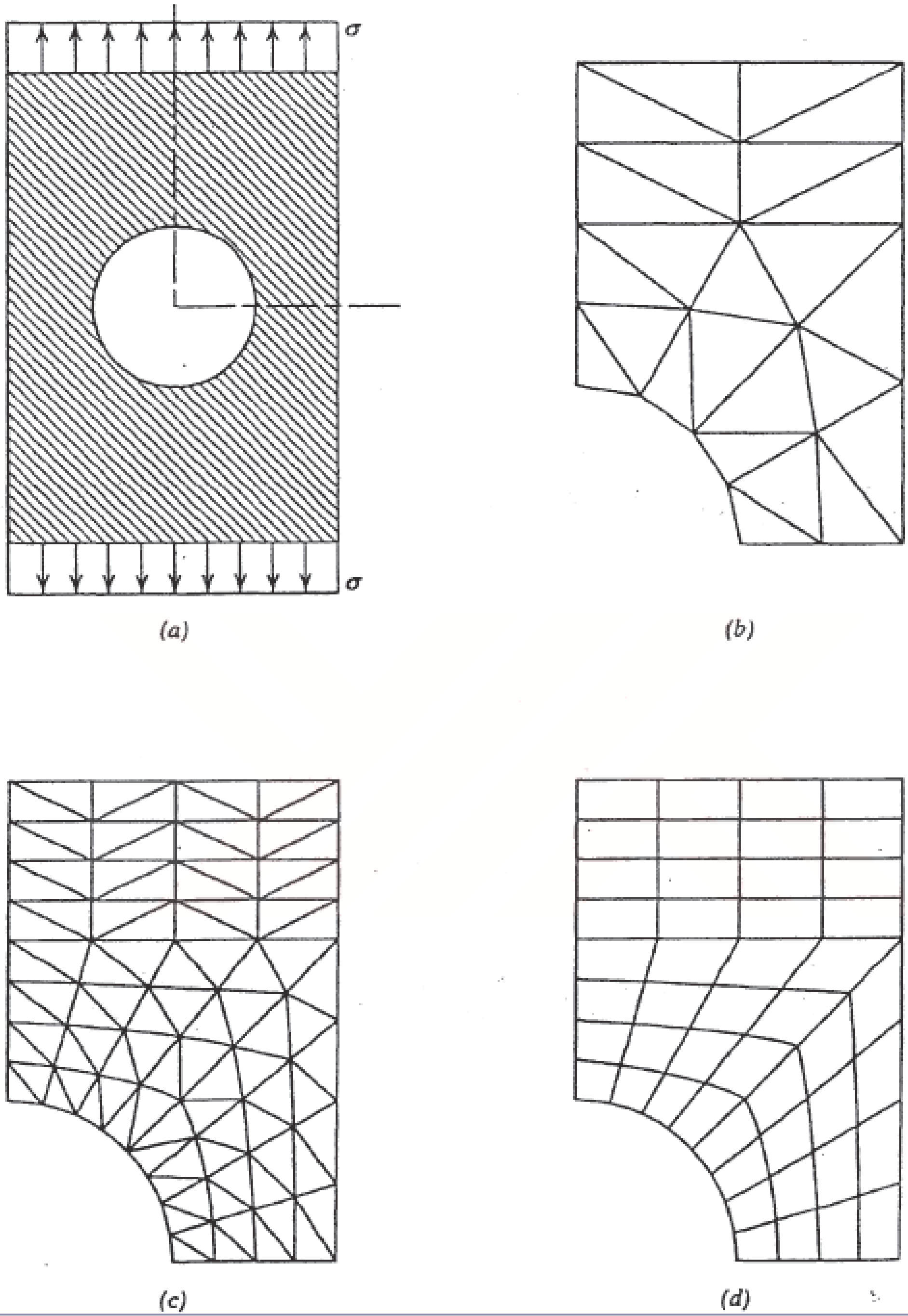

Figure 4.2: Finite element models of plate with centrally located hole. (a) plate geometry and loading. b) Coarse mesh of triangles. (c) Fine mesh of triangles. (d) Mesh of quadrilaterals with curved edges [16].

Add to these, powerful programs cannot be used without training. Their results cannot be trusted if users have no knowledge of their internal workings and little understanding of the physical theories on which they are based. An error caused by misunderstanding or oversight is not correctible by mesh refinement or by use of a more powerful computer. Some authorities have suggested that users be "qualified", somewhat in the .manner of practitioners having be licensed before engaging in a profession in which the potential for damage to the public is substantial. Although the finite element method can make a good engineer better, it can make a poor engineer more dangerous.

Computed results must in some way be judged or compared with expectations. Alternative results, useful for comparison, might be obtained from a different computer program that relies on a different analytical basis, from a simplified model amenable to hand calculation, from the behavior of similar structures already built, and from experiment. Experiment may be expensive and has its own pitfalls, but is desirable if the analytical process is pushed beyond previous experience and established practice.

4.3 About ANSYS and APDL

In order to evaluate stress intensity factors at the crack tips in this study, a finite element analysis program, ANSYS, is used. ANSYS is a comprehensive general purpose finite element computer program that contains over 100,000 lines of code [31].

ANSYS is one of the most powerful commercial finite element programs used in the world. It is due to various application fields of ANSYS. ANSYS product family consists of many parts. By means of this sub-parts of ANSYS, linear and non-linear analysis, buckling, heat transfer, fluid, acoustic problems and so on can be both modelled and solved.

Treatment of engineering problems basically contains three main parts: create a model, solve the problem, analyse the results. ANSYS, like many other FE-programs, is also divided into three main parts (processors) which are called preprocessor, solution processor, postprocessor. Other software may contain only the preprocessing part or only the postprocessing part. During the analysis, communication with ANSYS will be via a Graphical User Interface (GUI). The ANSYS program has a comprehensive GUI that gives users easy, interactive access to program actions, commands, documentation and reference material. Users can input data using a mouse, a keyboard, or a combination of both [32].

For users, there are two possibilities to work with ANSYS. The first one is to work directly by G.U.I. (i.e., by menus). The second one is to work by A.P.D.L. (ANSYS

Parametric Design Language). APDL allows one to build his model in terms of parameters (variables), which in turn allows one to make design changes easily. For simple models, directly working is very efficient but for the case of complex parts and models A.P.D.L. is advisable, because a parametric program can be written. A.P.D.L. allows user to enter program parameters from dialog boxes. Actually these two ways are same in the basis, but the main difference is that the pushing task automatically writes the command line of task in APDL language in the former and one can see what he has done at the same time on the computer screen. The programming logic of A.P.D.L. presented in Appendix A is similar with the other high level programming languages like C and Pascal. [33]

There are two options to start with A.P.D.L., first a text file is opened and program is written in this file or log file of the program can be used to edit data.

APDL allows one to build his model in terms of parameters (variables), which in turn allows one to make design changes easily. Actually these two ways are same in the basis, but the main difference is that the pushing task automatically writes the command line of task in APDL language in the former and one can see what he has done at the same time on the computer screen. Add to these, ANSYS has no limits on the number of the nodes, elements, or degrees of freedom. And also it should be noted that ANSYS uses dynamic memory allocation and the parameters managing the memory usage have been left to their default values.

For fracture mechanics, ANSYS is very ideal program. Stress Intensity Factors can be calculated directly by the program provided that the model is correct, the material used is isotropic and state of stress is plane stress, plane strain or axisymmetric.

4.4 Preprocessing

The first step of the finite element method starts with preprocessing. In the preprocessing part, one can select the type of elements, define the material properties, build the model, give attributes to the model and mesh the model. The first step is to select the element type which is Plane82 in this study. Plane82 is a 2-D eight-node structural solid element. (See Appendix B)

The next step is to define the material properties. More than one material property can be defined by giving different material numbers to them. In structural analysis, Elastic Modulus, Poisson's ratio and/or Shear Modulus are needed to be defined:

The material properties in this study are taken as:

Elastic Modulus (E) : 210000 MPa

Poisson's ratio (v) : 0.3

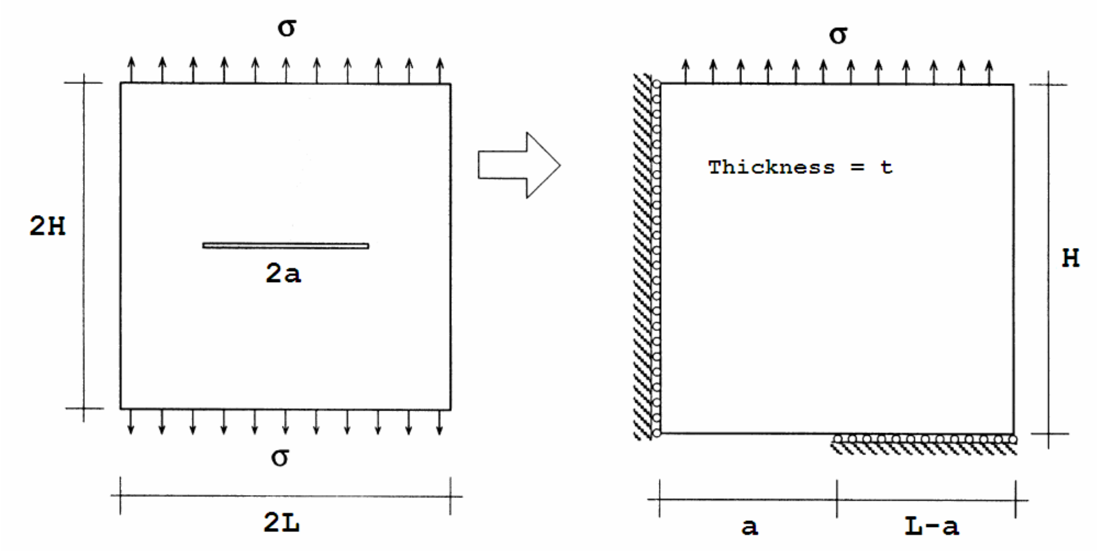

Figure 4.3: Model used in analysis

We will take advantage of symmetry in modelling since we have two symmetry planes which are normal to x and y axis. Due to the symmetry, it will be sufficient to model only one quarter of the crack region for the sake of simplicity and computational efficiency.

In the model five keypoints have been defined as shown in the Figure 4.4. Keypoint number 2 represents the crack tip. Keypoint number 1 represents the model symmetry point and center of the crack.

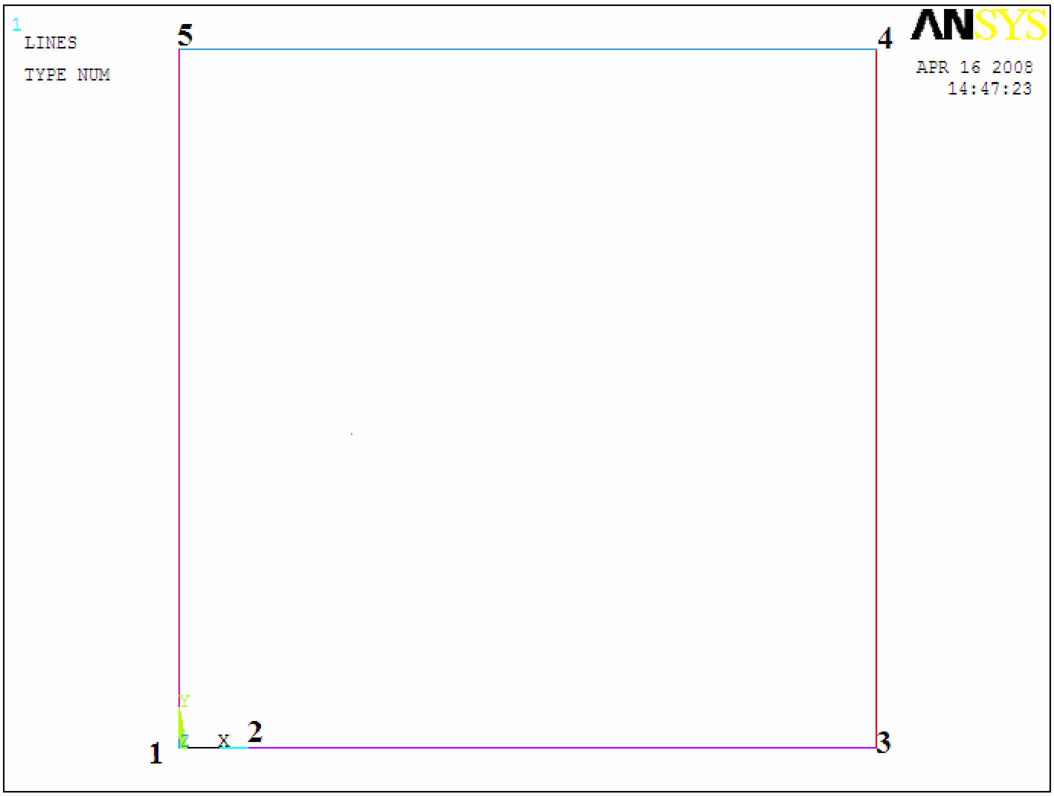

Figure 4.4: Defined keypoints represents quarter plate

A square could also be formed without creating these keypoints. However it is essential to use the uniqueness of command KSCON, which is used for obtaining singular elements at the crack tips in an area automatically for crack modelling. Since in order to use the KSCON command, it is required to define a keypoint at the crack tip.

The most important region in a fracture model is the region around the edge of the crack. This region is referred as a crack tip in 2-D model and crack front in a 3-D model as shown in Figure 4.5.

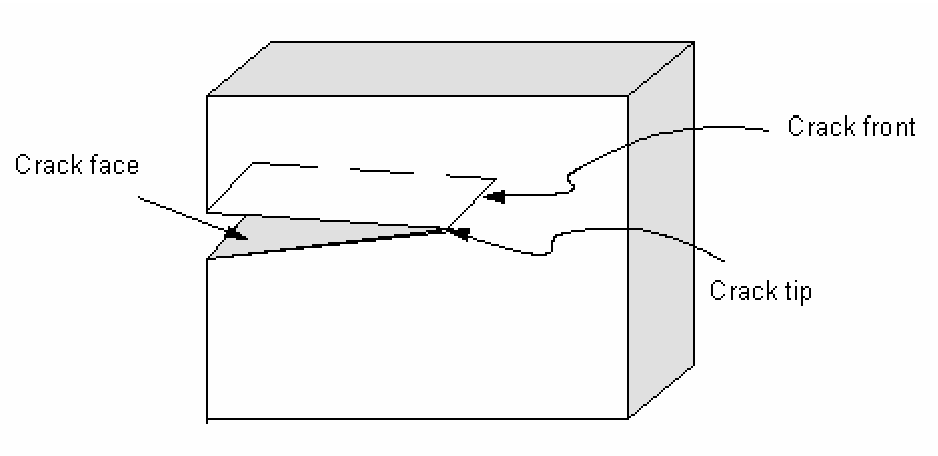

Figure 4.5: Crack tip, crack face and crack front

In linear elastic problems, it has been shown that the displacements near the crack front vary as $\sqrt{r}$, where r is the distance from the crack tip. The stresses and strains are singular at the crack tip, varying as $1/\sqrt{r}$. To pick up the singularity in the strain, the crack faces should be coincident, and the elements around the crack front should be quadratic, with the midside nodes placed at the quarter points. Such elements are called singular elements. Figure 4.6 shows examples of singular elements for 2-D and 3-D models. Notice that the element is wedge-shaped, with the KLPO face collapsed into the line KO.

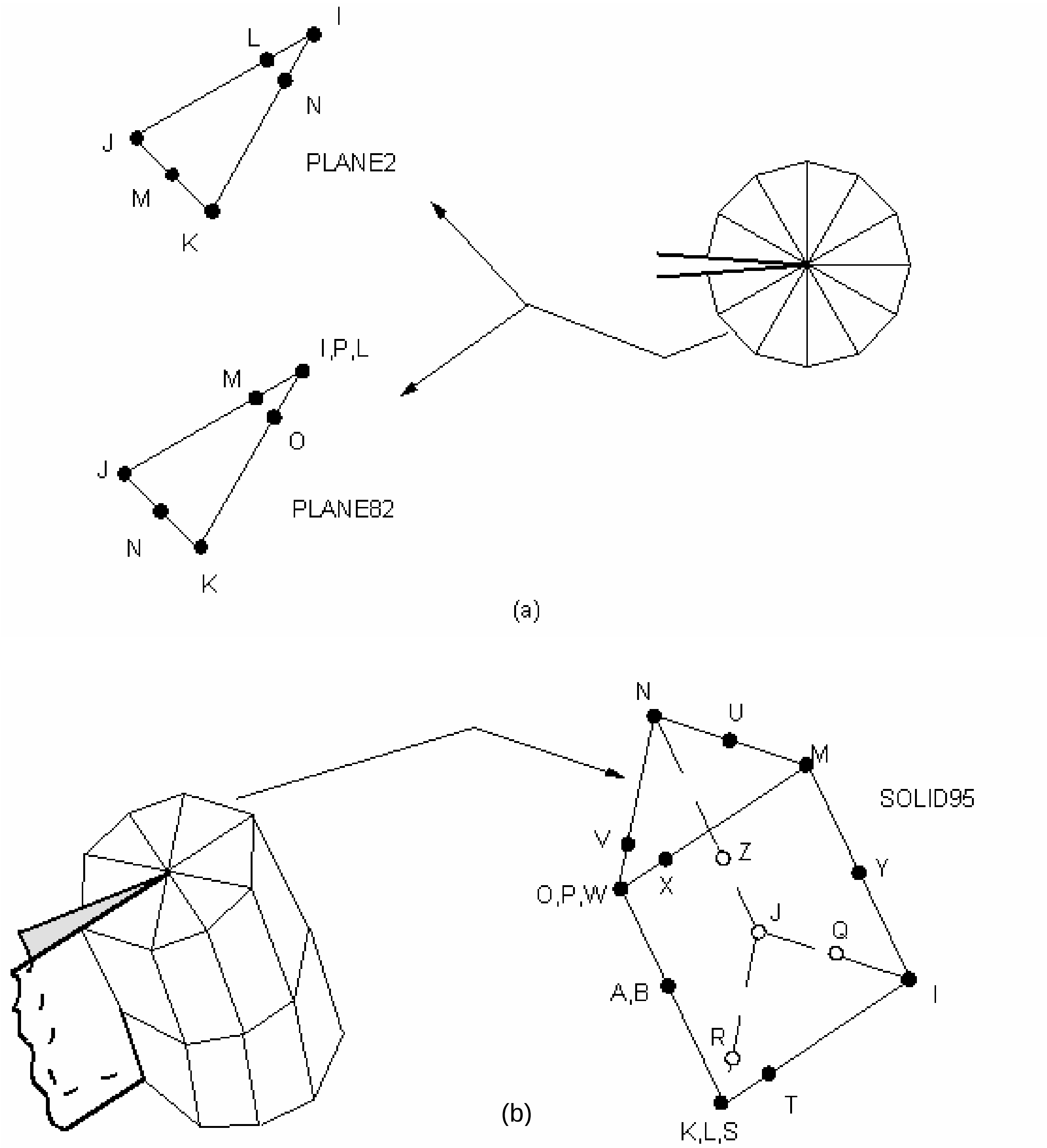

Figure 4.6: Examples of Singular Elements used in ANSYS (a) 2-D models and (b) 3-D models

KSCON defines a concentration keypoint about which an area mesh will be skewed. It is useful for modeling stress concentrations and crack tips. During meshing, elements are initially generated circumferentially about, and radially away, from the keypoint. Lines attached to the keypoint are given appropriate divisions and spacing ratios. Only one concentration keypoint per unmeshed area is allowed.

The first step is to define the required properties of KSCON command in order to form singular elements at the crack tips. If a special element is introduced in order to consider the singularity of the stress-strain in the vicinity of the crack tip a more accurate solution can be obtained. This is the way that an accurate stress intensity factor value can be obtained with a rather coarse mesh [33].

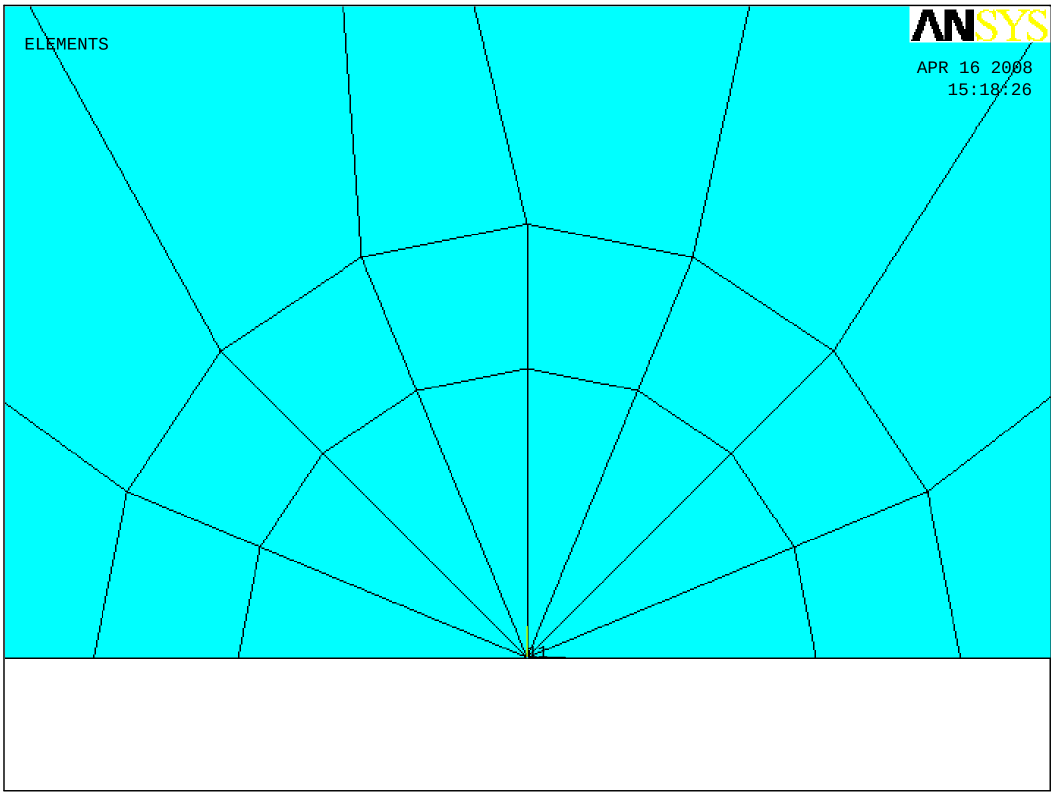

Figure 4.7: Singular crack tip elements generated by the use of KSCON command

In order to efficiently model the $1/\sqrt{r}$ type variation of displacements near the crack tip (r being the distance from the crack tip), quarter-point elements (QPEs) have been used to mesh the region surrounding the tip. QPEs were introduced by Barsoum [22] and are essentially six-noded triangular elements with their mid-side nodes shifted to quarter-point positions. It has been shown that, depending on the mesh and crack configuration, there exists an optimum size of QPE and smaller or larger QPEs compromise the accuracy of results. Murti and Valliappan [42] have suggested that the optimum size of QPE is 15-25% of the crack length.

On the other hand, ANSYS guidelines recommend that the radius of 1st row of elements should be "crack length/8" or smaller and in the circumferential direction, there should be roughly one element every 30 or 40 degrees. In this study, the maximum radius used is "crack length/16", the number of elements is 16, so roughly every 11-12 degrees there is one singular element and radius ratio is taken as 0.5 which is also advised by ANSYS [33]. Add to these, despite the offer of Murti and

Vallipan [42] about the optimum radius of 1st row of elements, it is seen that the value of this radius doesn't affect the results significantly. On the other hand, the number of elements is the most important and effective parameter, so a high number of elements at the crack tip should be taken.

Generating a 3-D fracture model is considerably more involved than a 2-D model. In order to generate a crack in 3-D, a brick element must be transformed into a wedge-shaped element by collapsing a surface along the crack front (Figure 4.6). Then midside nodes on both front and back surfaces near the crack front must be placed to quarter point. Another way to get wedge-shaped 3-D element is to generate singular isosceles triangles in 2-D, and then to drag them with some thickness or to rotate them to have curved crack front.

It should be noted that KSCON command does not support 3-D modeling, and we need to make sure that the crack front is along edge KO of the elements. Due to this problem first of all we have to form the 2-D area and extrude to generate the 3-D model by using SOLID95 elements in order to have a correct crack model element arrangement around the crack tip. This method will also satisfy the crack tip elements not to be distorted as it is recommended by ANSYS. Accordingly the crack tip elements will take the shape of isosceles triangles as shown in Figure 4.7.

Modeling guidelines of 3-D modeling in ANSYS are as follows:

1. Element size recommendations are the same as for 2-D models. In addition, aspect ratios should not exceed approximately 4 to 1 in all directions.

2. For curved crack fronts, the element size along the crack front will depend on the amount of local curvature. As a rough guide, you should have at least one element every 15° to 30° along a circular crack front.

3. All element edges should be straight, including the edge on the crack front.

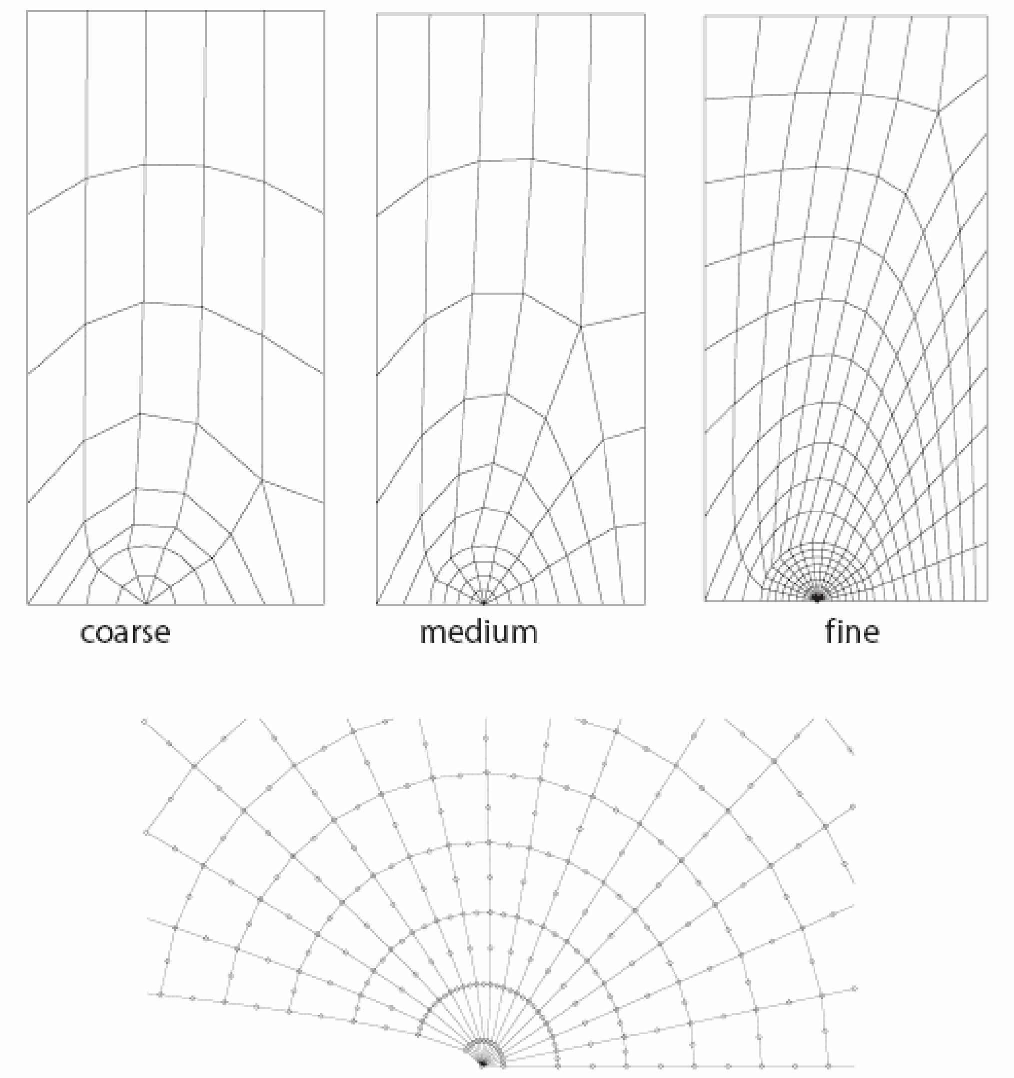

Figure 4.8: Detail of crack tip fine mesh, showing displaced shape and positions of nodes. Mid-side nodes are moved to quarter points in the first ring of elements around the crack tip.

After defining the required properties of singular elements, the next step is to define mesh size properties of the lines in the model in order to obtain a fine meshed model which is commonly used in this study.

After picking lines which one wants to modify the mesh size properties, it is needed to give the value of the required "element edge length" or "number of element divisions". For a finer meshed model, smaller values should be given to element edge length property. There is another parameter as "spacing ratio" on this table which has a default value of "1". If one changes this value, lengths of the meshes on lines increase or decrease linearly. This is generally an important property in the finite element method, which is needed to use coarser meshing far from the critical points.

Since crack tip is the critical point in the model, spacing ratio has been used to ensure a more dense element configuration near the vicinity of the crack tip.

The next step after modifying the default values of meshing parameters is to mesh the model:

After picking the required commands for meshing, the meshed model of the whole geometry (Figure 4.9) is obtained and the model is discretized into a high number of elements. Meshing is the last step of the preprocessor part.

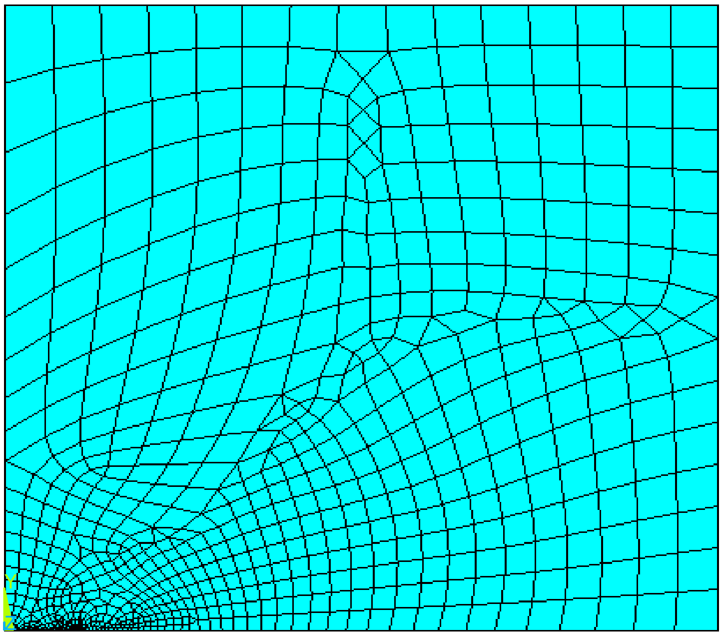

Figure 4.9: The meshed model of the whole geometry

As explained previously, for 3D analysis, 8-noded PLANE82 elements must be chosen for 2D area meshing and 20-noded SOLID95 elemets must be chosen for the volumetric mesh. We have introduced the PLANE82 element before. So that, second element (SOLID95) type must be introduced by the command ET and to activate it by the command TYPE. SOLID95 element type must be activated as the default element type.

It should be noted that the number of element division defines the number of elements through the thickness of the plate. A finer mesh should have a higher value of this sizing option. Nevertheless, this value must not be so high that the element size through thickness is below the radius of the quarter point elements around the crack tip. Otherwise an error message occurs to modify the element size.

Meshed area will be extruded along normal in order to get a 3-D model. By using this method that meshing the 2-D area first and then extruding into a volumetric meshing, the crack pattern will be maintained along the crack front.

Boundary conditions must be applied on the structure by using DSYM command to apply symmetry or antisymmetry boundary conditions on a plane of nodes. The command generates the appropriate DOF constraints for the nodes. In a structural analysis, for example, a symmetry boundary condition means that out-of-plane translations and in-plane rotations are set to zero, and an antisymmetry condition means that in-plane translations and out-of-plane rotations are set to zero. (Figure 4.10) All nodes on the symmetry plane are rotated into the coordinate system specified by the KCN field on the DSYM command.

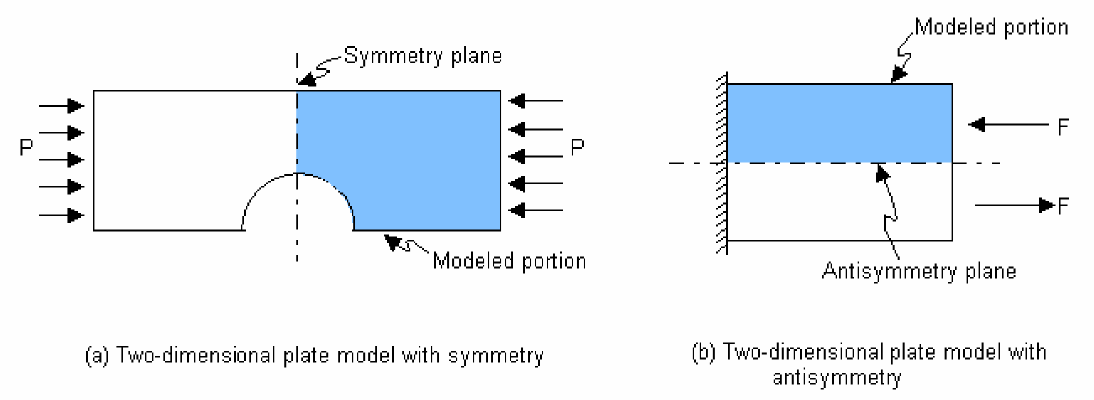

Figure 4.10: (a) Two-dimensional plate model with symmetry (b) Two-dimensional plate model with antisymmetry

First step of applying boundary conditions is to constrain translation of nodes where needed. In our crack model, UY degree of freedom of the nodes at the base line except the nodes on the crack line is constrained because of the symmetry condition according to x-axis.

At y = 0, the nodes on the x axis remain constant in the y-direction except the nodes on the crack line. Add to this, this constrained condition lets us to obtain a crack when a tensile load applied at the upper part of the model.

Subsequently, out-of-plane translations and in-plane rotations of these nodes must be set to zero. In the 3-D analysis, the plane strain condition is achieved by constraining UZ degrees of freedom of all the nodes (displacements in the Z-direction).

Also -1 MPa of tension must be applied at the upper line of the model (y = H)

Figure 4.11 represents how the model looks like after the boundary conditions and the pressure is applied.

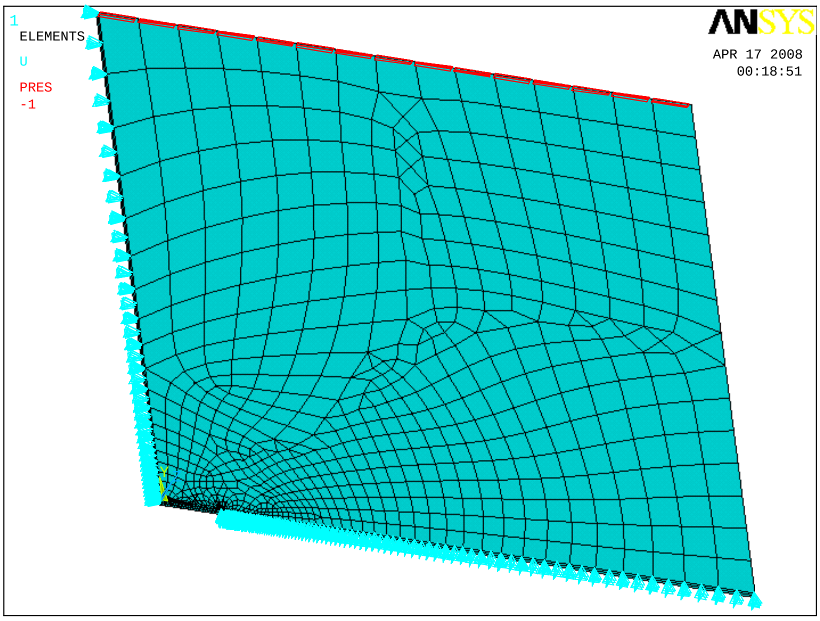

Figure 4.11: Meshed model with boundary conditions and tension applied

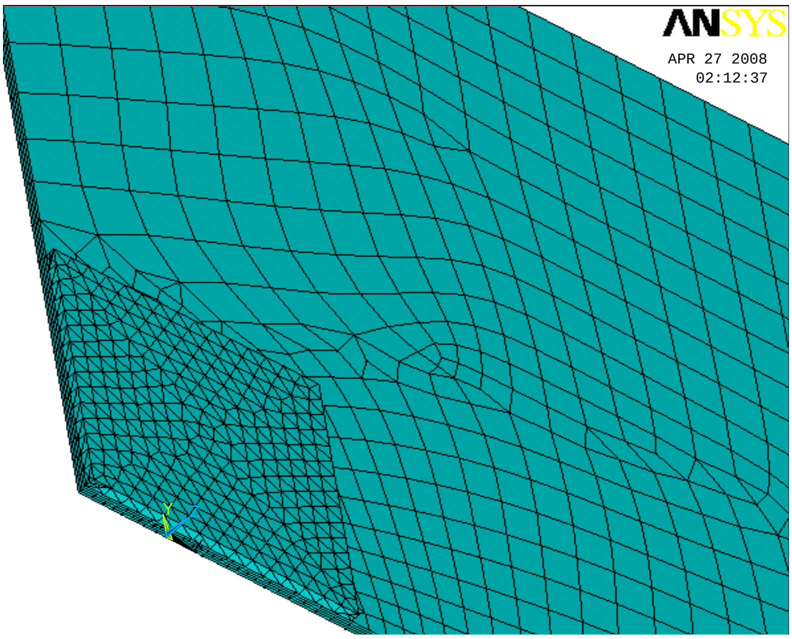

Figure 4.12: Bonded patch onto the plate

Note that the transition of y-component of displacement contours between the plate and the patch is smooth and continuous

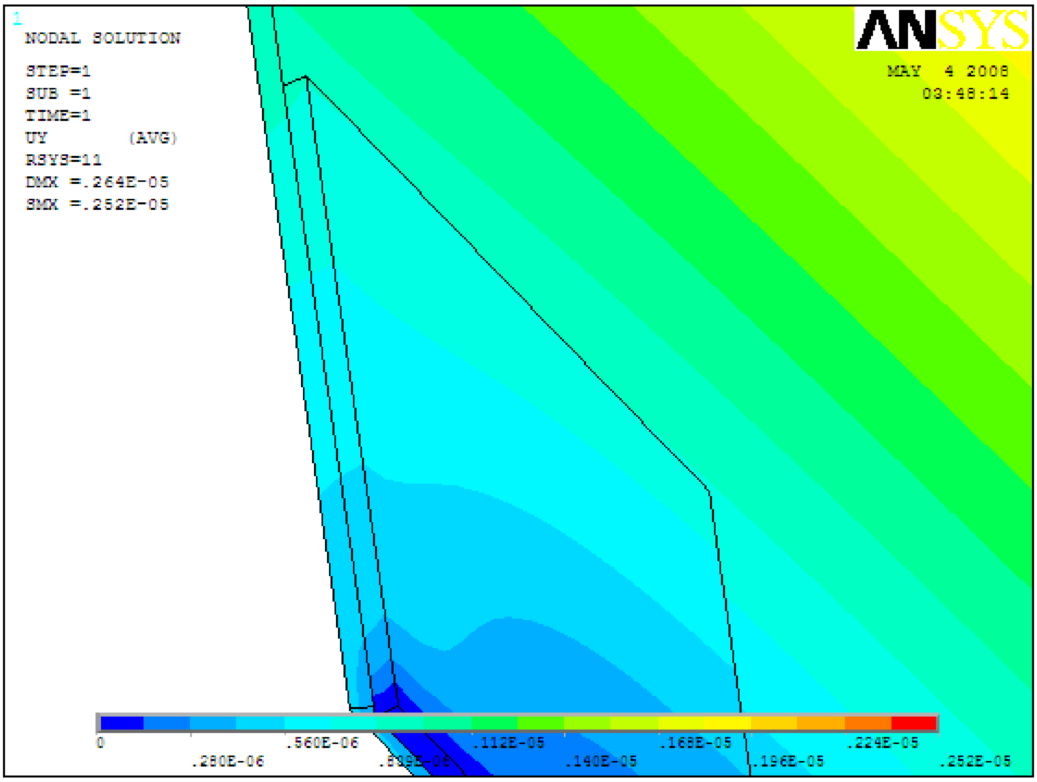

Figure 4.13: y-component of displacement contours between the patch and the plate

The finite element model of matrices and equations which are formed by the given data from the beginning of the analysis should ready to be solved.

4.5 Postprocessing part

Once the static analysis is completed, postprocessing part (POST1) can be used, the general postprocessor, to calculate fracture parameters such as stress intensity factor. In this study, the results of SIFs at the two crack tips and stress distribution inside the model have special importance. Calculation of SIFs at the crack tips can be accomplished in the Postprocessing part of the ANSYS by KCALC command with the displacement extrapolation method. There are also different methods such as the J-integral via the domain integral method [34], modified crack closure technique [35], virtual crack extension method [36].

To use KCALC properly, some essential steps must be followed beforehand in POST1:

1. A local crack-front coordinate system, with X perpendicular to the crack front and Y perpendicular to the crack face must be defined, as shown in the Figure 4.14.

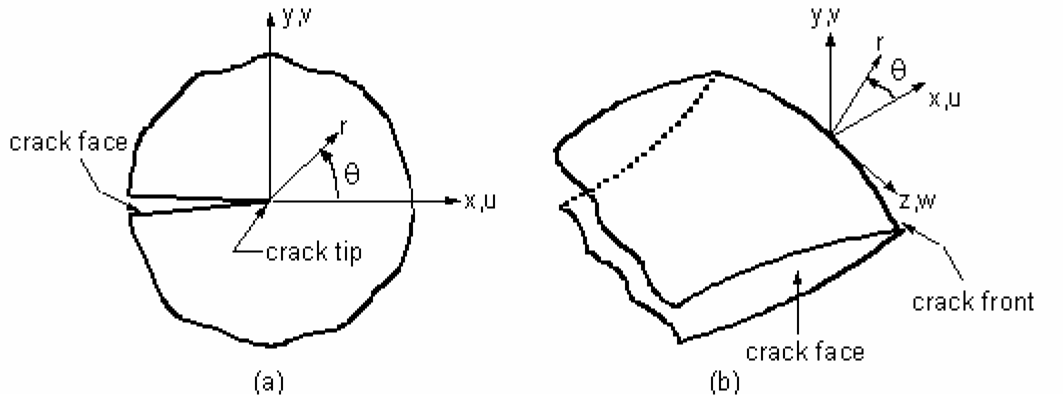

Figure 4.14: Local crack-front coordinate system (a) 2-D Models (b) 3-D Models

This local coordinate system must be the active model coordinate system [CSYS] and results coordinate system [RSYS] when KCALC is issued.

2. A path along the crack face must be defined. The first node on the path should be the crack-tip node. For a half-crack model, two additional nodes are required, both along the crack face. For a full-crack model, where both crack faces are included, four additional nodes are required: two along one crack face and two along the other. Since we have a half-crack model we need to select three nodes in order to define a path.

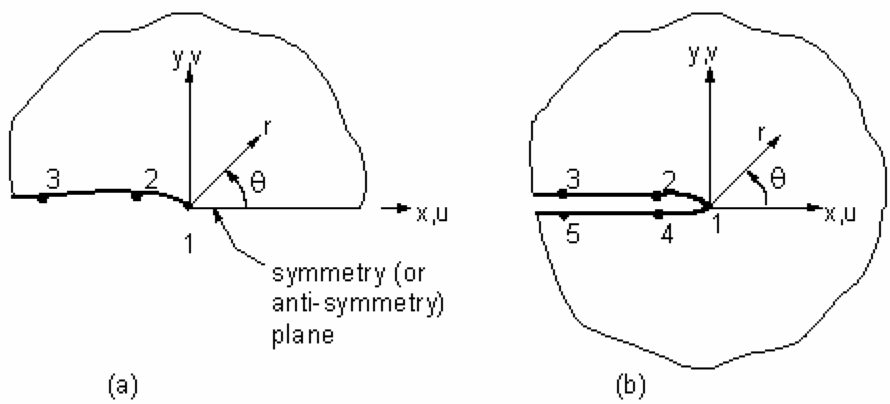

Figure 4.15: Typical path definitions (a) a half-crack model and (b) a full-crack model

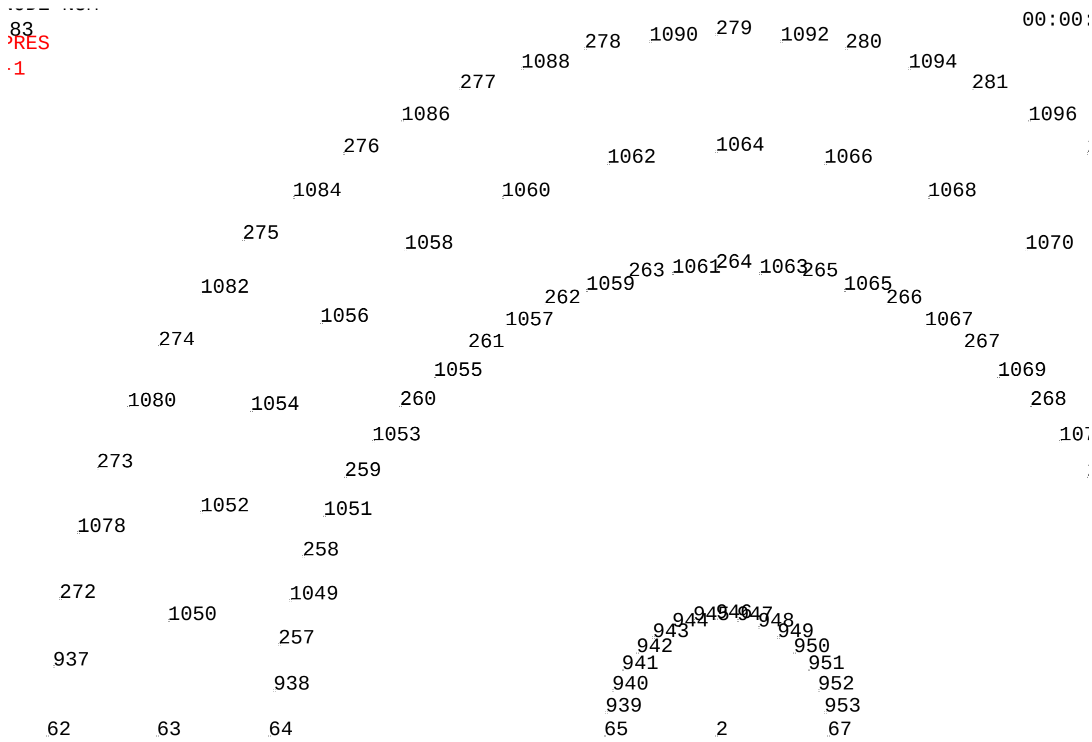

Figure 4.16: Nodes #2, #65 and #64 can be selected for the path.

The POST1 KCALC command calculates the mixed-mode stress intensity factors K_I, K_{II}, and K_{III}. This command is limited to linear elastic problems with a homogeneous, isotropic material near the crack region.

The KPLAN field on the KCALC command specifies whether the model is plane-strain or plane stress. Except for the analysis of thin plates, the asymptotic or near-crack-tip behavior of stress is usually thought to be that of plane strain. The KCSYM field specifies whether the model is a half-crack model with symmetry boundary conditions, a half-crack model with antisymmetry boundary conditions, or a full-crack model. The advantage of symmetry will be taken and model will be considered as half-crack model.

It can easily be seen that, there is intensification at the crack tips. In this-case, it is clear that the regular stress distribution of the whole body is disturbed by the effect of the crack.

As mentioned before, instead of using the graphical user interface, APDL can be used in all steps of the analysis. Throughout this study, a log file written parametrically in APDL language is used. So, the repeating steps in all analyses are done very fastly and parameters are changed very easily. A sample log file used in this study is given in Appendix A.

Add to these, a convergence test should be done in order to get accurate results and prevent from more time consuming than the optimum analysis. This test can be done by increasing the number of meshes and doing the same analysis, then comparing the results with each other. With the increasing number of mesh, the differences between the results become smaller, so the minimum number where the constantancy starts is the optimum mesh number of the analysis. In this study, it is not need to do such a test in every analysis, because there is not a significant difference between the results whether the coarse or fine mesh used.

5. ANALYSIS AND RESULTS

5.1 Plate with a Central Crack

A symmetrical finite rectangular plate with a height of 2H, width of 2L, thickness equal to t contains a transverse symmetrical crack of width 2a as shown in Figure 5.1 is examined to evaluate stress intensity factor. Uniformly distributed axial tension of intensity σ is applied to the ends of the plate. The material of the plate is assumed to be linearly elastic and isotropic. Both edges of the strip are free of stresses. Due to double symmetry, only one quadrant of the plate is needed to be modeled. The boundary conditions for the model are determined by symmetry conditions.

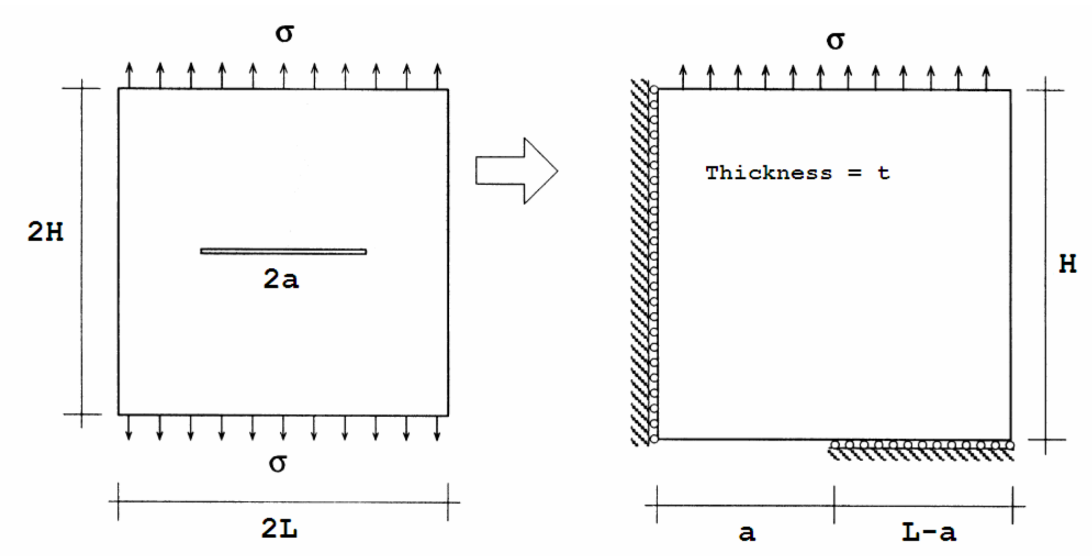

Figure 5.1: Centrally cracked finite rectangular plate

Plate with a central crack is a well examined for which solutions are available for example in [15, 16], making it possible to evaluate the accuracy of the finite element model used.

Stress Intensity Factor (S.I.F.) values at the crack tip are obtained for the plate with a central crack with various geometries depending on the crack length, plate width and plate height values by giving incremental changes for each parameter. The model involves focusing a tremendous amount of attention to the crack tip in order to obtain the stress field accurately. Throughout the numerical solution of the cracked plate, general purpose finite element code ANSYS is implemented. MATLAB code is written in order to achieve the tabulation of the results obtained by ANSYS. In the iteration process, MATLAB creates an input file containing the model geometries to be evaluated by ANSYS in order to calculate the stress intensity factor values. MATLAB executes the ANSYS APDL parametric code and tabulates the output of ANSYS. See Appendix A for a written APDL sample program. NASGRO, and stress intensity solutions tabulated handbooks [15, 21] and previous studies in the literature [8, 16] comes in handy for the verification of the results. In order to analyze the stress intensity factor with a reasonable accuracy and to examine the mesh dependency of the results, three different mesh densities used. In the theses, it is intended to see how the geometry and meshing parameters affect the SIF values. Following parameters are changed and examined during the study.

- Crack length
- Plate width
- Plate height
- Plate thickness
- Mesh density (Coarse, Medium, Fine)
- Number of elements around circumferential direction around crack tip
- Effect of Poisson's ratio
- Effect of Young's modulus

Some of the finite element results were compared with the analytical results.

Three commercial software packages were used during analysis, ANSYS, NASGRO and MATLAB. ANSYS was used for pre-processing, processing the finite element analyses of the case studied. NASGRO was used in order to verify the SIF results obtained from the finite element analyses as a secondary verification to the tabulated solutions from the references [15, 16]. MATLAB is the platform to run and list the results during iterations.

Material properties of the finite element model;

Young's modulus, $E = 2.1 \times 10^5$ MPa

Poisson's ratio = 0.3

For general calculations tension σ is applied to the ends of the plate is calculated as follows,

$$K_I = Y\sigma\sqrt{\pi a} \tag{5.1}$$

For the condition:

$$K_I = Y$$
$$\sigma\sqrt{\pi a} = 1$$

$$\sigma = \frac{1}{\sqrt{\pi a}} \tag{5.2}$$

For a typical crack length of 0.01 m.

$\sigma = 5{,}64189583\ N/m^2$

If the above stress value used for tension, the geometric correction factor will be equal to stress intensity factor for the crack length of 0.01 m. Thus we can get the dimensionless geometric correction factors directly from the computations through analysis without doing further calculations..

For the plate with a central crack subject to tensile loading, the precision of results using different types of mesh is discussed and assessed by comparison with values obtained in the literature, Ref. [16].

5.1.1 Accuracy of the model

In general the stress intensity factor depends on the applied stress, crack size, and the geometry with the equation,

$$K_I = Y\sigma\sqrt{\pi a}$$

where Y is called the geometry factor or dimensionless stress intensity factor (SIF). Normally this geometry factor can be looked up in technical reference books. For a centre crack in an infinite plate, Y = 1.0 [21]. The geometry of the cracked body imposes an effect on the new crack tip stress field, thus modifying the value of the stress intensity factor. In general, if the edge crack is situated in a strip of finite width, L, then the correction factor becomes a function of *(a/L).*

$$Y = f(a/L) \tag{5.3}$$

The determination of this geometry factor is a problem of stress analysis. Any realistic geometry requires recourse to numerical methods, as very few closed form solutions exist. The most popular and efficient method is finite element analysis. By using the MATLAB code developed which executes the ANSYS APDL batch file to obtain stress intensity factor values for general geometry depends on many parameters. Table 2.1 lists dimensionless stress intensity factors (Y) for a number of values depending on f(a/L). A more comprehensive list could be found in a two-volume handbook Murakami [37].

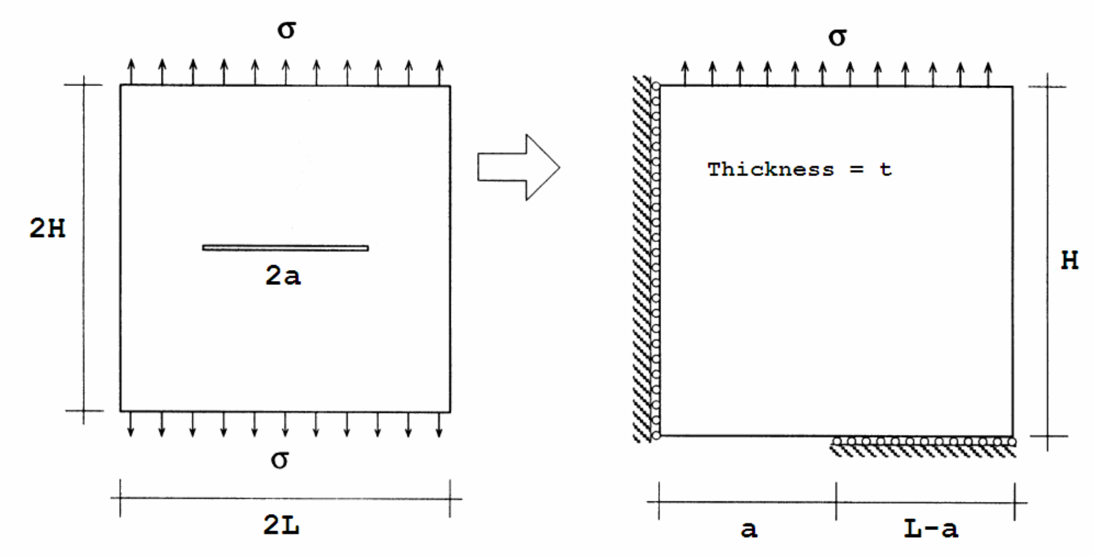

Figure 5.2: Model used for the analysis

Evaluation Range:

a/L = [0.0 – 0.7] by increments 0.1 (m)

H/L = [0.4 – ∞] by increments 0.1 (m)

t, thickness = 0.001 m

$$\sigma = \frac{1}{\sqrt{\pi a}} \text{ N/m}^2$$

Young Modulus = E = 2.1 x 10^5 MPa

Poisson's ratio = 0.3

Stress intensity factors (dimensionless geometry correction factors) are obtained and tabulated with varying (a/L) and (H/L) parameters. In Table 5.3, the finite element solution of the stress intensity factor values are compared with the results of isida [16] and it is clearly seen that the results are in perfect agreement.

Table 5.1: Change of Y (dimensionless stres intensity factor) values versus c/b and a/b ratios for a Mode I loaded of centrally cracked rectangular plate under uniform tension.[Ref 33, Isida**]**

表 2 $\dfrac{K_{\mathrm{I}}}{\sigma_0\sqrt{\pi a}}$ （一様引張り）

	c/b	0.4	0.5	0.6	0.7	0.8	0.9	1.0	1.2	1.5	1.8	∞ (5)
$\frac{a}{b}=$	0	1.000	1.000	1.000	1.000	1.000	1.000	1.000	1.000	1.000	1.000	1.000
	0.1	1.069	1.046	1.033	1.026	1.021	1.017	1.014	1.010	1.007	1.006	1.006
	0.2	1.256	1.175	1.130	1.103	1.083	1.067	1.055	1.039	1.029	1.025	1.025
	0.3	1.520	1.371	1.285	1.228	1.184	1.150	1.123	1.088	1.066	1.060	1.058
	0.4	1.843	1.629	1.497	1.400	1.323	1.262	1.216	1.158	1.122	1.112	1.109
	0.5	2.247	1.967	1.773	1.619	1.496	1.403	1.334	1.251	1.203	1.190	1.187
	0.6	2.806	2.424	2.123	1.883	1.702	1.572	1.481	1.38	1.32	1.31	1.303
	0.7	3.67	3.04	2.55	2.19	1.94	1.78	1.68	—	—	—	1.488

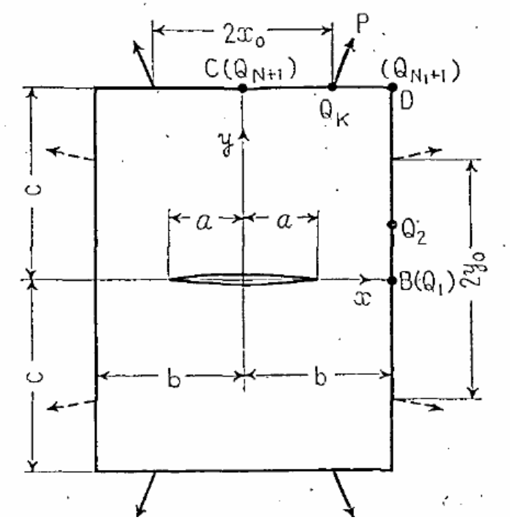

Table 5.2: Change of Y (dimensionless geometry correction factor) Values Versus H/L and a/L ratios for a Mode I loaded of centrally cracked rectangular plate under uniform tension. [ANSYS results] Note: Infinite values are obtained from NASGRO

		H/L													
		0.4	0.5	0.6	0.7	0.8	0.9	1.0	1.1	1.2	1.5	1.8	2.5	4.0	Infinite
a/L	0.0	1.0000	1.0000	1.0000	1.0000	1.0000	1.0000	1.0000	1.0000	1.0000	1.0000	1.0000	1.0000	1.0000	1.0000
	0.1	1.0695	1.0459	1.0336	1.0262	1.0211	1.0171	1.0140	1.0117	1.0099	1.0069	1.0058	1.0053	1.0039	1.0062
	0.2	1.2561	1.1750	1.1309	1.1033	1.0833	1.0679	1.0558	1.0465	1.0396	1.0289	1.0252	1.0245	1.0239	1.0254
	0.3	1.5206	1.3716	1.2861	1.2285	1.1848	1.1504	1.1237	1.1035	1.0888	1.0664	1.0599	1.0578	1.0574	1.0594
	0.4	1.8447	1.6304	1.4980	1.4006	1.3236	1.2629	1.2167	1.1826	1.1583	1.1224	1.1125	1.1097	1.1093	1.1118
	0.5	2.2487	1.9684	1.7740	1.6199	1.4972	1.4033	1.3344	1.2855	1.2516	1.2032	1.1904	1.1870	1.1865	1.1892
	0.6	2.8073	2.4258	2.1250	1.8847	1.7031	1.5725	1.4817	1.4198	1.3784	1.3216	1.3073	1.3037	1.3031	1.3043
	0.7	3.6679	3.0425	2.5476	2.1895	1.9455	1.7840	1.6782	1.6094	1.5648	1.5061	1.4919	1.4887	1.4880	1.4841
	0.8	4.9642	3.7795	3.0150	2.5503	2.2698	2.0987	1.9927	1.9263	N/A	N/A	1.8194	1.8159	1.8103	1.7989

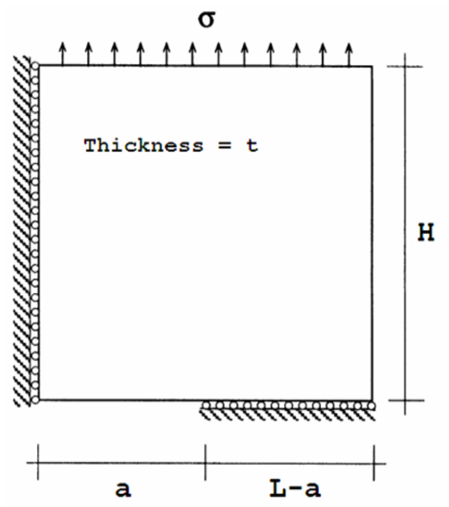

Table 5.3: Percentage of relative errors computed by comparing the FE results according to Isida's [33] results. $Err(\%) = \frac{Y_{I(Isida)} - Y_{I(FE)}}{Y_{I(Isida)}} \times 100$

		H/L									
		0.4	0.5	0.6	0.7	0.8	0.9	1.0	1.2	1.5	1.8
a/L	0.0	0.0	0.0	0.0	0.0	0.0	0.0	0.0	0.0	0.0	0.0
	0.1	0.0	0.0	-0.1	0.0	0.0	0.0	0.0	0.0	0.0	0.0
	0.2	0.0	0.0	-0.1	0.0	0.0	-0.1	-0.1	-0.1	0.0	0.0
	0.3	0.0	0.0	-0.1	0.0	-0.1	0.0	-0.1	-0.1	0.0	0.0
	0.4	-0.1	-0.1	-0.1	0.0	0.0	-0.1	-0.1	0.0	0.0	0.0
	0.5	-0.1	-0.1	-0.1	-0.1	-0.1	0.0	0.0	0.0	0.0	0.0
	0.6	0.0	-0.1	-0.1	-0.1	-0.1	0.0	0.0	0.1	-0.1	0.2
	0.7	0.1	-0.1	0.1	0.0	-0.3	-0.2	0.1	N/A	N/A	N/A

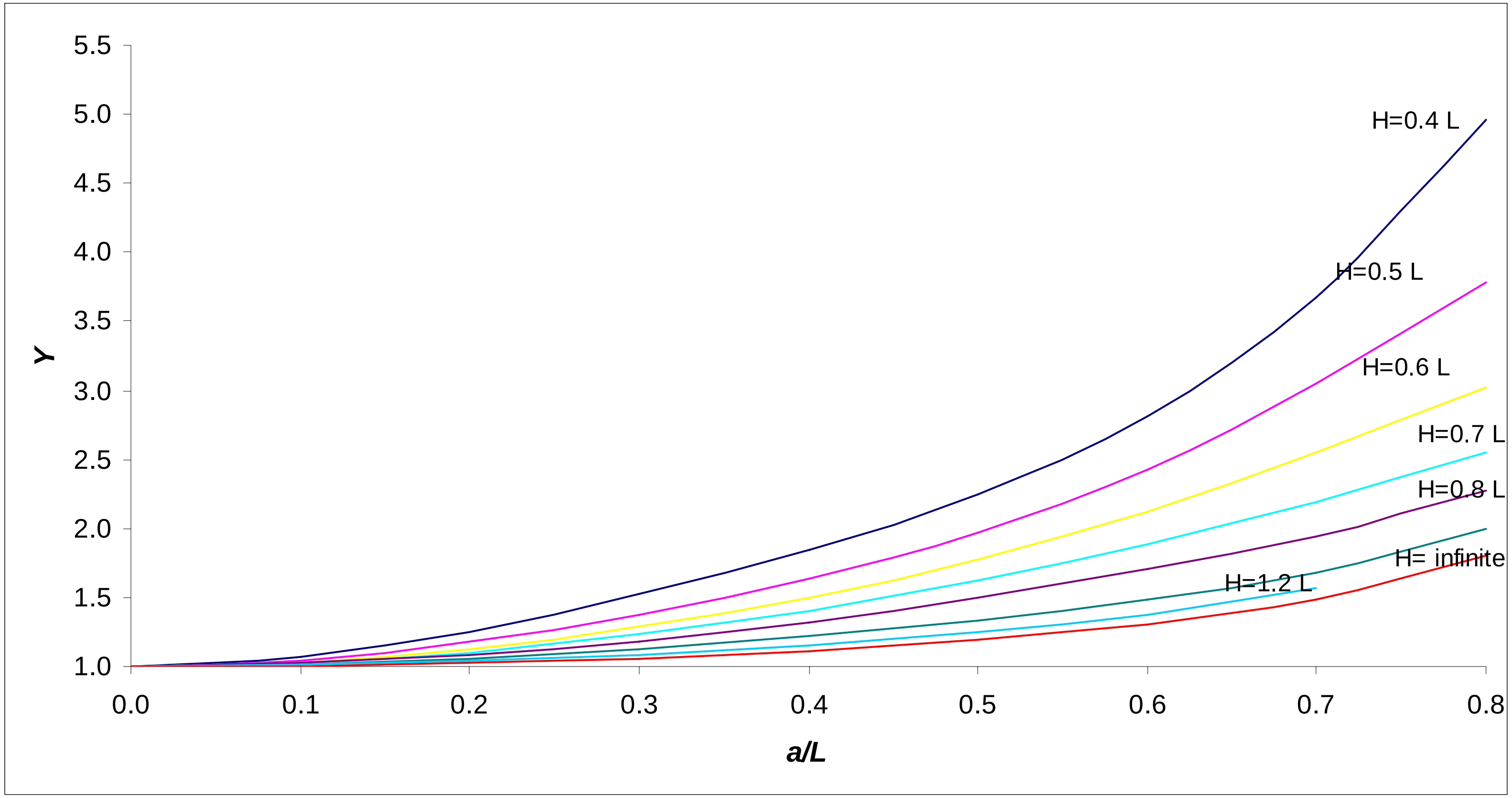

Figure 5.3: Variation of Stress Intensity Factors vs. (a/L), (H/L) ratios, when L =0.1 m, v = 0.3, t = 0.001 m, $\sigma = \dfrac{1}{\sqrt{\pi a}}$ N/m^2, E = 2.1 x 10^5 MPa

5.1.2 Stress intensity factor vs. plate thickness

Table 5.4: Variation of dimensionless SIF with respect to the thickness of plate

t	Y a = 0.1L, H = L	Y a = 0.5L, H = L	Y a = 0.1L, H = infinite
0.0005	1.01411	1.33453	1.00590
0.001	1.01404	1.33444	1.00584
0.0015	1.01398	1.33435	1.00578
0.002	1.01392	1.33427	1.00572
0.0025	1.01386	1.33418	1.00566
0.003	1.01380	1.33410	1.00560
0.0035	1.01374	1.33402	1.00554
0.004	1.01368	1.33393	1.00548
0.0045	1.01362	1.33386	1.00542
0.005	1.01356	1.33378	1.00536
0.0055	1.01349	1.33370	1.00529
0.006	1.01343	1.33362	1.00523
0.0065	1.01336	1.33355	1.00517
0.007	1.01330	1.33348	1.00510
0.0075	1.01323	1.33340	1.00504
0.008	1.01317	1.33333	1.00497
0.0085	1.01310	1.33326	1.00490
0.009	1.01303	1.33319	1.00484
0.0095	1.01296	1.33312	1.00477
0.01	1.01289	1.33305	1.00470

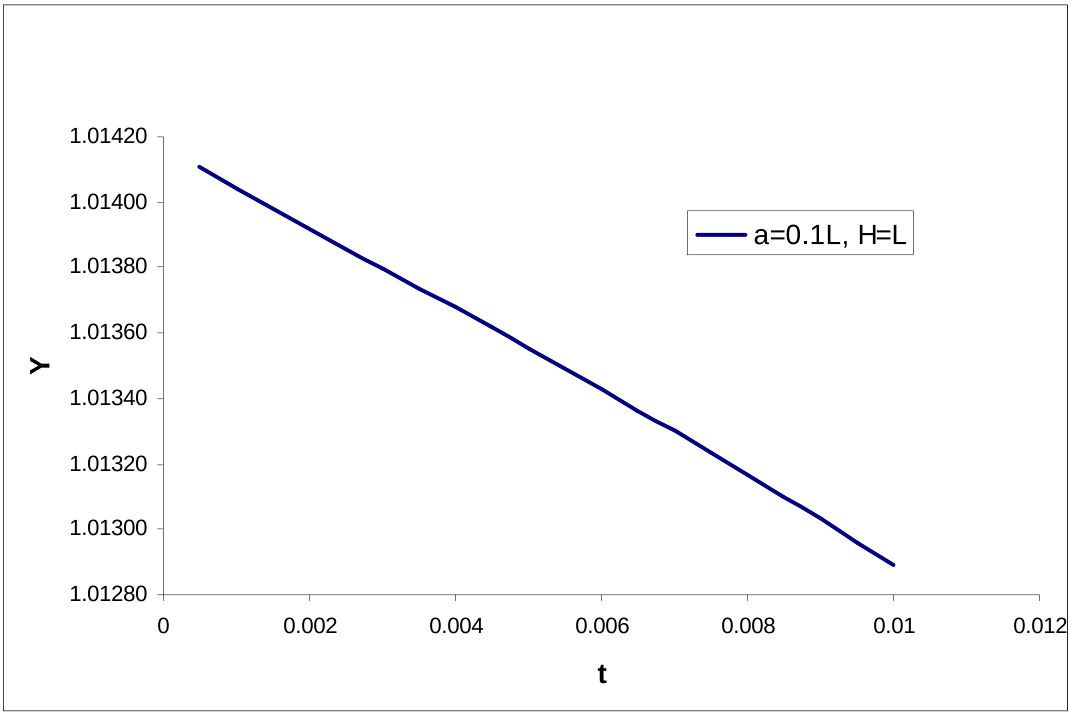

Figure 5.4: Variation of dimensionless stress intensity factor vs. thickness of plate when a = 0.1L, H = L

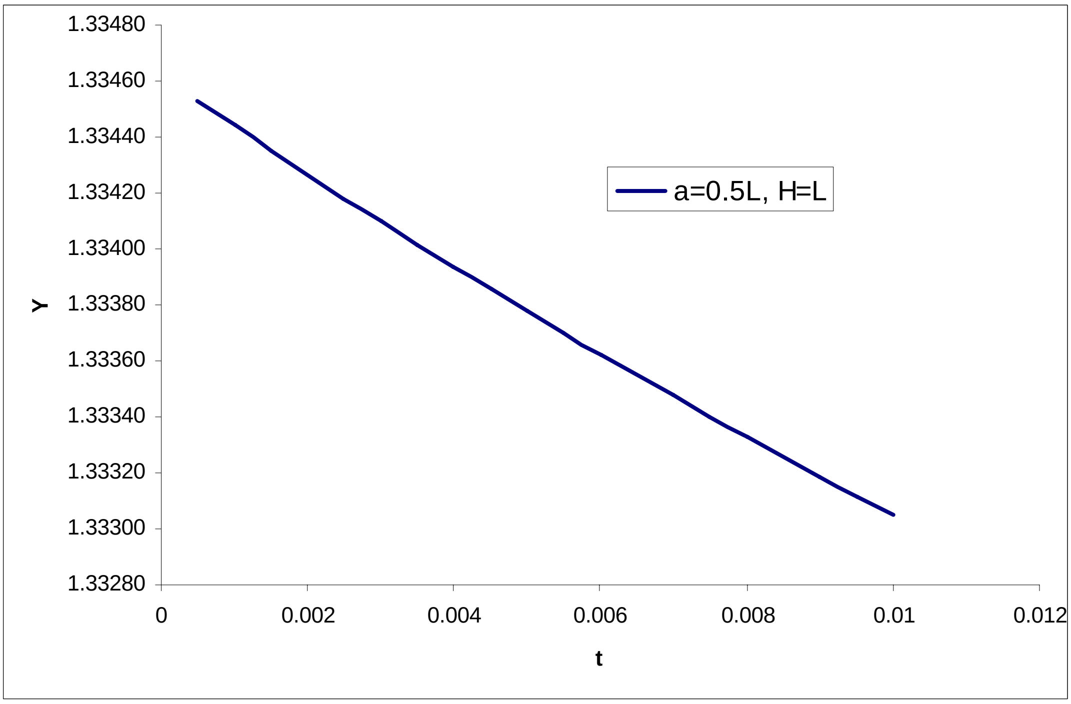

Figure 5.5: Variation of dimensionless stress intensity factor vs. thickness of plate when a = 0.5L, H = L

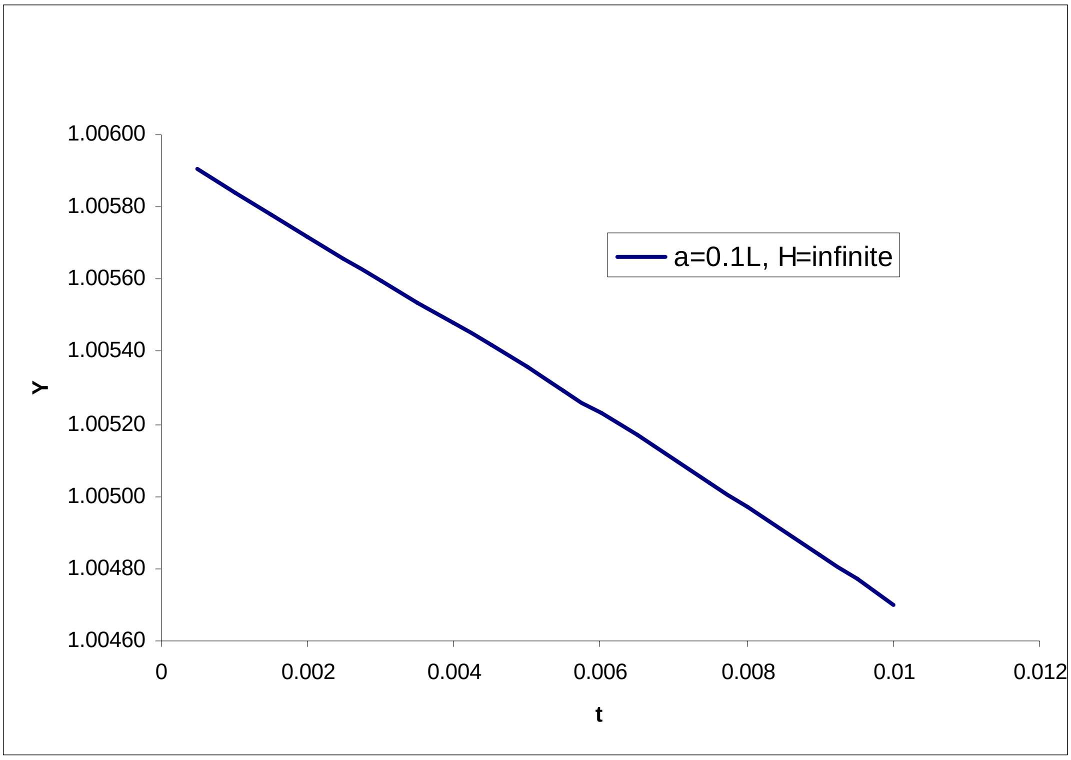

Figure 5.6: Variation of dimensionless stress intensity factor vs. thickness of plate when a = 0.1L, H = infinite

5.1.3 Infinite stripe condition

As we had already mentioned, the stress intensity factor depends on the geometry of the plate we are considering. For the most general and simple case, dimensionless stress intensity value for an infinite plate with a center through crack under tension is equal to Y = 1 as shown in Figure 5.7. In particular, it depends on the ratio H/L. On Table 5.2 we display the values of dimensionless stress intensity factor Y, determined again using ANSYS, for different geometries. We note that as the value of H/L increases, the values of Y tend to the values of the right column ($H/L = \infty$), which refers to values that we would expect for an infinite stripe with a center through crack under tension, as in Figure 5.8. These values have been computed by using the software package NASGRO.

The condition that how the infinity condition of the height of the solid is achieved should also be investigated. This task is achieved by doing the same analysis and increasing the height of the geometry. Then, the results are compared with each other and when the discrepancy between them are insignificant, it can be said that the condition of infinity for the height of the geometry is obtained.

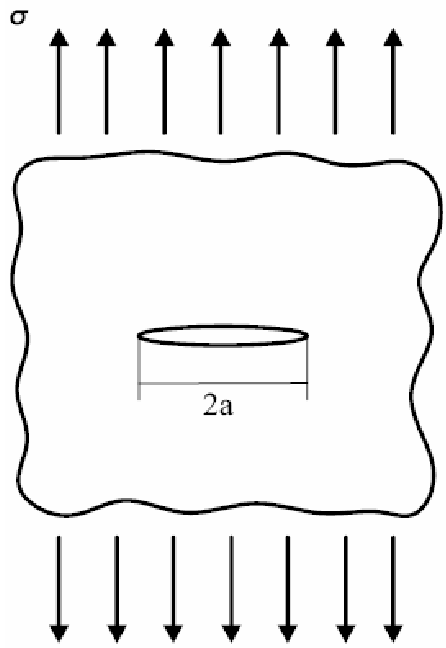

Figure 5.7: Infinite plate with a center through crack under tension

$K_I = \sigma\sqrt{\pi a}$, $\qquad Y = 1$

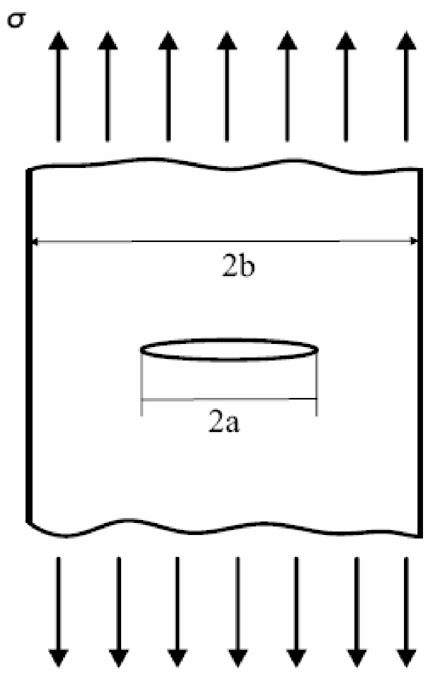

Figure 5.8: Infinite stripe with a center through crack under tension

When the height (*H*) of the plate goes to infinity plate shape becomes a strip and some analytical equations are available such as shown below.

Irwin [45]: $K_I = \sqrt{\frac{2b}{\pi a}\tan\frac{\pi a}{2b}}\sigma\sqrt{\pi a}$, $Y = \sqrt{\frac{2b}{\pi a}\tan\frac{\pi a}{2b}}$ (5.4)

Feddersen [83]: $K_I = \sqrt{\sec\frac{\pi a}{2b}}\sigma\sqrt{\pi a}$, $Y = \sqrt{\sec\frac{\pi a}{2b}}$ (5.5)

Tada [15]: $K_I = \left[1 - 0.025(a/b)^2 + 0.06(a/b)^4\right]\sqrt{\sec\frac{\pi a}{2b}}\sigma\sqrt{\pi a}$,

$$Y = \left[1 - 0.025(a/b)^2 + 0.06(a/b)^4\right]\sqrt{\sec\frac{\pi a}{2b}} \tag{5.6}$$

These equations are theoretically derived based on geometries of infinite dimensions ($H \rightarrow \infty$). Using the software ANSYS, we also determined the value of the dimensionless stress intensity factor Y for high ratios of H/L. In Table 5.5 we display some values of Y calculated for various plate thicknesses from abovementioned theoretical approaches and also ANSYS, up to three significant digits. It can be seen that our results, identified by finite element method, are in line with those predicted by those theoretical and empirical equations.

Table 5.5: Variation of dimensionless stress intensity factor vs crack length under infinite stripe condition

t	H/L=1.8	H/L=2.5	H/L=4	NASGRO	Irwin	Feddersen	Tada
0.1	1.006	1.005	1.004	1.006	1.004	1.006	1.006
0.2	1.025	1.025	1.024	1.025	1.017	1.025	1.024
0.4	1.113	1.110	1.109	1.112	1.075	1.112	1.109
0.6	1.307	1.304	1.303	1.304	1.208	1.304	1.303
0.8	1.819	1.816	1.810	1.799	1.565	1.799	1.814

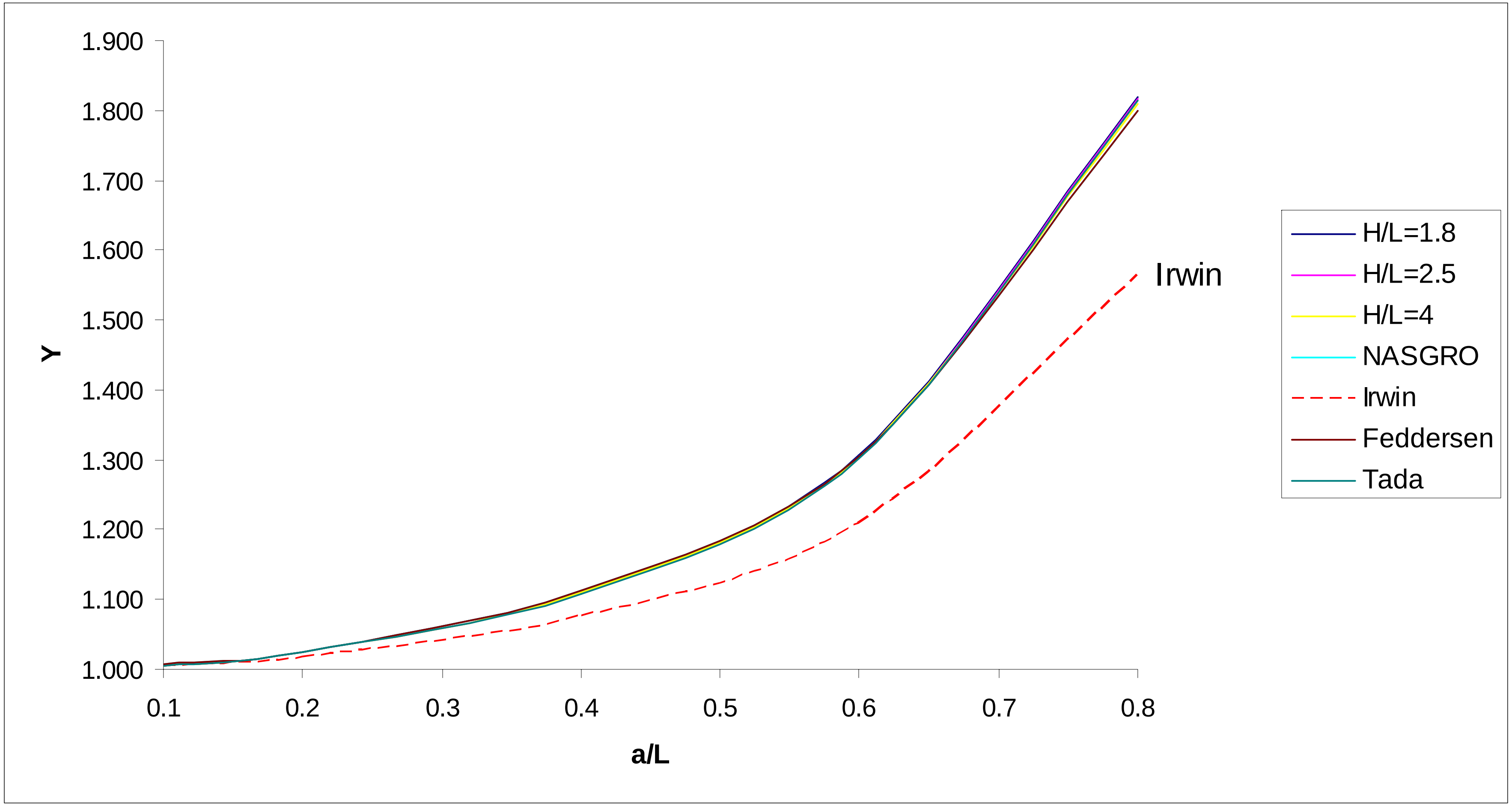

Figure 5.9: Compared results for infinite plate (strip) conditions

As can be seen from Figure 5.9, other than the Irwin's approach for the infinite strip condition, ANSYS solution and NASGRO software, Feddersen and Tada have results in very good agreement. In order to achieve the infinite plate conditions by using ANSYS, it is sufficient to model the height of the plate equal to H = 1.8 with less than %0.4 error percentage comparing to the Feddersen (and also NASGRO) results.

Table 5.6: Error percentage of infinite strip conditions from analytical solutions

a/L	Error % H=1.8L	Error % H=2.5L	Error % H=4.0L
0.1	0.02	0.07	0.21
0.2	-0.07	0.00	0.06
0.4	-0.31	-0.06	-0.02
0.6	-0.35	-0.07	-0.03
0.8	-0.28	-0.09	0.22

5.1.4 Aggrement with Analytical solution

Aliabadi [38] computed the stress intensity factor for the finite geometry represented in Figure 5.10.

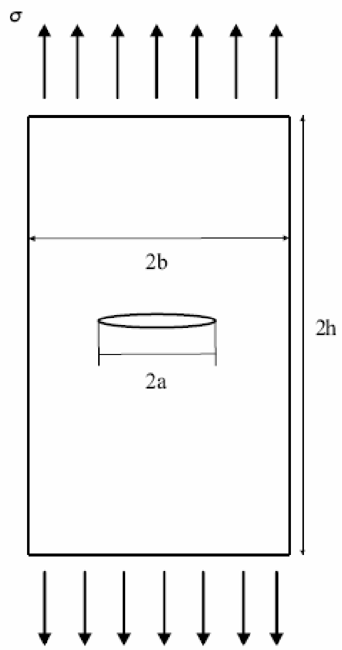

Figure 5.10: Finite plate with a center through crack under tension

He considered a rectangular plate, of height 2h, width 2b, with a central through crack of length 2a, which was loaded from its upper and lower edges by a uniform tensile stress σ. For the special case of h = b, he estimated

$$K_I = \sigma\sqrt{\pi a}\begin{pmatrix} 1 + 0.043\left(\dfrac{a}{b}\right) + 0.491\left(\dfrac{a}{b}\right)^2 + 7.125\left(\dfrac{a}{b}\right)^3 - 28.403\left(\dfrac{a}{b}\right)^4 \\ + 59.583\left(\dfrac{a}{b}\right)^5 - 65.278\left(\dfrac{a}{b}\right)^6 + 29.762\left(\dfrac{a}{b}\right)^7 \end{pmatrix} \tag{5.7}$$

K_I values were computed using Equation 5.7, we also determined the value of the dimensionless stress intensity factor Y for the same geometry, using the numerical package ANSYS. In Table 5.7, some values of Y are displayed. It can be seen that our results, identified by finite element method in the present study, are in line with those predicted by Aliabadi. We further illustrate this analysis in Figure 5.11, for which more data points were taken.

Table 5.7: Comparison of FEM results with Aliabadi's [38] results

	a = 0	a = 0.1L	a = 0.2L	a = 0.3L	a = 0.4L	a = 0.5L	a = 0.6L	a = 0.7L	a = 0.8L
Aliabadi	1.0000	1.0140	1.0551	1.1231	1.2162	1.3342	1.4812	1.6803	2.0162
FEM	1.0000	1.0140	1.0558	1.1237	1.2167	1.3344	1.4817	1.6782	1.9927
Error %	0.0	0.0	-0.1	-0.1	0.0	0.0	0.0	0.1	1.2

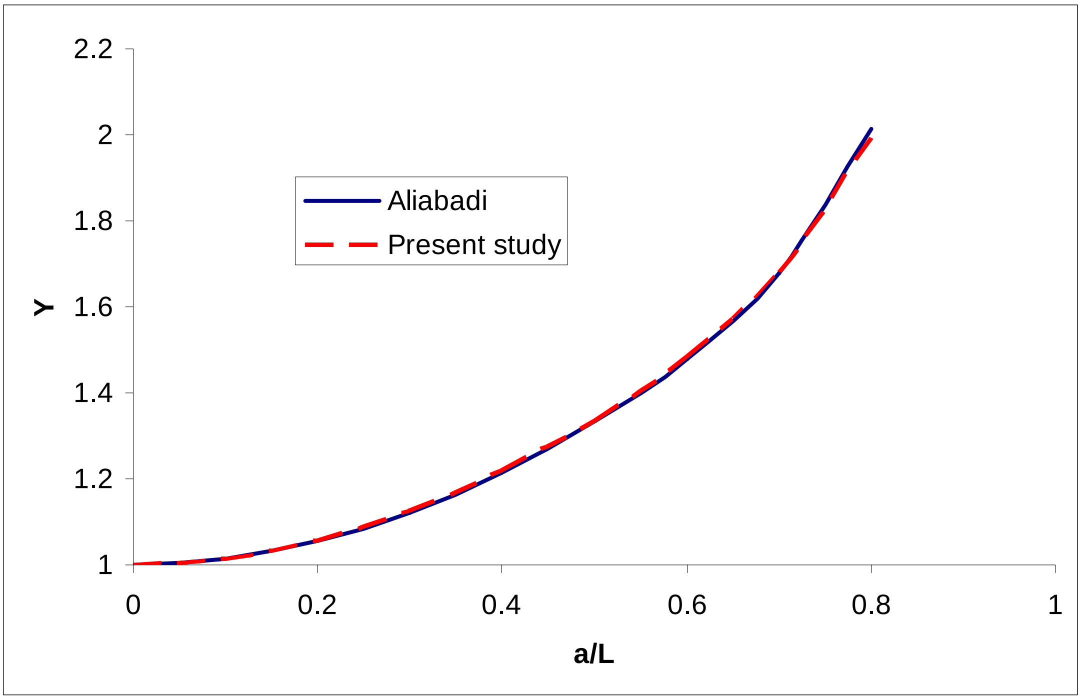

Figure 5.11: Compared FEM results with Aliabadi [38]

5.1.5 Dependancy of SIF on Young's Modulus and Poisson's ratio

By changing the Young's modulus values from $E_0 = 1x10^5$ MPa to $E = 3x10^5$ MPa, it is seen that stress intensity factors do not depend on the value of the Young's modulus.

Table 5.8: Effect of Poisson's ratio on dimensionless SIF

Poisson's ratio	a = 0.1 L, H = L	a = 0.4L, H = 0.5L
0.20	1.0140233	1.6304454
0.25	1.0140430	1.6304131
0.30	1.0140418	1.6303505
0.35	1.0140075	1.6302368

For the special case of a = 0.1L and H = L, the dependancy of stress intensity factor to poisson's ratio is as below

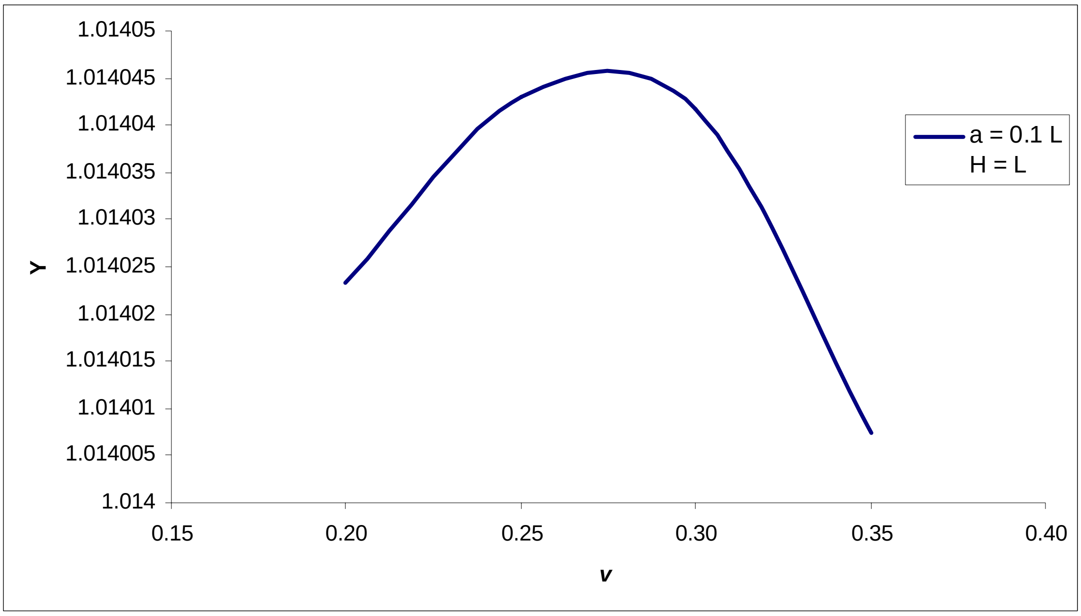

Figure 5.12: Variation of poisson ratio

In this thesis, it is presented that the dependency of the stress intensity factor to Poisson's ratio is insignificant. It is also shown that the stress state and Poisson's ratio ν can negatively influence the results, particularly in any of these circumstances: plane strain, large value of ν, and/or coarse angular discretization. To circumvent this effect, a null Poisson's coefficient is recommended. Besides, a fine angular discretization helps to minimize the error.

5.1.6 Mesh convergence

In the finite element analysis, it is obvious that more meshes approximate to exact solution. But it also leads to spending more computational time. Finding out the balance between the mesh density and the computational time is necessary. Optimum mesh can be obtained by a trial and error procedure. Therefore, the following cases are taken to simulate the effects on the sensitivity and converge of SIF with different mesh parameter.

In the model, crack length a is set as a reference for the element sizing. Simulations are performed for different sets of element lengths near crack tip. The element lengths near crack tip are varied from a/4 to a/8, where a is 0.01m. The procedure indicates that an a/10 mesh density is sufficient for the analysis. By comparing to Isida's [16] results of Table 5.1, it can easily be seen that there is a good agreement (less than 0.1% error) between numerical and analytical results for the fine mesh configuration with the element length of a/10, so the model is proved to be reliable for further analyses. According to these results, the element length a/10 near crack tip has been used throughout the study. The mesh characteristics of model for a specific geometry is given in Table 5.9.

Table 5.9: Result Convergence of Element Size Near Crack Tip

Mesh Type	Element length	K_I	Node #	Element #
Coarse mesh	a/4	1.01218	12875	1235
Medium mesh	a/8	1.01394	21356	3756
Fine mesh	a/10	1.01401	32035	5480

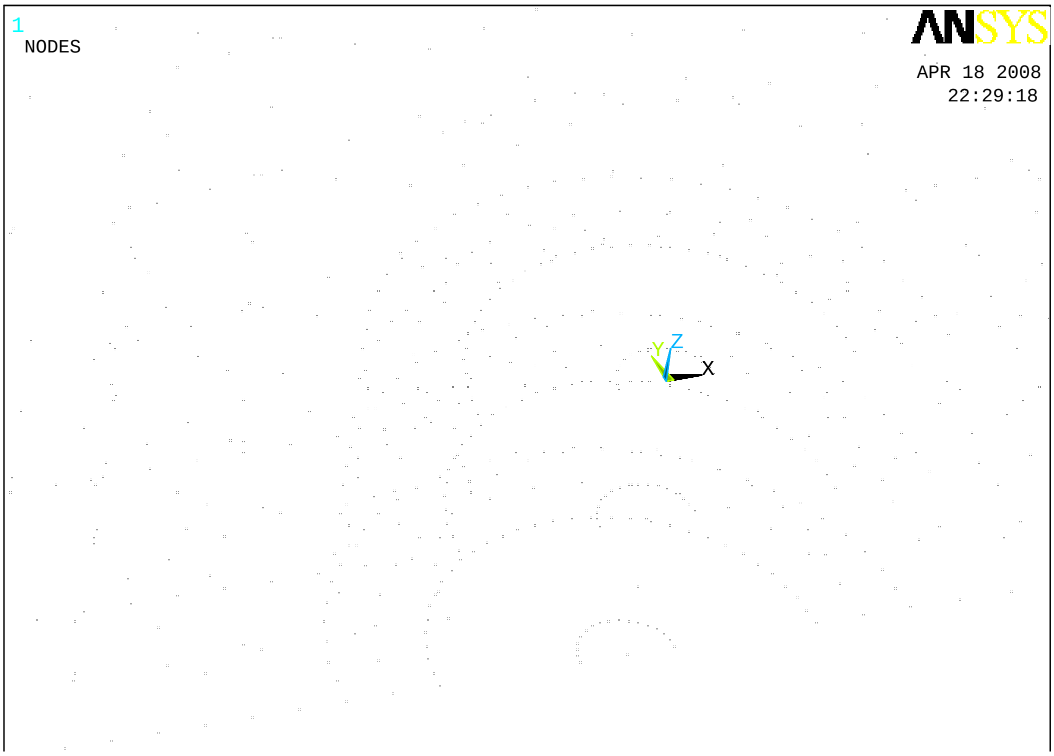

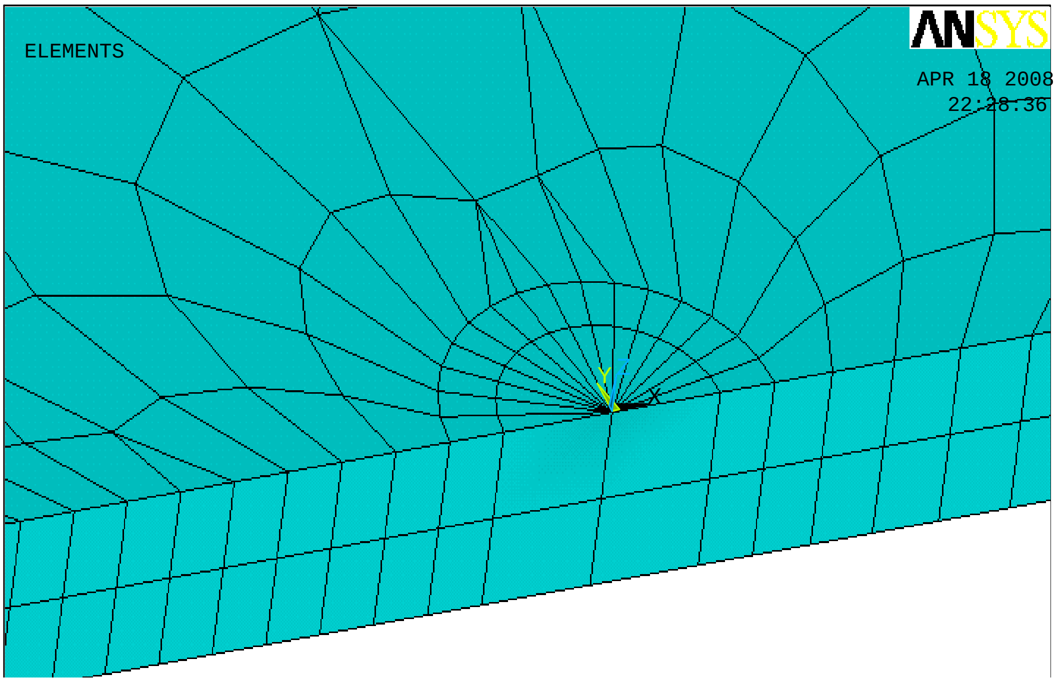

Figure 5.13: Zoom on crak tip region. Detail of nodes and quarter-point elements when radius of singular elements = a/16

Also the concentration point about which an area mesh will be skewed for modelling crack tip has been examined. The concentration has been performed by using ANSYS KSCON command which assigns element division sizes around a keypoint and generates singular elements around the crack tip. As a rule of thumb, for reasonable results, the first row of elements around the crack tip should have a radius of approximately *a*/8 or smaller, where *a* is the crack length. In the circumferential direction, roughly one element every 30° or 40° is recommended [33].

So the radius of the first row of elements around the crack tip is an essential parameter in the calculation of stress intensity factor values if quarter point elements are used to model in finite element method. This radius has been given three other values such (a/8), (a/16), (a/32) and the accuracy has been investigated.

Table 5.10: Result Convergence of singular element radius

Mesh Type	Element length	K_I	Node #	Element #
Coarse mesh	a/8	1.01389	21564	3756
Medium mesh	a/16	1.01401	32035	5480
Fine mesh	a/32	1.01402	58765	9845

First, it has been shown that the displacement extrapolation technique can give very accurate predictions, even for coarse meshes, if a good angular discretization is made around the crack tip. The method based on a two-term extrapolation of the displacement field, brings the best results for large element sizes, with differences from the reference value of K_I well under 1%.

A mesh refinement attending only to the element length, *l*, brings no benefits to the accuracy of K_I predictions. Even worse, if the angular discretization is too rough, e.g. 90° or 60° elements, a wrong K_I limit can be reached when *l* tends to zero. A minimum angular discretization with six elements around the tip, 30° each, is recommended [8].

5.2 Patch Repaired Plate with a Central Crack

A thin rectangular sheet of parametrical dimensions shown in Figure 5.14 is subjected to a uniform, uniaxial tensile stress of 1MPa perpendicular to crack is considered. The sheet contains a central crack 0.01 long (1/10 of the plate width) which is patched on both ends by the same material of the plate. The plate and the patch is isotropic and various thicknesses of patch are considered. Further, the bond between the cracked plate and the patch is assumed to be complete, i.e. without any interface between the two structural components.

Because of the symmetrical nature of the problem, only one-quarter of the structure was analyzed. Table 5.11 and Figure 5.15 shows the effect of the increasing patch thickness.

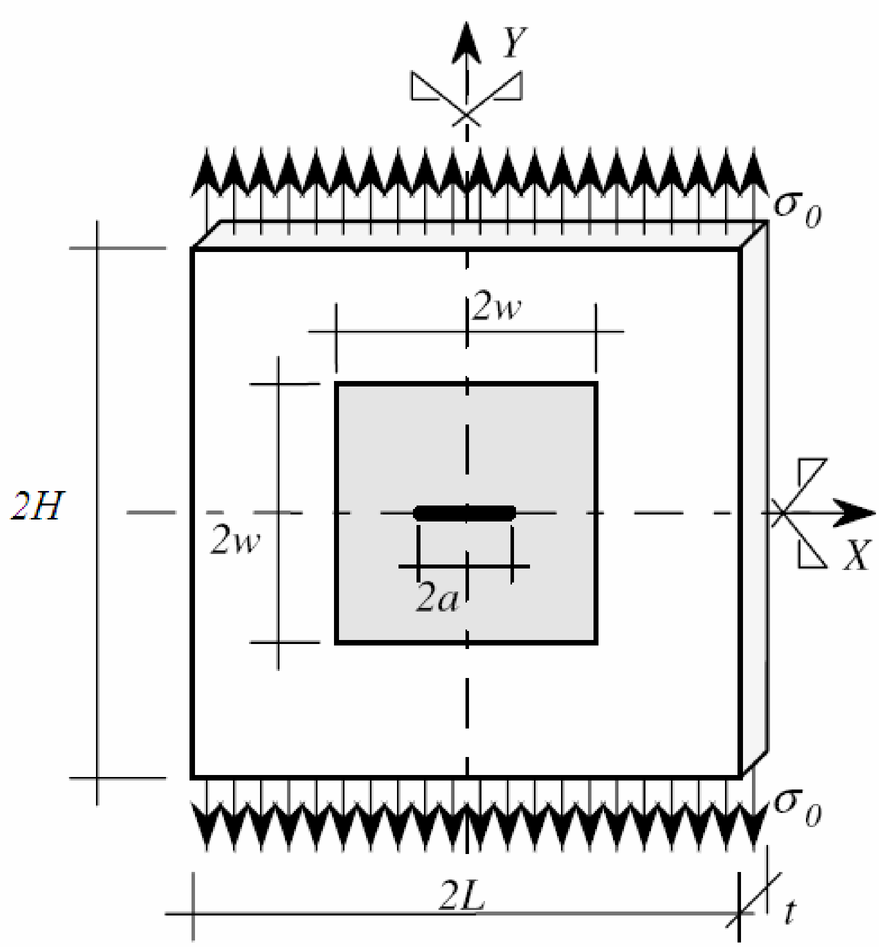

Figure 5.14: Patch repaired plate with a central crack

Geometry:

- L = 0.1 m
- H = 0.1 m
- a = 0.01 m
- t = 0.001 m
- E, Young modulus = 210000 MPa
- v, Poisson ratio = 0.3
- w = 0.03 m

- σ_0 = 1 MPa

Table 5.11: Dimensionless stress intensity factor vs. bonded patch thickness

Patch thickness (m)	K_I (MPa.m$^{1/2}$), Present Method
0	1.0140
0.001	0.17186071
0.002	0.11064065
0.003	0.08243152
0.004	0.06539785
0.005	0.05594784
0.006	0.05182539
0.007	0.04585213
0.008	0.04320349
0.009	0.04048982
0.010	0.03822103

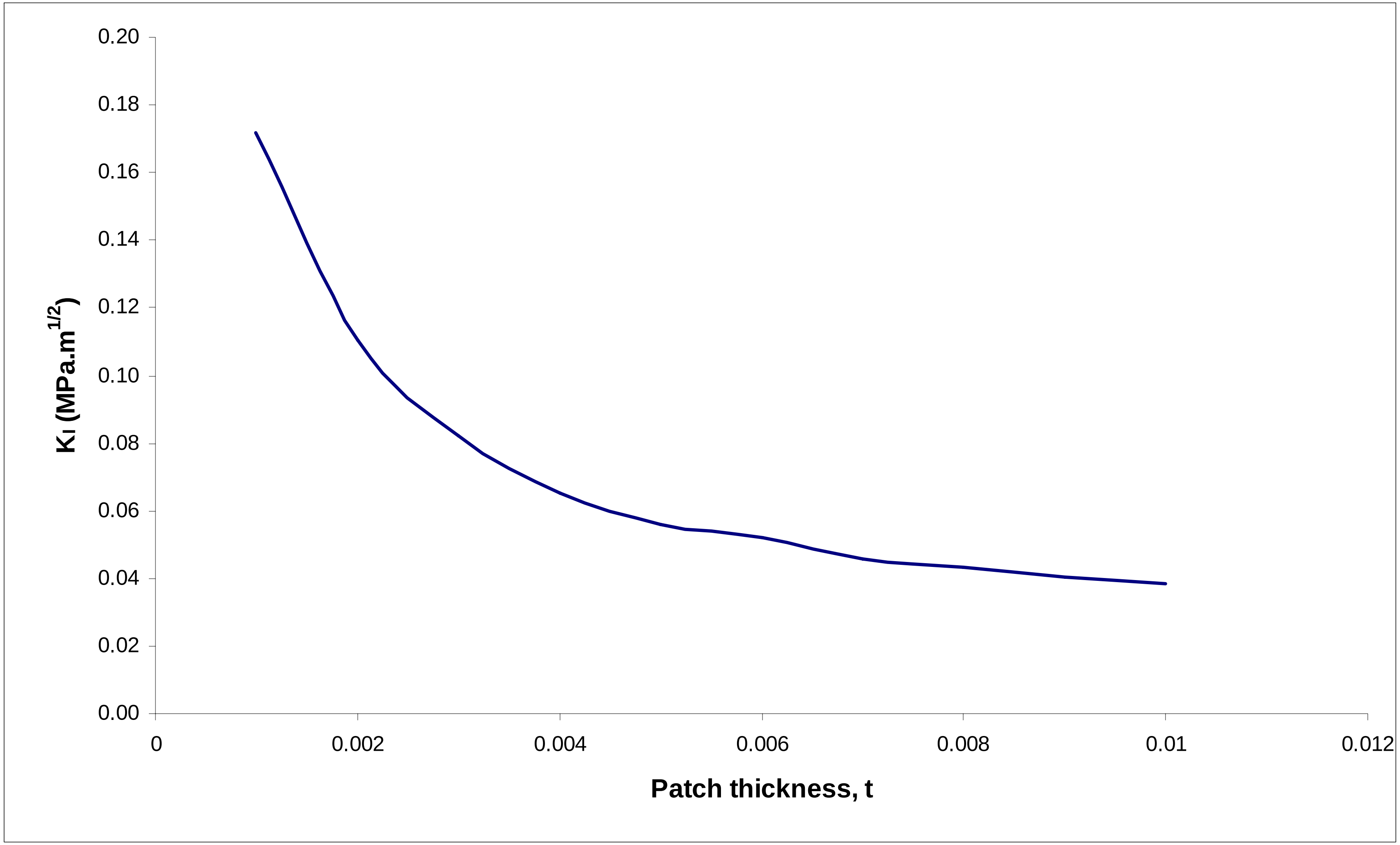

Figure 5.15: Variation of K_I with respect to patch thickness

5.2.1 Variation of stress intensity factor with a/L ratio

For the patch width of w = 0.5L as shown in Figure 5.17, the values in Table 5.12 are calculated with ANSYS APDL.

Table 5.12: Change of dimensionless SIF with respect to crack length

a/L	K_I (MPa.m$^{1/2}$)
0.1	0.1834
0.13	0.1614
0.16	0.1487
0.19	0.1341
0.22	0.1273
0.25	0.1172
0.28	0.1168
0.31	0.1079
0.34	0.1083
0.37	0.0972
0.40	0.0932

These results and a sixth polynomial trendline representing the variation are plotted in Figure 5.16.

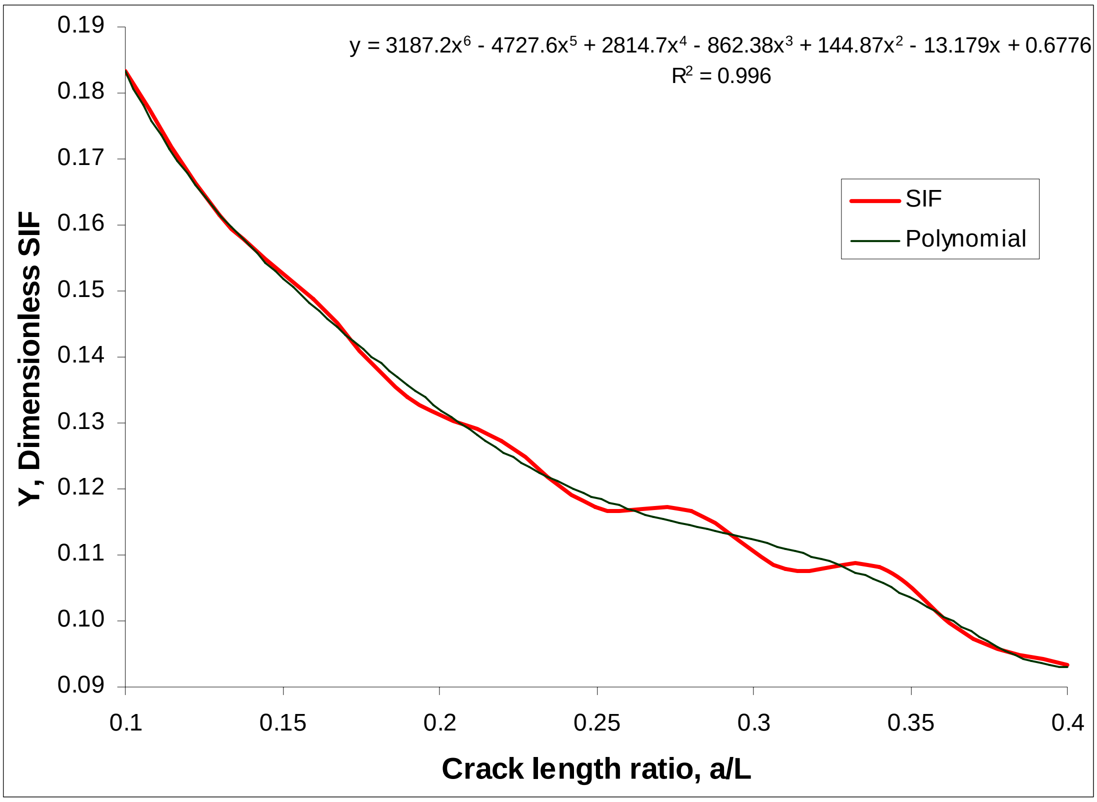

Figure 5.16: Variation of dimensionless stress intensity factor with respect to a/L when w = 0.5

A trendline shows the trend in a data set and is typically associated with regression analysis. Creating a trendline and calculating its coefficients allows for the quantitative analysis of the underlying data and the ability to both interpolate and extrapolate the data for forecast purposes.

An order of six polynomidal trendline is added in order to quantitatively analyze the behaviour of the crack length and Y dependancy. Notice that the R-squared value is 0.996, which is a perfect fit of the line to the data.

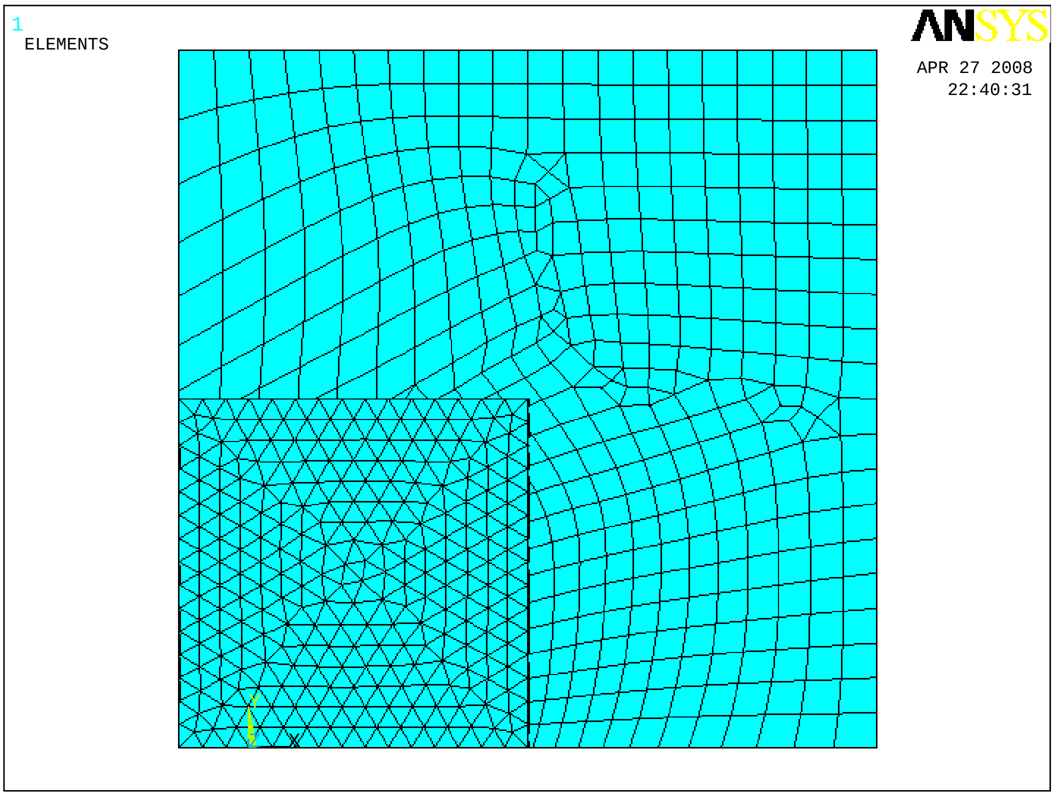

Figure 5.17: Mesh model for w = 0.5L

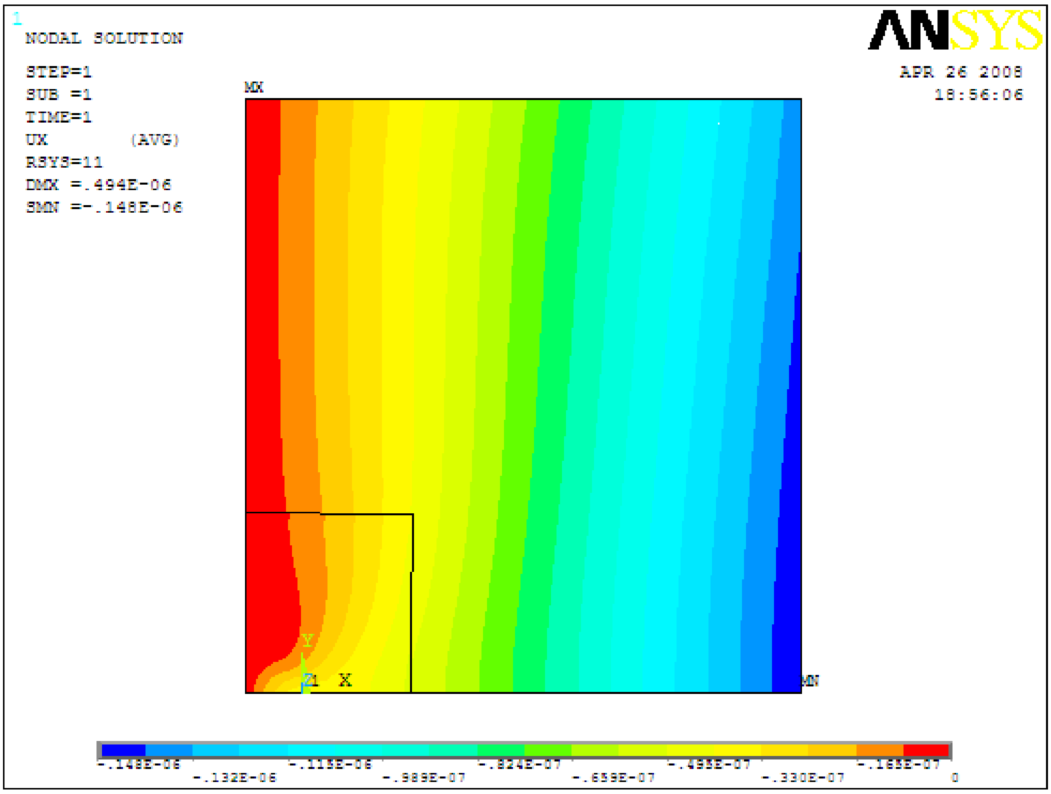

Figure 5.18: x-component of displacement contours

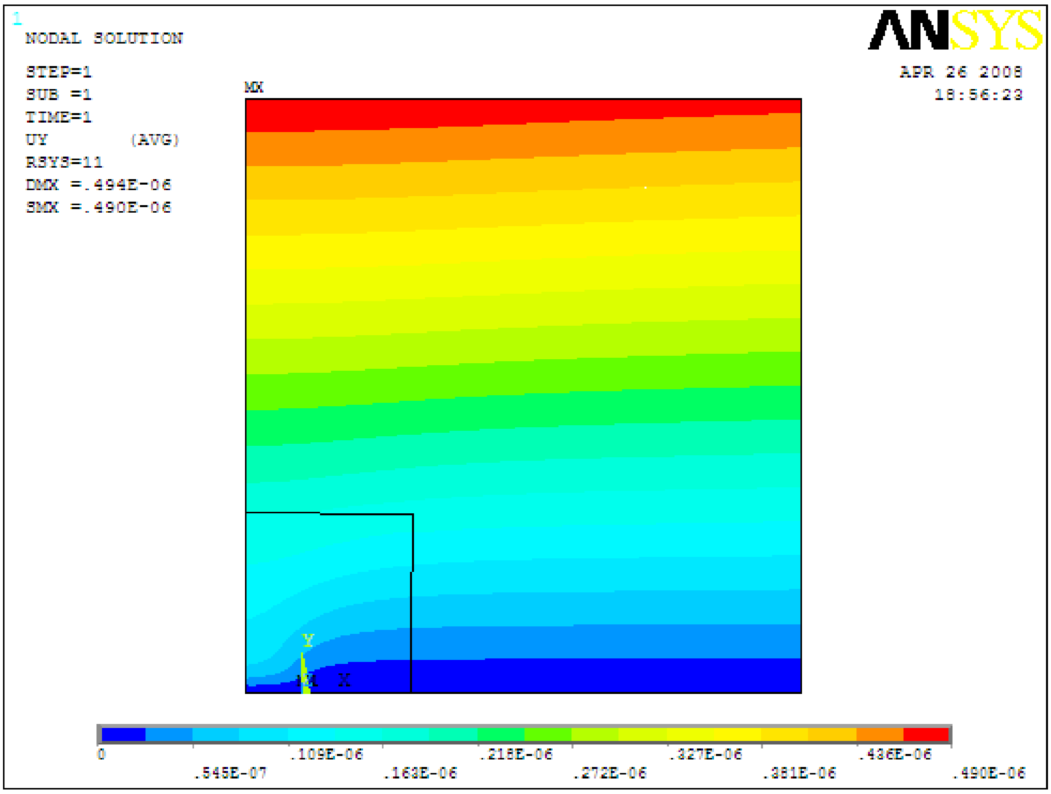

Figure 5.19: y-component of displacement contours

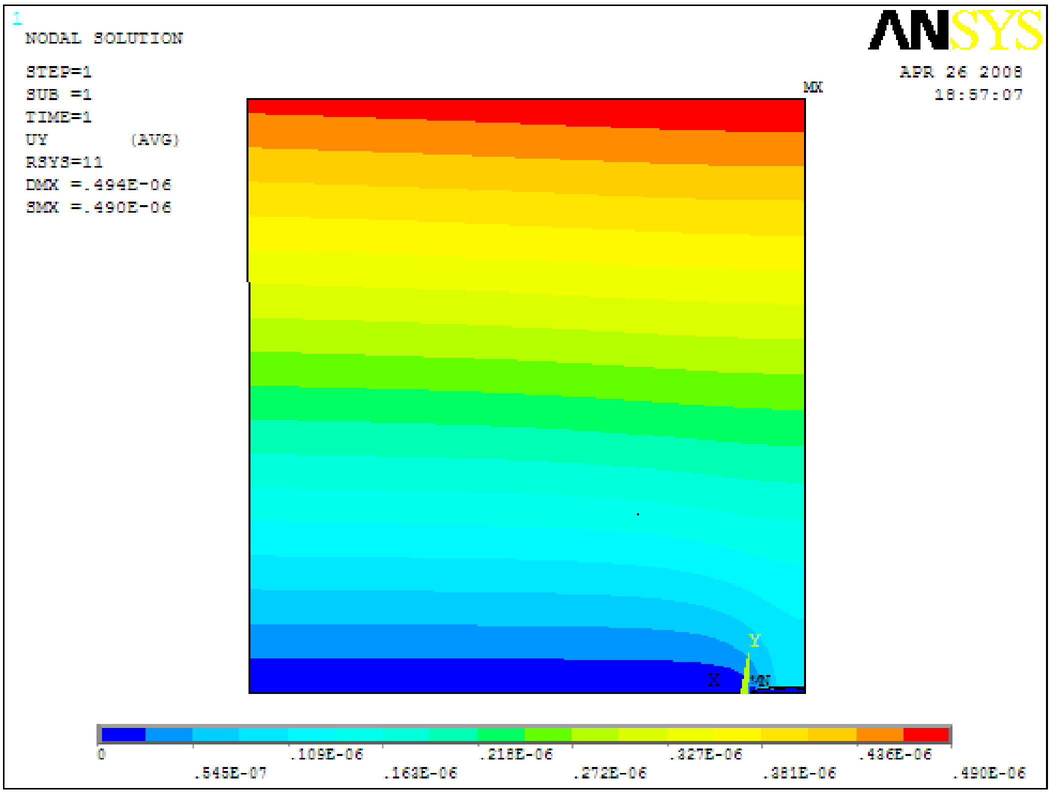

Figure 5.20: y-component of displacement contours from the back side

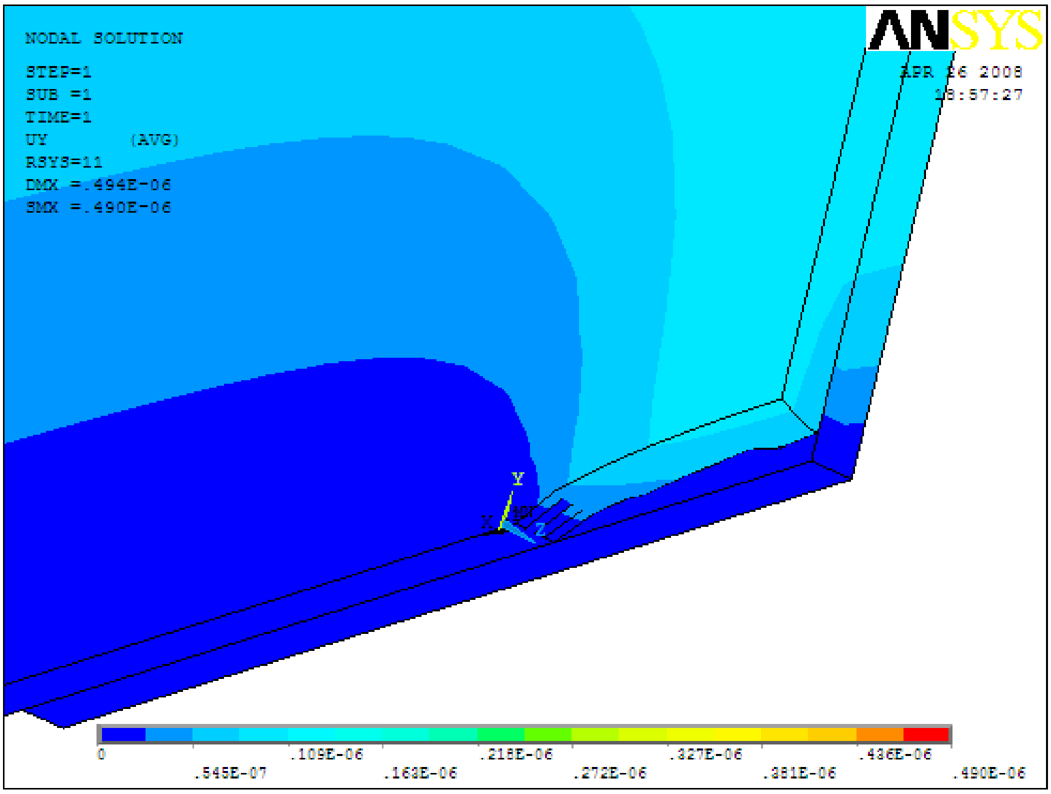

Figure 5.21: Zoom on crack tip. Note the crack deformation on the crack face.

5.2.2 Accuracy of the model

In this section, the numerical codes written in ANSYS APDL is applied to a specific geometry, which was solved by Jones and Callinan [39], and the results are compared and analysed.

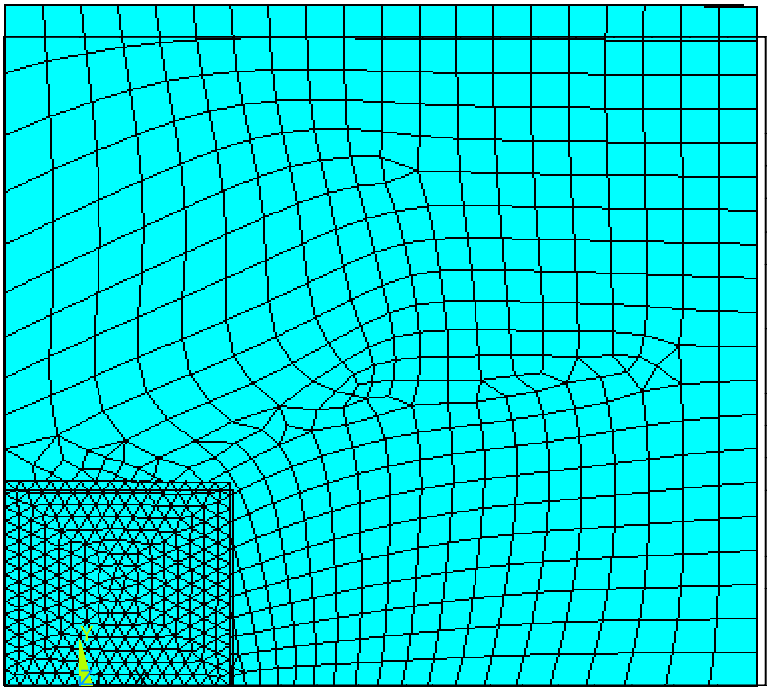

Figure 5.22: Meshed model used in analysis

Geometry: (Same as Ref [39])

- L = 508 mm
- H = 635 mm
- a = 38.1 mm
- t = 2.3 mm
- E, Young modulus = 71020 MPa
- v, Poisson ratio = 0.32
- w = 100.8 mm
- h = 12.7 mm
- σ_0 = 689 kPa

Table 5.13: Comparison of K_I values with previous studies

Patch thickness (mm)	K_I (kPa.m$^{1/2}$), Present study	K_I (kPa.m$^{1/2}$), Jones & Callinan [39]	K_I (kPa.m$^{1/2}$), Arin [40]
0	168.52	166.2	N/A
0.127	85.70	77.8	75.4
0.254	65.31	65.0	61.4
0.381	55.68	57.9	51.9
0.508	49.80	53.1	44.7
0.635	45.69	N/A	N/A
0.762	42.57	46.7	31.3

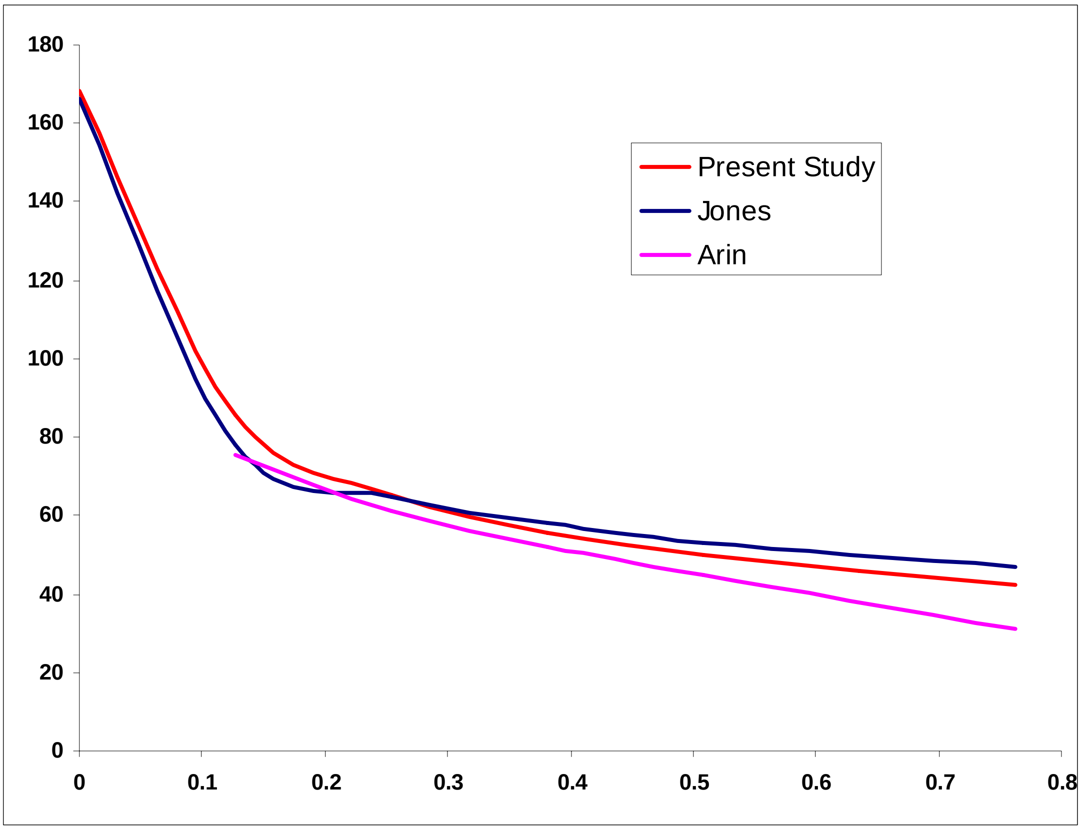

Figure 5.23: Comparision of K_I values with previous studies

From Table 5.12 we see that patching is a very efficient way of lowering the stress intensity factor and that the increasing of patch thickness continually decreases the value of the stress intensity factor.

The stresses in the patch are predominantly σ_y stresses ($\sigma_x \cong \tau_{xy} \cong 0$) and are fairly constant across the width of the patch, the only exception being at the crack, i.e., on the x axis. These stresses are shown in Figure 5.24 where we see that for each thickness of patch the maximum stresses occur in the region of the crack and decay monotonically toward the edges of the patch. Far from crack tip to the edge of the patch it can be seen that the σ_y stress becomes very close to the applied stress. And also as shown in Figure 5.24 and Table 5.14, for increasing thickness of the patch, the maximum σ_y stress and the average stress decreases. The maximum σ_y stress is shown in Table 5.14 for various thicknesses of the patch.

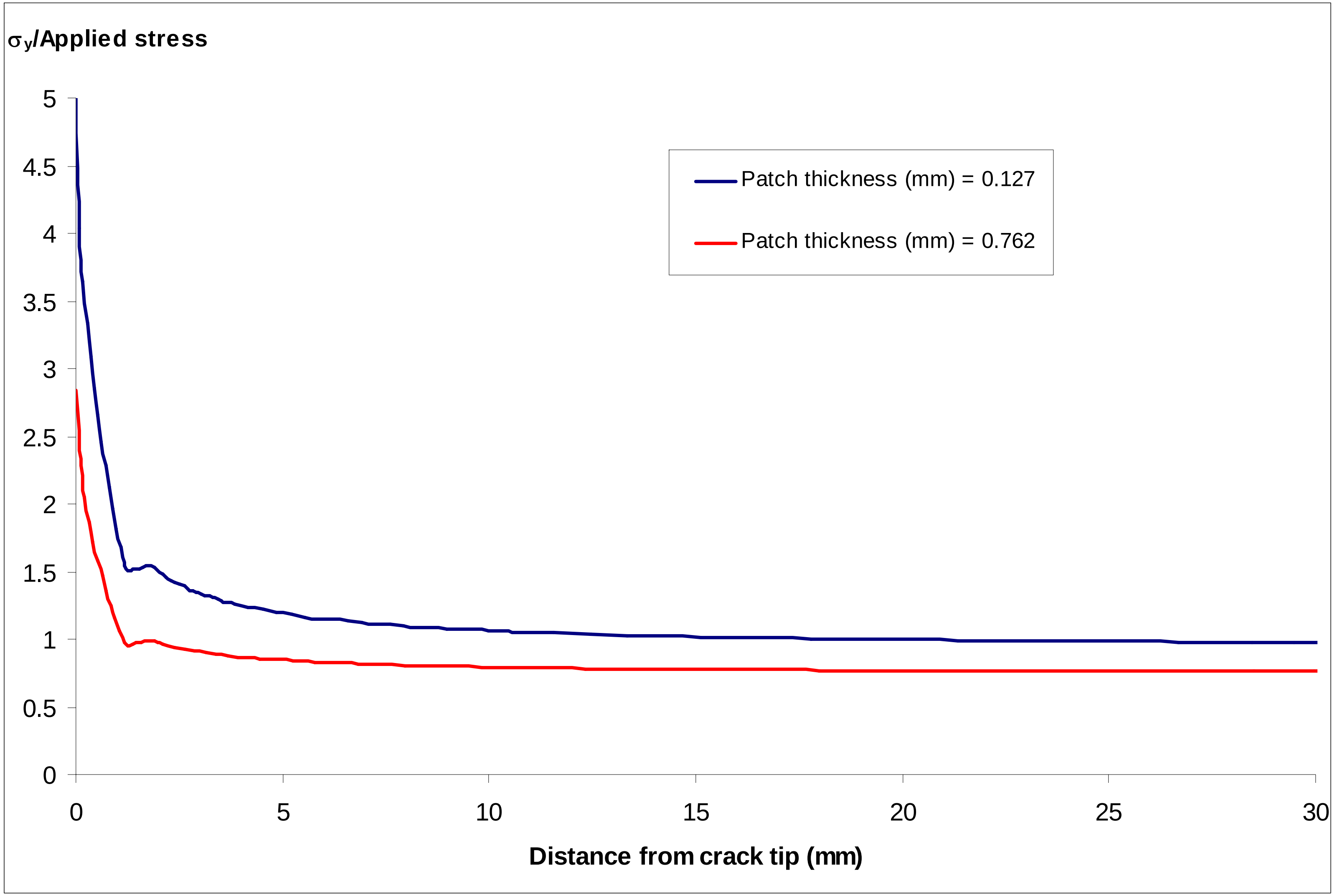

Figure 5.24: Variation of patch stress (σ_y) with distance from crack

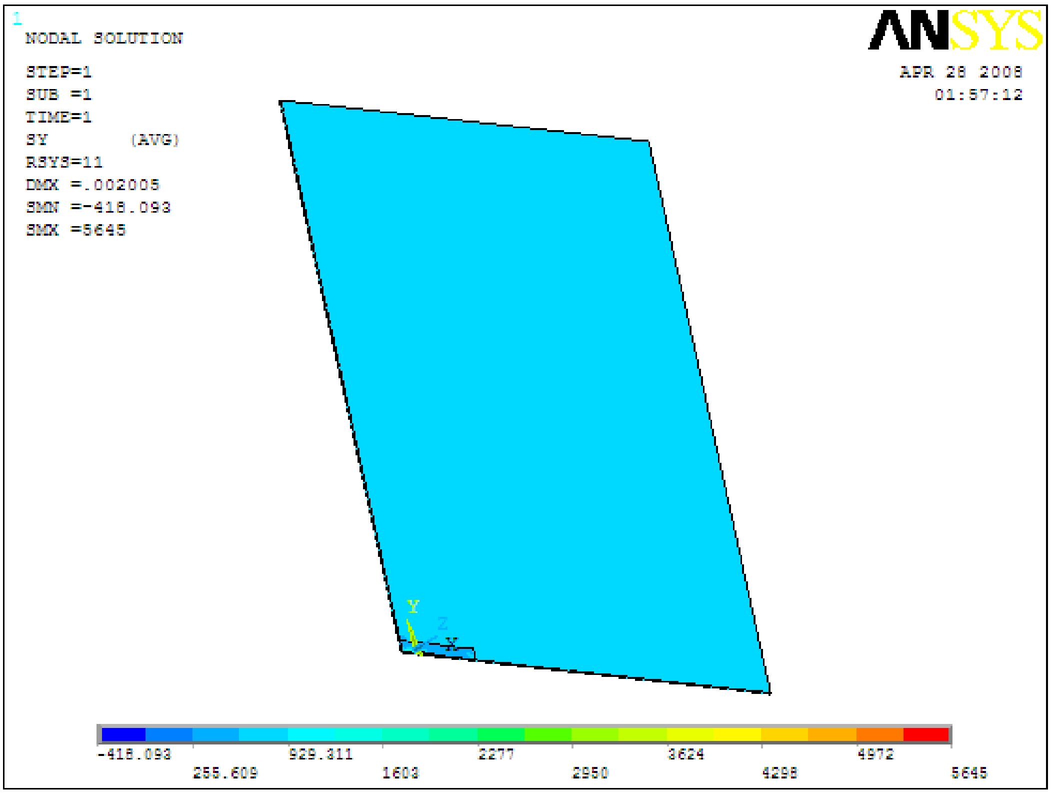

Figure 5.25: σ_y stresses throughout the plate for patch with thickness 0.508. Note that the stress is constant across the plate except the crack region.

Table 5.14: Maximum σ_y stresses occurred for varying patch thicknesses

Patch thickness (mm)	$\sigma_{y\ max}$ (kPa)
0.127	18419
0.254	10120
0.381	7164
0.508	5645
0.762	4235

Applied tensile stress = 689 kPa

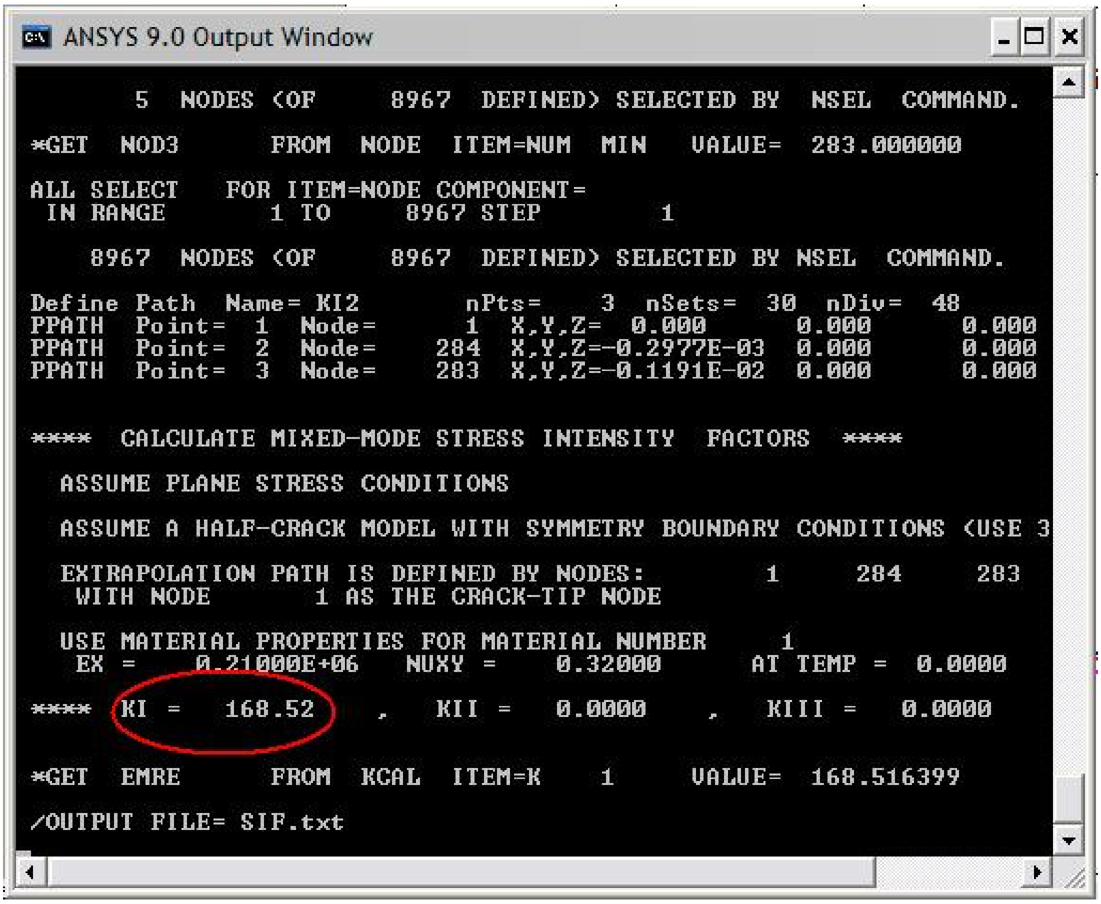

Figure 5.26: ANSYS output window shows the K_I value for the specified geometry when the patch is not present. K_I = 168.52

It is remarkable to note that the result of the patchless solution (168.52 kPa) is even more accurate than the reference solution (166.2 kPa). Reference [39] states "It is interesting to note that, when the patch is not present, the method yields the value K_I = 166.2 kPa, which differs by only 1% from the exact analytical result of 168.5 kPa." The result we found yields the exact analytical result without any error.

5.3 Plate With Irregular Patch

In this section, a patch bonded onto the plate with irregular shape as shown in Figure 5.27 is examined. The shape of the patch is determined with eleven keypoints which are joined by a spline fitted through the keypoints. The patch shape is under the geometric constraint that the extension of the patch must remain inside the allowable square region with width of w = 0.3 L.

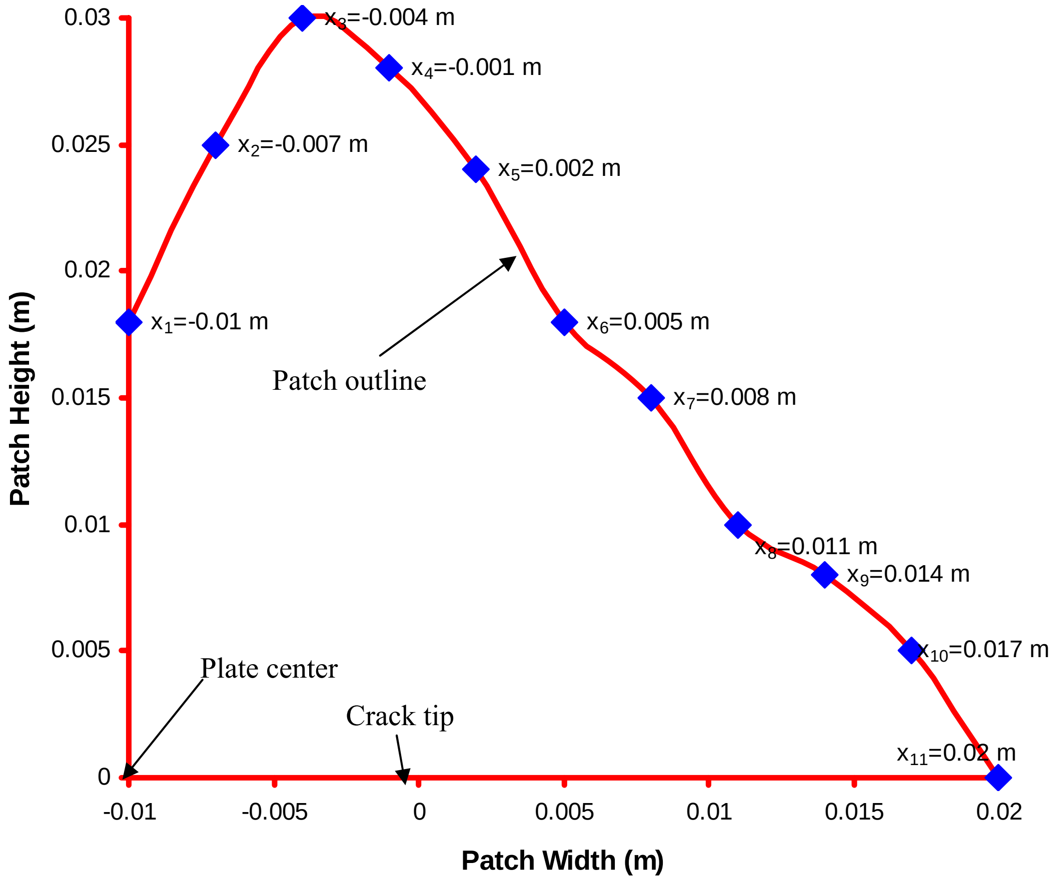

Figure 5.27: The example of an outline of the patch shape, which is determined by the blue spline keypoints

Geometry

- a/L = 0.1
- H/L = 0.1
- t/L = 0.01
- t_p/L= 0.01
- E = 210000 MPa
- v = 0.3
- w = 0.03 m
- σ_0 = 5.6419 MPa (In order to satisfy K_I = Y)
- Spline keypoints: y_1=0.02, y_2=0.025, y_3=0.035, y_4=0.05, y_5=0.043, y_6=0.038, y_7=0.03, y_8=0.025, y_9=0.015, y_{10}=0.01

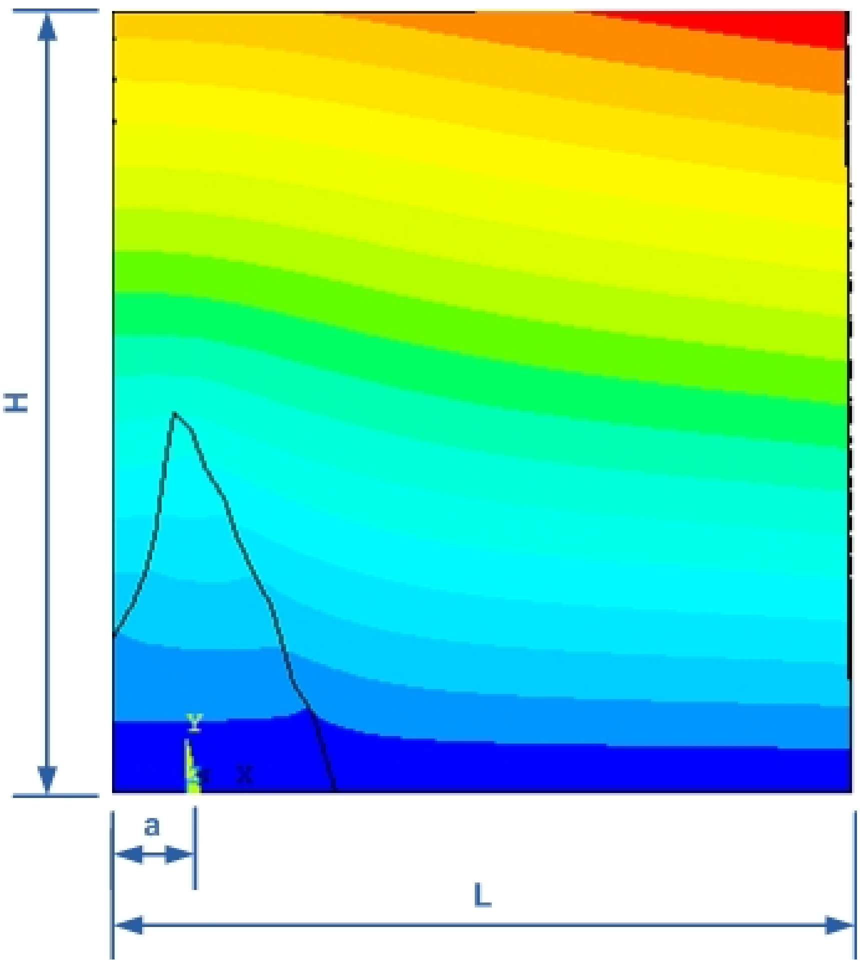

Figure 5.28: y component of displacement curves for the irregular curved patch for spline keypoints of y_1=0.02, y_2=0.025, y_3=0.035, y_4=0.05, y_5=0.043, y_6=0.038, y_7=0.03, y_8=0.025, y_9=0.015, y_{10}=0.01

The stress intensity factor is calculated through the given data by the developed APDL code (Appendix A) and the calculations yielded the result as below:

$K_I = 0.18064$ MPa.m$^{1/2}$

σ_{ymax} = 12.073 Mpa

By referring to Table 5.11, for the same configuration with a w = 0.3L square patch (Figure 5.29) yielded the result of

$K_I = 0.17186$ MPa.m$^{1/2}$

σ_{ymax} = 11.47 MPa

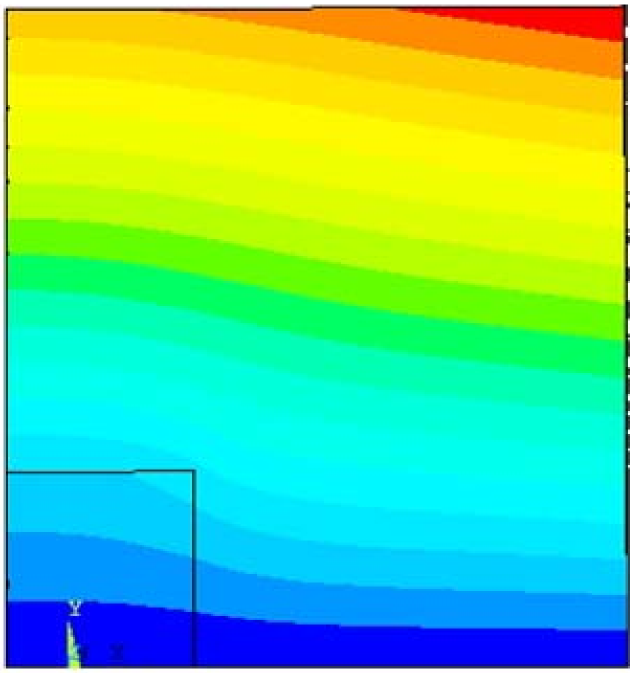

Figure 5.29: y component of displacement curves for the square patch of with width equals to 0.3L

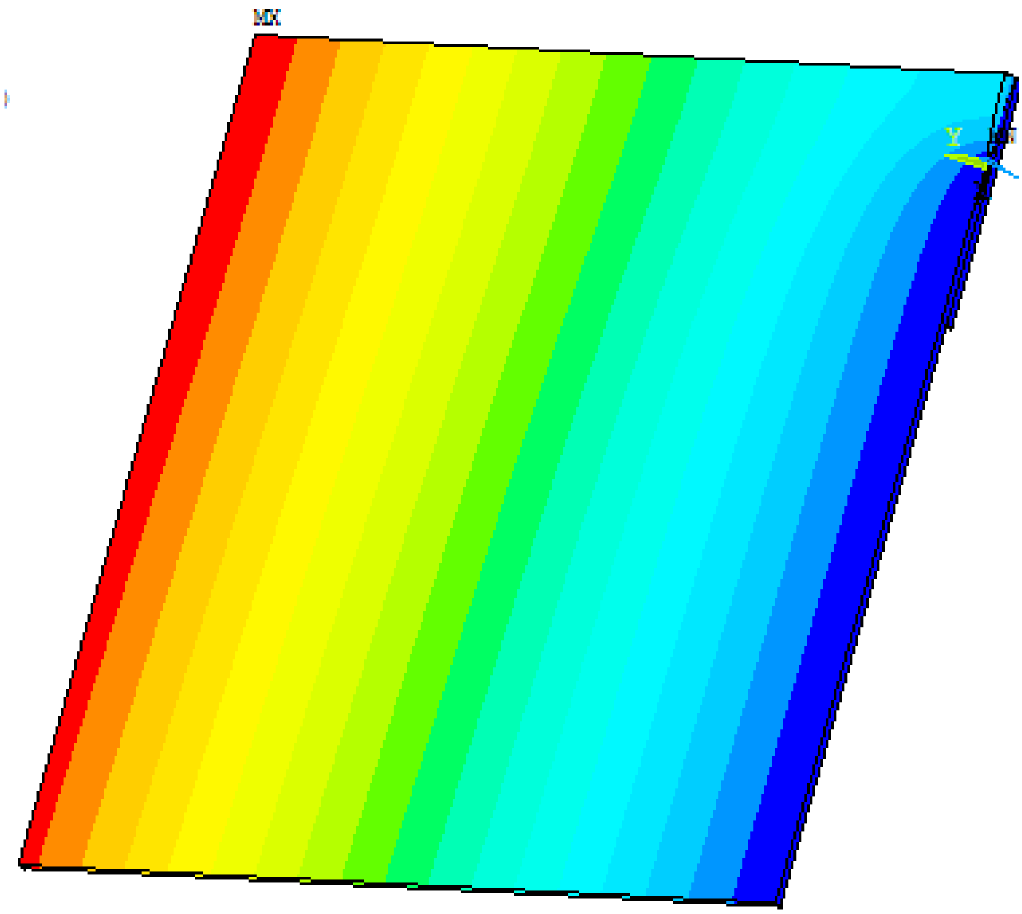

Figure 5.30: y component of displacement contours from the back for the square patch with width of w = 0.3L

Geometry

- $a/L = 0.1$
- $H/L = 0.1$
- $t/L = 0.01$
- $t_p/L = 0.01$
- $E = 210000$ MPa
- $v = 0.3$
- $w = 0.03$ m
- $\sigma_0 = 5.6419$ MPa (In order to satisfy $K_I = Y$)
- Spline keypoints: y_1=0.05, y_2=0.045, y_3=0.04, y_4=0.03, y_5=0.025, y_6=0.020, y_7=0.015, y_8=0.01, y_9=0.010, y_{10}=0.005

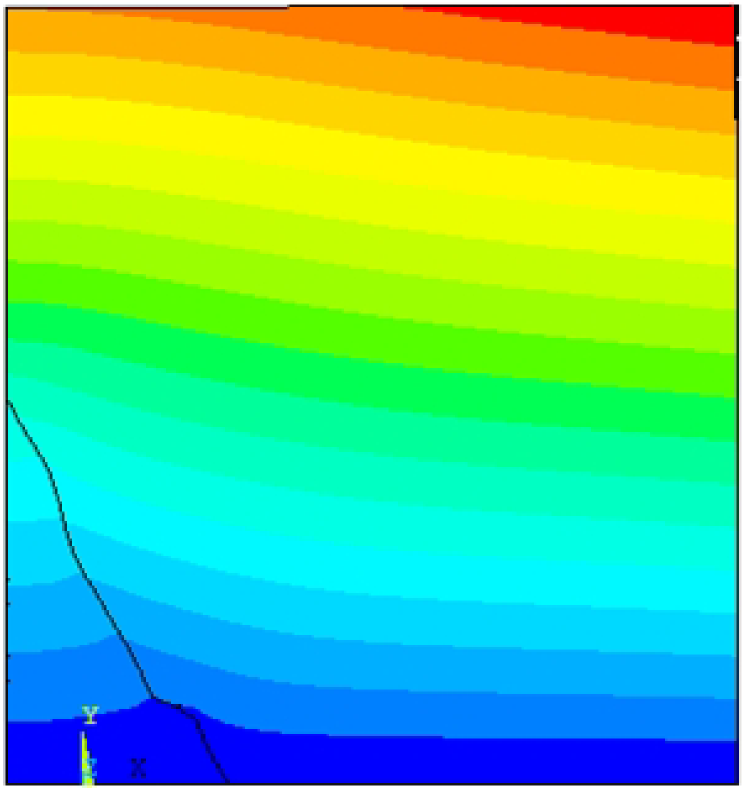

Figure 5.31: –y component of displacement curves for the irregular curved patch for spline keypoints of y_1=0.05, y_2=0.045, y_3=0.04, y_4=0.03, y_5=0.025, y_6=0.020, y_7=0.015, y_8=0.01, y_9=0.010, y_{10}=0.005

Calculated results for stress intensity factor and the maximum stress value achieved through the plate is:

$K_I = 0.1889$ MPa.m$^{1/2}$

σ_{ymax} = 12.63 Mpa

With the same plate geometry but with the following patch

Spline points: y_1=0.008, y_2=0.006, y_3=0.003, y_4=0.002, y_5=0.004, y_6=0.01, y_7=0.015, y_8=0.02, y_9=0.025, y_{10}=0.03

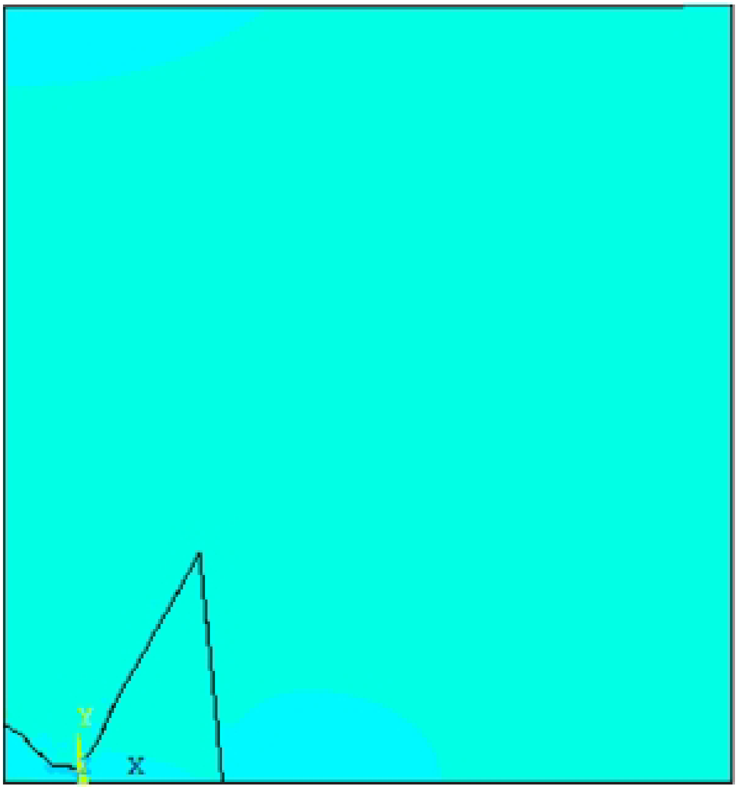

Figure 5.32: Schematic of the irregular curved patch for spline keypoints of y_1=0.008, y_2=0.006, y_3=0.003, y_4=0.002, y_5=0.004, y_6=0.01, y_7=0.015, y_8=0.02, y_9=0.025, y_{10}=0.03

$K_I = 0.1570$ MPa.m$^{1/2}$

σ_{ymax} = 10.50 MPa

Note the decrease in the stress intensity factor and maximum y component of stress achieved on the plate values. Various irregular patch configurations are examined and observed that the patch shape which is similar to Figure 5.32 yields to minimum stress intensity factor values comparing to other irregular patch shapes. The effectiveness of some patch shapes (square, circular, elliptical, modified skewed) are examined by former authors before such as [13,43]. They have found that an efficient patch repair corresponds to the so-called “modified skewed patch” satisfies the most optimum patch shape to lower stress intensity factor values. The modified skewed patch which has been found (in [13,43]) to be a very effective crack repair, can be considered to be very similar to the patch shape determined in the present study with Figure 5.32. It can be concluded that the patch shapes smilar to Figure 5.32 is found to satisfy the most efficient way of lowering stress intensity factors.

The stress intensity for the repaired and unrepaired configurations is determined using the present finite element code. Table 5.15 provides a comparison for both configurations with the plate height of H = L and patch size of w = L/2. As it can be seen from Figure 5.33, the SIF values for repaired configuration are considerably smaller than the corresponding unrepaired configuration.

Table 5.15: Comparison of Stress Intensity Factor Values for repaired and unrepaired configurations.

Patch size L/2 x L/2		
Crack length	**K_I Repaired**	**K_I Unrepaired**
L/10	0.183	1.014
1.2L/10	0.165	1.020
1.4L/10	0.158	1.027
1.6L/10	0.149	1.036
1.8L/10	0.140	1.045
2L/10	0.134	1.056

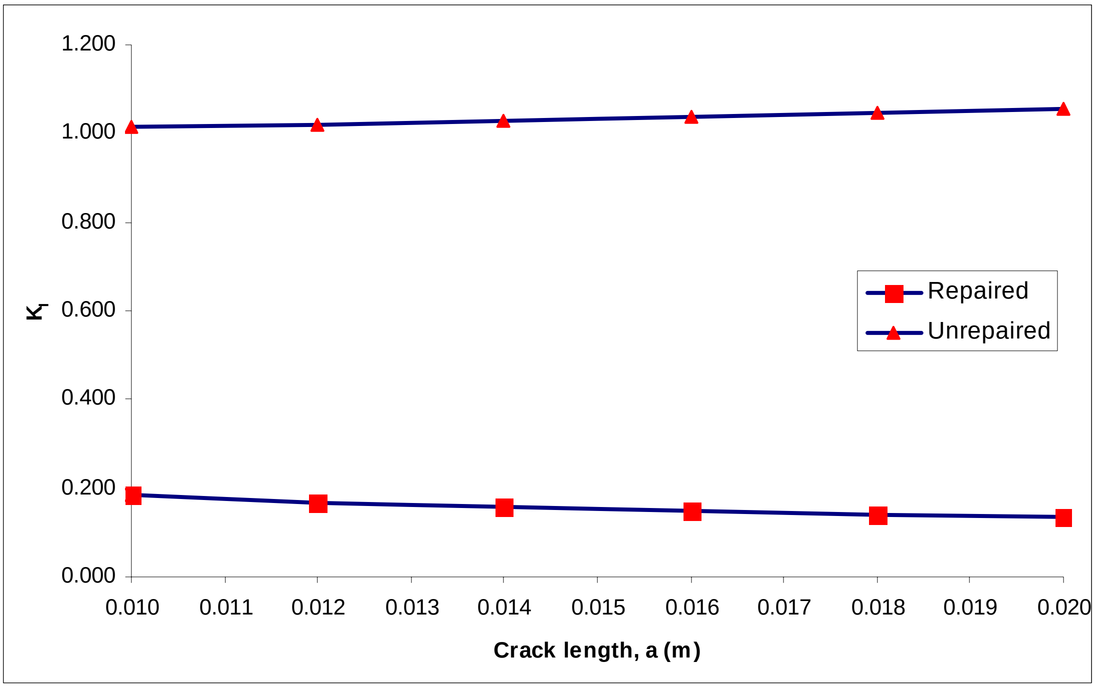

Figure 5.33: Stress Intensity Factor values for unrepaired skin and corresponding skin repaired bonded patch

5.4 Conclusion

Patching is a very efficient way of lowering the SIF and that the increasing of patch thickness continually decreases the value of the SIF. Realistic finite element modeling plays an important role in the analysis of patched cracks. In this study, 3-D finite element models were created by finite element software ANSYS for investigating the stress intensity factors at the crack tip for patched cracks.

Several case studies were performed by using ANSYS Parametric Design Language (A.P.D.L) in order to test the reliability of the model. Many sample crack problems found from various publications [8, 13, 16, 38, 39, 40] which provides analytical or numerical results data are solved in order to verify the results and validate the used model.

One of the earliest studies of cracks in materials was done by Isida [16], where the method of expansion of complex stress potentials was utilized to obtain numerical results for stress intensity factors for the crack configurations that are geometrically same with that studied in this research. It has been proved that for the unpatched condition, the finite element model developed in this study produced results which are in perfect agreement with Isida's results.

The finer elements around the crack tip are recommended (converged from large to small element) for the accuracy of stress intensity factor calculation. There is a tendency that Displacement Correlation Technique is acceptable for cracked plate analysis as far as coupled with the appropriate mesh arrangement.

Analytical results given in abovementioned references were compared with finite element results. The error among the results is at most 0-1%. Hence, finite element method can be suggested as the best candidate at the present time for obtaining approximate stress intensity factors, whenever exact solutions are not available. This method can be adopted rapidly in structural analysis. The reason is that the method is conceptually simple, easily adoptable to high speed computations, applicable to large classes of geometries, materials and loading conditions and can be made quite accurate.

The method presented here can be easily implemented and is a versatile tool for the determination of SIFs in fractured plates with patch of varied shapes not found in handbooks. Furthermore, such high level of accuracy was easily achieved with no more than a few elements along the cracks. It can be seen that the method presented in this paper could be an extremely powerful method for analysing a wide range of problems. Because of the automatic mesh creation it is also ideal for parametric analyses. Different models with varying repair configurations to choose the optimum one can be generated very quickly.

The main contribution of this thesis is the development of a reliable finite element model for the evaluation of Stress Intensity Factors on various configuration and shape of patch repaired and unrepaired plates.

Suggestions for Further Studies:

1. Bending effect for Mode III or out-of-plane effects for Mode II may be included and investigated

2. Central crack may be replaced by edge cracks.

3. The material of the patch may be assumed to be anisotropic.

4. The effect of the bonding adhesive between the patch and the plate can be taken into account to represent a more realistic model

5. An optimal shape of a patch repair for a cracked plate could be investigated by implementing various optimization techniques including biology-based method genetic algorithm embedded in APDL codes developed in the present study. The best topology can be deduced by determining the optimal material density distribution of the patch. The optimisation can be performed keeping constant the total patched area and minimising the SIF function.

REFERENCES:

[1] **Broek D.,** 1999. Elementary Engineering Fracture Mechanics, Kluwer Academic Publishers, London

[2] **Shukla, A.,** 2004. Practical Fracture Mechanics in Design, CRC, New York

[3] **Wang, C.H**., 1996. Introduction to Fracture Mechanics, DSTO Aeronautical and Maritime Research Laboratory, Melbourne

[4] **Gdoutos E. E.,** 2005. Fracture Mechanics, Springer, The Netherlands

[5] **Pereira J.P. and Duarte C.A.,** 2005. Extraction of stress intensity factors from generalized finite element solutions, Engineering Analysis with Boundary Elements, 29, 397-413

[6] **Lin X.B., Smith R.A**., 1999. Stress intensity factors for corner cracks emanating from fastener holes under tension, Engineering Fracture Mechanics, 62, 535-553

[7] **Araújo T. and Bittencourt T.N.,** 2000. Numerical Estimation Of Fracture Parameters In Elastic And Elastic-Plastic Analysis, European Congress on Computational Methods in Applied Sciences and Engineering, Barcelona, 11-14 September 2000

[8] **Guinea G.V. and Planas J.,** 2000. K_I evaluation by the displacement extrapolation technique, Engineering Fracture Mechanics, 66, 243-255

[9] **Utomo P. and Nikraz H.,** 2006. Evaluation Of Finite Element Mesh Arrangements And Stress Intensity Factor Calculation Methods For Opening Mode Fracture Of Cracked-Cemented Materials, Civil Engineering Dimension, Volume 9, Number 2

[10] **Lim I. L. and Johnston I.W.,** 1992. On Stress Intensity factor Computation From the Quarter-point Element Displacements, Communications in Applied Numerical Methods, 8, 291-300

[11] **Tsamasphyros G. and Marioli-Riga Z.,** 2003. Computer Software For The Stress Analysis Of Repaired Aircraft Structures With The Method Of Composite Patch Repair, Mechanics, Automatic Control and Robotics, 3, 729-738

[12] **Aour B. and Rahmani O.,** 2007. A Coupled FEM/BEM Approach And Its Accuracy For Solving Crack Problems In Fracture Mechanics, International Journal of Solids and Structures, 44, 2523–2539

[13] **Brighenti R. and Carpinteri A.,** 2006. A Genetic Algorithm Applied To Optimisation Of Patch Repairs For Cracked Plates, Comput. Methods Appl. Mech. Engrg, 196, 466–475

[14] **Liu C.F. and Jou H.S.,** 1997. Stress intensity factor of a patched crack, Int. J. Solid Struct., 34, 1557–1562.

[15] **Tada, H. and Paris, P. C.,** 1973. The Stress Analysis of Cracks Handbook, Del Research Corporation, Missouri, USA,

[16] **Isida M.,** 1976. Arbitrary Symmetric Loading Problems of Centrally Cracked Rectangular Plates, Trans. Jpn. Mech. Engrs., 42, 3019–3030.

[17] **Anderson T.L.,** 2005. Fracture Mechanics, CRC Press, Florida,

[18] **Bui H.D.,** 2006. Fracture Mechanics Inverse Problems and Solutions, Springer, The Netherlands

[19] **Erdogan F.,** 1983. Stress Intensiy Factors, Journal of Applied Mechanics, 50, 992- 1002.

[20] **Chan S., Tuba I, and Wilson W.,** 1970. On the Finite Element Method In Linear Fracture Mechanics, Engineering Fracture Mechanics, 2, 1–17.

[21] **Sih G.C.,** 1974. Handbook of Stress Intensity Factors, Institute of Fracture and Solid Mechanics Lehigh University Bethlehem, Pennsylvania.

[22] **Barsoum R.S.,** 1976. On the Use of Isoparametric Finite Elements in Linear Fracture Mechanics, International Journal for Numerical Methods in Engineering, 10, 25-37.

[23] **Zehnder A.T.,** 2008. Lecture Notes on Fracture Mechanics, Cornell University, New York

[24] **Freese C.E. and Tracey D.M**., 1976. The Natural Isoparametric Triangle Versus Collapsed Quadrilateral For Elastic Crack Analysis, International Journal of Fracture, 12, 767–770.

[25] **Banks-Sills L. and Sherman D.,** 1986. Comparison of Methods For Calculating Stress Intensity Factors With Quarter-point Elements, International Journal of Fracture, 32, 127–140

[26] **Shih C.F. and Delorenzi H.G.,** 1976. Crack Extension Modelling With Singular Quadratic Isoparametric Elements, Int. J. Fract., 12, 647-651

[27] **Paris, P. C. and Sih, G. C.,** 1965. Stress Analysis of Cracks, Fracture Toughness and Testing and its Applications, American Society for Testing and Materials, Philadelphia, 381, 30-83

[28] **Beer G. and Watson J.O.,** 1992. Introduction to Finite and Boundary Element Methods for Engineers, John Wiley & Sons Ltd.

[29] **Cook R. D., Malkus D. S. and M. E. Plesha**, 1989. Concepts and Applications of Finite Element Analysis, John Wiley and Sons, Inc.

[30] **Boresi A. P. and Schmidt R. J.,** 1993. Advanced Mechanics of Materials, John Wiley and Sons, Inc.

[31] **ANSYS Theory Reference,** SAS IP Inc.

[32] **Moaveni S.,** 1999. Finite Element Analvsis Theory and Apulication with ANSYS, Prentice-Hall, Inc.

[33] **ANSYS Modeling and Meshing Guide,** SAS IP Inc.

[34] **Williamson R. L., Wright J. K., Steffler E. D. and Cannon R. M**., 2002. Numerical Analysis of Surface Cracks at Regions of Curvature in Oxide Scales, Materials Science & Engineering, 1-11.

[35] **Bouiadjra B. B., Belhouari M. and Serier B.,** 2002. Computation of the stress intensity factors for repaired cracks with bonded composite patch in mode I and mixed mode, Composite Structures, 56, 401-406.

[36] **Pan N. and Sheppard S. D.,** 2002. Stress intensity factors in spot welds, Engineering Fracture Mechanics, 70, 671-684

[37] **Murakami Y. and Aoki S.,** 1987. Stress Intensity Factors Handbook, Pergamon, Oxford, New York.

[38] **Aliabadi M.H. and Rooke D.P.,** 1992. Numerical Fracture Mechanics, Kluwer Academic Publishers, Great Britain

[39] **Jones R. and Callinan R. J.,** 1979. Finite Element Analysis of Patched Cracks, J. Struct. Mech., 7, 107-130

[40] **Arin K.,** 1974. A Plate with a Crack Stiffened By a Partially Debonded Stringer, Eng. Fract. Mech., 6, 133-140

[41] **Yehia N. A. B. and Shephard M. S**., 1985. On the Effect of Quarter-point Element Size on Fracture Criteria, Int. J. Numer. Methods Eng., 21, 1911-1924

[42] **Murti V. and Valliappan S.,** 1986. A universal optimum quarter point element, Engineering Fracture Mechanics, 25, 237-258

[43] **Kumar A. M. and Hakeem S. A.,** 2000. Optimum design of symmetric composite patch repair to centre cracked metallic sheet, Comp. Struct. 49, 285–292.

[44] **NASGRO** < http://www.swri.org/4org/d18/mateng/matint/nasgro>, accessed at 24.06.2008.

[45] **Irwin, G.R.,** 1961. Plastic Zone near a Crack and Fracture Toughness, Sagamore Research Conference Proceeding, Sagamore.

[46] **Westergaard, H.M.,** 1939. Bearing pressures and cracks, Trans. ASME J. Appl. Mech., 6, 49–53

[47] **Rice, J.R.,** 1968. A path independent integral and the approximate analysis of strain concentration by notches and cracks, Trans. ASME J. Appl. Mech. 35, 379-386

[48] **Sneddon I.N.,** 1969. Crack problems in the classical theory of elasticity, Wiley

[49] **Williams J. G.,** 1984. Fracture under complex stress - The angled crack problem, International Journal of Fracture, 8, 441-446

[50] **ASTM E399-90,** 1993. Standard Test Method for Plane-Strain Fracture Toughness of Metallic Materials, Annual Book of ASTM Standards, American Society for Testing and Materials, 03.01, 509-539

[51] **Feddersen C. E.,** 1973. Analysis of fatigue, fatigue-crack propagation, and fracture data, NASA Langley Research Center, Ohio

APPENDIX A

SAMPLE APDL CODES, FOR UNPATCHED CONDITION

```
/PREP7
/input,data,txt
*DIM,aaa,ARRAY,8,1,1, , ,
*SET,AAA(1,1,1) , a1
*SET,AAA(2,1,1) , a2
*SET,AAA(3,1,1) , a3
*SET,AAA(4,1,1) , a4
*SET,AAA(5,1,1) , a5
*SET,AAA(6,1,1) , a6
*SET,AAA(7,1,1) , a7
*SET,AAA(8,1,1) , a8
/NERR,0
ET,1,PLANE82
MPTEMP,,,,,,,,
MPTEMP,1,0
MPDATA,EX,1,,a4
MPDATA,PRXY,1,,a5
K,1                    ! DEFINE KEYPOINTS AND LINE SEGMENTS
K,2,a2-a1
K,3,a2-a1,a3
K,4,-a1,a3
K,5,-a1
L,    1,    2
L,    2,    3
L,    3,    4
L,    4,    5
L,    5,    1
FLST,5,2,4,ORDE,2
FITEM,5,2
```

```
FITEM,5,3
CM,_Y,LINE
LSEL, , , ,P51X
CM,_Y1,LINE
CMSEL,,_Y
LESIZE,_Y1, , ,15, , , , ,0
FLST,5,1,4,ORDE,1
FITEM,5,4
CM,_Y,LINE
LSEL, , , ,P51X
CM,_Y1,LINE
CMSEL,,_Y
LESIZE,_Y1, , ,20,0.1, , , ,0
FLST,5,1,4,ORDE,1
FITEM,5,5
CM,_Y,LINE
LSEL, , , ,P51X
CM,_Y1,LINE
CMSEL,,_Y
LESIZE,_Y1, , ,8,10, , , ,0
FLST,5,1,4,ORDE,1
FITEM,5,1
CM,_Y,LINE
LSEL, , , ,P51X
CM,_Y1,LINE
CMSEL,,_Y
LESIZE,_Y1, , ,15, , , , ,0
FLST,2,5,4
FITEM,2,1
FITEM,2,2
FITEM,2,3
FITEM,2,4
FITEM,2,5
AL,P51X
KSCON,1,a1/a7,1,a7
```

```
MSHKEY,0
CM,_Y,AREA
ASEL, , , ,       1
CM,_Y1,AREA
CHKMSH,'AREA'
CMSEL,S,_Y
AMESH,_Y1
CMDELE,_Y
CMDELE,_Y1
CMDELE,_Y2
ET,2,SOLID95
TYPE,   2
EXTOPT,ESIZE,2,0,
EXTOPT,ACLEAR,0
EXTOPT,ATTR,0,0,0
MAT,1
REAL,_Z4
ESYS,0
VOFFST,1,-a8, ,
ASEL,S, , ,       6
NSLA,S,1
DSYM,SYMM,X, ,
ALLSEL,ALL
ASEL,S, , ,       3
NSLA,S,1
DSYM,SYMM,Y, ,
ALLSEL,ALL
ASEL,S, , ,       5
NSLA,S,1
SF,ALL,PRES,-1/(3.14159265358979323846264338327 95*a1)**0.5
!SF,ALL,PRES,-a6
ALLSEL,ALL
NSEL,ALL
D,ALL,UZ
!CS,11,0,2,70,259,1,1,
```

```
CSWPLA,11,0,1,1,
CSYS,11,
ALLSEL,ALL
FINISH
/SOL
SOLVE
FINISH
/POST1
RSYS,11
NSEL,S,LOC,Y,0              ! SELECT NODES FOR LPATH COMMAND
NSEL,R,LOC,X,0
*GET,NOD1,NODE,,NUM,MIN
NSEL,A,LOC,Y
NSEL,R,LOC,X,-a1/8/a7,-a1*99/a7/100
*GET,NOD2,NODE,,NUM,MIN
NSEL,A,LOC,Y
NSEL,R,LOC,X,-a1*99/a7/100,-a1*101/a7/100
*GET,NOD3,NODE,,NUM,MIN
NSEL,ALL
PATH,KI2,3,,48              ! DEFINE PATH WITH NAME = "KI2"
PPATH,1,NOD1                ! DEFINE PATH POINTS BY NODE
PPATH,2,NOD2
PPATH,3,NOD3
KCALC,1,1,0,0
*GET,result,KCAL,,K,1
/OUTPUT, SIF,txt,,APPEND
*VWRITE,result
(E14.8)
/OUTPUT
```

APPENDIX B

PLANE82 ELEMENT

PLANE82 provides more accurate results for irregular shapes without as much loss of accuracy. The 8-node elements have compatible displacement shapes and are suitable for curved boundaries.

The 8-node element is defined by eight nodes having two degrees of freedom at each node: translations in the nodal X and Y directions. The element may be used as a plane or an axisymmetric element.

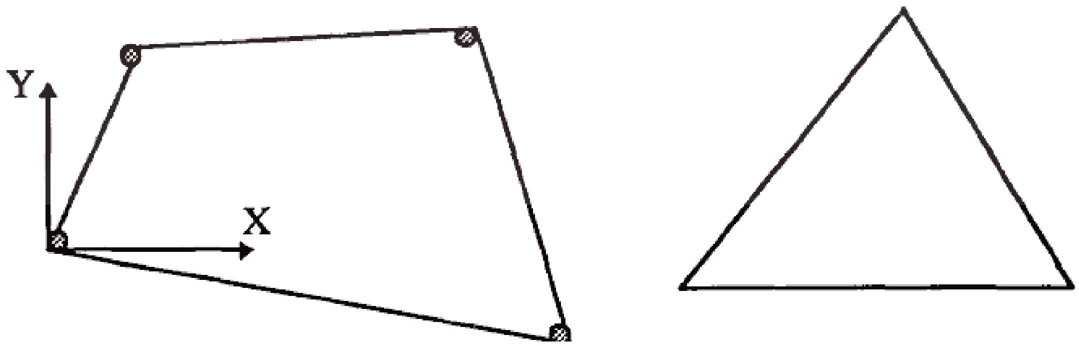

Figure B.1: PLANE82 Solid Element, Triangular Shape Option

APPENDIX C

SOLID95 ELEMENT

SOLID95 is a higher order version of the 3-D solid element. It can tolerate irregular shapes without as much loss of accuracy. SOLID95 elements have compatible displacement shapes and are well suited to model curved boundaries.

The element is defined by 20 nodes having three degrees of freedom per node: translations in the nodal X,Y, and Z directions. The element may have any spatial orientation.

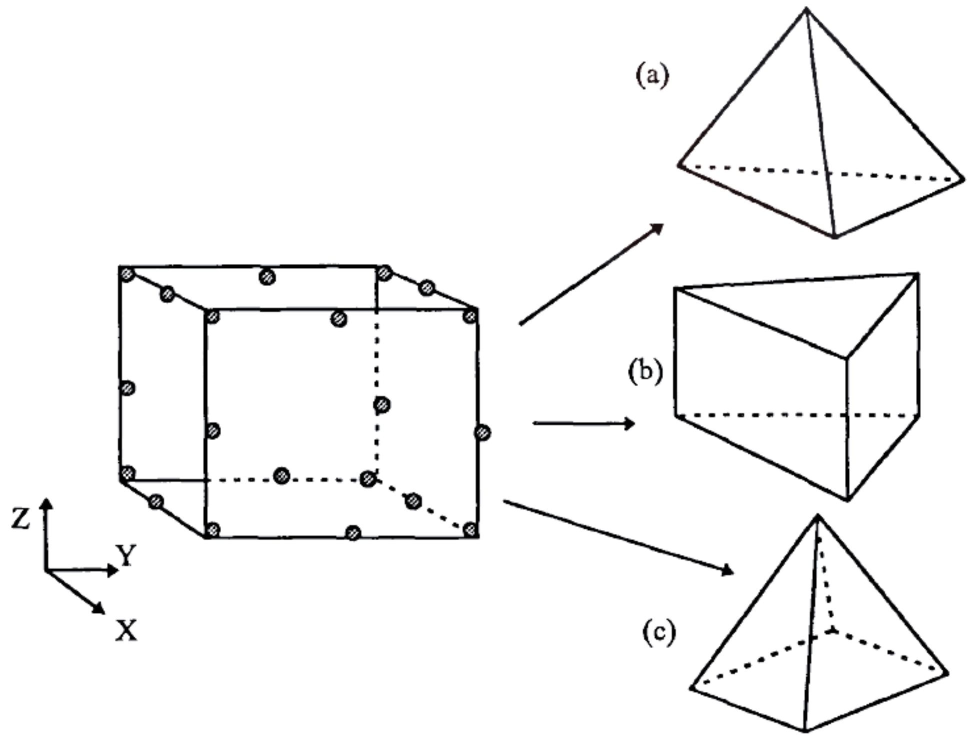

Figure C.1: SOLID95 and Shape Options: (a) Tetrahedral, (b) Prism, (c) Pyramid

ÖZGEÇMİŞ

Emre Civan was born in Zonguldak on December 3, 1979. He received his High School Degree from İzmir Yamanlar College and B.S. Degree from I.T.U. Aeronautical & Astronautical Engineering Department as an Aeronautical Engineer. He started M.S. in Aeronautical Engineering Program at Istanbul Technical University, Institute of Science and Technology in 2005.